Digital Transmission by Hermite N-dimensional Antipodal Scheme

Wachira Chongburee

Dissertation submitted to the faculty of the Virginia Polytechnic Institute and State University in partial fulfillment of the requirements for the degree of

Doctor of Philosophy
In
Electrical Engineering

Timothy Pratt, Chair
Charles W. Bostian
William A Davis
Dennis G. Sweeney
Surot Thangjitham

February 11, 2004
Blacksburg, Virginia

Keywords: Hermite Keying, Orthogonal Waveforms, Antipodal Scheme, N-dimensional PSD, Optimal Synchronization, Digital Modulation

Digital Transmission by Hermite N-dimensional Antipodal Scheme

Wachira Chongburee

Abstract

A new N-dimensional digital modulation technique is proposed as a bandwidth efficient method for the transmission of digital data. The technique uses an antipodal scheme in which parallel binary data signs baseband orthogonal waveforms derived from Hermite polynomials. Orthogonality guarantees recoverability of the data from N simultaneously transmitted Hermite waveforms. The signed Hermite waveform is transmitted over a radio link using either amplitude or frequency modulation. The bandwidth efficiency of the amplitude Hermite method is found to be as good as filtered BPSK in practice, while the bit error rates for both modulations are identical. Hermite Keying (HK), the FM modulation version of the N-dimensional Hermite transmission, outperforms constant envelope FSK in terms of spectrum efficiency. With a simple FM detector, the bit error rate of HK is as good as that of non-coherent FSK. In a frequency selective fading channel, the simulation results suggest that specific data bits of HK are relatively secure from errors, which is beneficial in some applications. Symbol synchronization is critical to the system. An optimal synchronization method for the N-dimensional antipodal scheme in additive white Gaussian noise channel is derived. Simulation results confirm that the synchronizer can operate successfully at E/N_o of 3 dB.

Acknowledgement

First and foremost, I would like to express my gratitude to Dr. Timothy Pratt, my advisor and career role model, for his revision of this dissertation over the Internet and for the technical and communication skills I have learned from him. I thank Dr. Charles Bostian, Dr. William Davis, Dr. Dennis Sweeney and Dr. Surot Thangjitham for serving as my committee members. My thanks also go to my family in Thailand and my colleagues at Kasetsart University for their unrelenting support. Finally, my special thanks are for my dear friends in Blacksburg for a place to stay and for the warm welcome I received during the time of defending my dissertation.

Table of Contents

List of Figures

List of Tables

Chapter 1
Introduction

Radio communications at the beginning focused on transmission of audio signals. Transmission of audio signals over radio links has been implemented by using the signals to modulate the carrier amplitude (amplitude modulation, AM) or carrier frequency (frequency modulation, FM). Analog transmission was natural for such a signal. Audio signals are not the only information that needs to be transmitted over radio links. Transmission of digital data, with finite valued form of information, has become important. Digital transmission allows many features which are not easy to implement in analog transmission, for example data encryption. In fact, any analog signals can be represented in digital format. Digital modulation techniques have been proposed and developed. One aim is to increase the data rate as much as possible with limited transmit power and limited bandwidth. There is a bound on the data rate that can be transmitted over a channel without error which is set by the bandwidth of the channel and the signal to noise ratio. [SHA48].

The digital data rate successfully transmitted over a radio communication channel is limited either by the allowed channel bandwidth or by the available transmit power. Generally, a higher data rate requires more transmit bandwidth and power. Speaking of bandwidth, an ideal transmission technique maximizes the ratio of the transmit bit rate and the transmit bandwidth. The ratio is known as bandwidth efficiency. Since bandwidth is limited and always expensive, maximizing bandwidth efficiency is one of the key goals of digital communication system design.

In digital radio communications, a modulation technique describes how the digital data is carried by the transmit carrier. Generally, the digital data are used to modulate the carrier's amplitude or phase, or both. Each particular modulation technique comes with a specific bandwidth efficiency and characteristics in the presence of noise. An ideal modulation technique must be bandwidth efficient and tolerate noise well. Unfortunately, there is always a trade-off between the two efficiencies. A modulation technique is proposed in this dissertation aiming to exploit both efficiencies.

Theoretically, if the information rate in bits/second (bps) is less than the channel capacity, the error rate could approach zero [SHA48]. The channel capacity is determined by the channel bandwidth and signal to noise ratio. Modulation techniques alone are unlikely to achieve the theoretical channel capacity. For instance, spectral efficiency of Binary Phase Shift Keying (BPSK) can reach 1 Hz/bps by using a raised cosine filter with zero roll-off factor. However, the signal to noise ratio (S/N) must be about 12 dB in practice to have the communication link considered error free. At a spectral efficiency of 1 Hz/bps, the S/N of BPSK exceeds the Shannon limit by more than 10 dB. Improvement is dramatically achieved by adding redundant bits to correct errors. The BCH (1023, 688) error correcting code [BOS60], which encodes 688 data bits into 1023 total bits, can lower the error-free S/N to about 6 dB. Recently, turbo codes [BER93] further reduce the minimum S/N required for near-error free operation to very close to Shannon limit, leaving little room of further improvement.

Nevertheless, the Shannon limit applies only to the case of additive white Gaussian noise (AWGN). In practice, interference is not restricted to thermal noise. In indoor communications, for example, the channel is modeled as a heavy multipath channel [SAL87]. Delayed multipath components play a key role in received signal distortion. The received signal is frequency-selective faded. The simulation results in [CHU87] show significant degradation due to multipath. Thus, modulation techniques designed to combat AWGN are not guaranteed to be robust in such an environment.

Spread spectrum is a technique used to mitigate the effects of multipath of the received signal [SKL97b], although spread spectrum implies inefficient use of the bandwidth. Although a number of users can share the spread spectrum, the bit error rate increases as the number of the users increases [PIC82]. As a result, there is a need to design a modulation technique that tolerates multipath impairment without sacrificing bandwidth.

This dissertation proposes a modulation technique that aims to combat such a multipath impairment. The new design is constrained by efficient use of the bandwidth. Additionally, the bit error rate (BER) performance of the proposed technique must be at least as good as existing modulation techniques in an AWGN environment. Its superior performance in the delayed multipath environment is expected. Performance improvement achieved by using channel coding is beyond the scope of this dissertation.

1.1 Proposed Modulation Scheme

The proposed digital modulation technique makes use of signal orthogonality. The orthogonality allows transmission of multiple orthogonal signals simultaneously. At the receiver, the orthogonality of the signal guarantees the capability to recover the original data transmitted. If M orthogonal signals are used, the system can be viewed as an M dimensional system.

In an already available M-ary orthogonal system, one symbol is sent at a time. Each symbol carries $\log_2(M)$ data bits. It is shown in [PRO95] that communication systems with M orthogonal symbols can reach the Shannon S/N ratio limit of -1.6 dB when the number of the orthogonal symbols approaches infinity. The drawback is that the bandwidth approaches infinity as well. Bandwidth usage becomes inefficient. As a result, this system is disqualified when bandwidth becomes a constraint.

In fact, orthogonality of M symbols allows simultaneous transmission of M orthogonal pulses. This research proposes a method of carrying M data bits on the signs of the M orthogonal symbols (pulses). First, M serial data bits are fed into a serial to parallel converter. The parallel M data bits are used to sign the M orthogonal pulses. The signed orthogonal pulses are then combined and transmitted. The signed M orthogonal symbols then form 2^M distinct symbols. Therefore, in one symbol (pulse) period, M bits of data are sent simultaneously. The system is titled N-dimensional antipodal. Since M

data bits are transmitted simultaneously, the antipodal system can be viewed as a parallel transmission system.

The antipodal scheme of M-orthogonal pulses, even when approaching an infinite number of pulses, would fail to reach the Shannon power limit. Questions of spectral efficiency and power performance along with implementation aspects then arise. An aim of this dissertation is to evaluate the bandwidth efficiency of the antipodal orthogonal system. Throughout the thesis, results are obtained by simulation using Matlab [MAT99], a widely used software package.

Generally, the orthogonal waveforms are baseband signals. Radio communications need to re-allocate the spectrum about DC of the orthogonal waveforms to a radio band. Two methods are proposed to carry the combination of the signed orthogonal pulses over the radio link. The first method keeps the combined orthogonal waveforms on the carrier's amplitude, i.e., amplitude modulation (AM). The other method lets the baseband orthogonal waveform modulate the carrier's frequency, i.e., frequency modulation (FM). The two methods require different occupied bandwidths and their immunities to channel impairments are distinct. The bandwidths of both methods are investigated in this research as well as the BER performances in both AWGN and frequency selective fading channels.

1.2 Selected Orthogonal Pulse Sets

Because of their spectral efficiency, in this research, Hermite waveforms are chosen over other orthogonal pulse sets. Hermite waveforms are developed from Hermite polynomials. The Hermite polynomials are not orthogonal and their values approach infinity when their argument gets large. However, multiplying the Hermite polynomials with a proper exponential term results in a set of orthogonal functions. The resultant functions are called Hermite waveforms. The Hermite waveforms are time-infinite but their values are packed in some period. Outside the symbol period, the values decay quickly to zero. Essentially, they are finite energy pulses.

Hermite waveforms have already been used in many applications. Recently, an ultra wide band (UWB) system proposed in [MIT03] invokes the orthogonality of Hermite waveforms to increase data rate and to add error correction code to achieve reliable communication. The UWB system is becoming of interest since it has useful properties for short-range communication in a dense multipath environment [WIN98]. Typical UWB uses a time hopping pattern as a multiple access technique. Its performance is analyzed in [CRA99]. Another application of the Hermite waveform set is proposed in [WAL93]. There, Hermite wavelets are used to replace sinusoid waves in multicarrier system in a high-rate digital subscriber loop (DSL). Applications of Hermite waveforms include image processing [MAR90].

Hermite waveforms are quite complex. Generation of the pulses for UWB use is discussed in [MIC02]. A special property of Hermite waveforms is that the time waveforms and their Fourier transforms have the same shapes [MAR90]. The property allows simultaneous extrapolation in both time and frequency domains [RAO99]. Invoking an additional pulse requires little extra bandwidth. This characteristic supports the claim that Hermite waveforms are the most bandwidth efficient orthogonal pulse [HAR72]. Discussion on Hermite waveforms is detailed in Chapter 2.

1.3 Survey of Similar Parallel Schemes

The concept of parallel transmission has been introduced in the 1950's. In this system, the available bandwidth is divided into narrower sub-channels by a number of independently modulated subcarriers (tones) modulated by rectangular pulses. The spectra of the sub-channels in the multitone system are overlapping and $\sin(x)/x$ shaped. An improved system proposed in [CHA66] replaces the modulating rectangular pulses by bandlimited raised cosine pulses. According to the system, each channel carries a binary data rate of R_b and the channels are spaced by $R_b/2$. Large numbers of channels allow transmission speeds close to the Nyquist rate with no resultant intersymbol interference or interchannel interference. The system performance is evaluated in [SAL67] and [CHA68].

In a multitone system with a larger number of carriers, the coherent demodulators required by the subcarriers become unreasonably expensive and complex. The system can be implemented indirectly through the discrete Fourier transform [WEI71]. Later, an orthogonal QAM using fast Fourier transform (FFT) was explored [HIR81]. Advances in Digital Signal Processing (DSP) technology have eased implementation of the FFTs required in these systems. Orthogonal Frequency Division Multiplexing (OFDM), a form of multi-carrier modulation that makes use of the FFT, has been developed and is now widely used. For instance, OFDM has been adopted by Europe for digital terrestrial broadcasting [EUR94]. The analysis in [CIM85] shows that OFDM provides a large improvement in bursty Rayleigh fading channels. In addition, advantages of OFDM include bandwidth efficiency, robustness to impulse interference, sampling time shift and implementation complexity. However, the down side is that OFDM suffers from a high peak-to-average power ratio, sensitivity to carrier frequency offset and proneness to tone interference [WU95].

Carrying baseband OFDM from a FFT processor over a radio channel can be done in many ways. In [CIM95], the baseband signal modulates an RF carrier. Optionally, frequency modulation (FM) is used in a system proposed and analyzed in [CAS91]. This system allows implementation of OFDM on existing low cost FM radio equipments. Additionally, FM is a constant envelope RF signal. The peak and average power are identical. In this research, FM is one choice of the newly proposed parallel transmission using M orthogonal pulses.

1.4 Result Summary

It is shown by simulation results that bandwidth occupied by the baseband Hermite antipodal scheme is practically efficient. The Hermite system requires a baseband bandwidth of $0.625R_b$ Hertz to transmit a bit rate of R_b bits per second. Ninety nine percent of the signal energy is guaranteed to lie in the band. The occupied bandwidth is equivalent to that of a raised cosine pulse with a roll off factor of 0.25.

The bit error rate performance of AM Hermite antipodal modulation is identical to that of binary phase shift keying (BPSK). Erroneous bits distribute uniformly over the Hermite waveforms used. In Hermite Keying, a modulation technique that carries the Hermite waveforms in the frequency of the transmit carrier, the power spectral density is monotonically decreasing. No side lobe is observed. The bandwidth efficiency of Hermite Keying is better than that of minimum shift keying (MSK). With a non-coherent FM receiver equipped with simple preemphasis/deemphasis, Hermite Keying performs as well as a non-coherent frequency shift keying (FSK). Identical signal power after the non-coherent demodulator is assumed.

In a frequency-selective fading channel, the long symbol period of Hermite Keying does not help improving the average BER. However, the data bits carried by the low order Hermite pulses are relatively secure. It might be useful in some applications.

1.5 Chapter Organization

Chapter 2 describes the proposed Hermite orthogonal antipodal system. This chapter focuses on bandwidth efficiency. A method to determine the power spectral density of an arbitrary N-dimensional antipodal system is developed. Then, the bandwidth of the system is evaluated numerically and compared with the bandwidth of the classical raised cosine pulse. The bandwidth efficiency is either reported in a format of the bandwidth and transmit bit period (BT) or normalized by the transmit bit rate (R_b).

Chapter 3 discusses N-dimensional direct detectors for the antipodal system and theirs alternatives. Highlights of this chapter are the derivation of an optimum synchronizer for general N-dimensional orthogonal systems. Construction of the detector and synchronizer are introduced. Performance of the synchronizer and its limitation are investigated.

Chapter 4 evaluates the power efficiency of the system. Complex envelope representation is briefly reviewed and used in the simulation of bandpass radio signals. The chapter is closed with a discussion of peak to average power ratio.

Chapter 5 reports an investigation of an FM orthogonal N-dimensional system. FM bandwidth and BER of the system are simulated. This chapter reviews FM noise and explains its effects on the dimensional bit error rate. The effects of preemphasis and deemphasis are examined. Chapters 3-5 restrict the channel disturbance to additive white Gaussian noise (AWGN) only.

Chapter 6 takes signal fading into account. A satellite mobile channel is reviewed. Performance of the FM antipodal system in a mobile satellite channel is simulated. Finally, Chapter 7 draws the dissertation to a conclusion. Chapter summaries are provided at the end of each chapter.

Chapter 2
Hermite Orthogonal Waveforms

In typical digital transmission, data bits are sent serially. A higher bit rate can be achieved by shortening the bit/symbol period. As long as the ratio of bit energy and the noise power spectral density is maintained constant, the bit error rate (BER) is unchanged. However, in multipath environments, multiple copies of delayed transmitted signal are received. Noise is not the only interference. In such an environment, the BER dramatically increases as either the ratio of the delay and the bit period or the power of the unwanted copies increases [FUN93]. As a result, in high-speed transmission, in which the bit period is narrow, BER is affected by the delayed signal directly.

An approach to mitigate the multipath effects is to extend the symbol period. A basic method to extend the symbol period is that the input data stream is first serial-to-parallel converted to N parallel data streams. The effective bit rate for each parallel stream is $1/N$ of the original serial data stream. As a result, the parallel bit period is N times wider than the bit period of the original serial stream. Then, N different waveforms (symbols) are assigned to each of the N parallel streams. The N resulting waveforms are combined to be a composite transmit waveform. As long as the N symbols are orthogonal, detection of the presence of a participating symbol on the composite waveform is possible. The parallel transmission system can be viewed as an N-dimensional system.

There are a number of candidate orthogonal waveforms. One important criterion in communications is that a good set of the orthogonal waveforms must consume as little bandwidth as possible. Hermite orthogonal waveforms, which are derived from Hermite polynomials, are said to be the best bandwidth-wise [HAR72]. The derivation of the Hermite waveforms and their bandwidth consumption are investigated in this chapter.

2.1 Review of Orthogonal Functions

A set of functions, $\{f_0(t), f_1(t), f_2(t), \ldots\}$ is said to be orthogonal over an interval $[t_1, t_2]$ if

$$\int_{t_1}^{t_2} f_m(t) f_n(t) dt = \begin{cases} 0, & m \neq n \\ \delta_{mm}, & m = n \end{cases} \quad \textbf{(2.1)}$$

where δ_{mm} is the energy of the function $f_m(t)$.

Let $s(t)$ be a signal composed from a linear combination of $f_p(t)$ with coefficients b_p

$$s(t) = \sum_{p=0}^{n-1} b_p f_p(t) \quad \textbf{(2.2)}$$

The coefficients b_p can be decomposed by

$$b_p = \int_{t_1}^{t_2} s(t) f_p(t) dt \quad \textbf{(2.3)}$$

In digital communications, b_p is used to carry the digital data. The capability to extract b_p from the composite signal $s(t)$ allows us to transmit n independent data sets simultaneously. However, the added basis orthogonal functions always cost extra bandwidth. We will refer to the orthogonal functions $f_k(t)$ as the k^{th} orthogonal basis pulses. The energy of $s(t)$ can be computed by

$$E_S = \int_{t_1}^{t_2} s^2(t) dt \quad \textbf{(2.4)}$$

$$E_S = \int_{t_1}^{t_2} \left(\sum_{p=0}^{n-1} b_p f_p(t) \right)^2 dt$$

$$= \sum_{p=0}^{n-1} \int_{t_1}^{t_2} \left(b_p f_p(t) \right)^2 dt \qquad \textbf{(2.5)}$$

Clearly, the energy of $s(t)$ is equal to the sum of the energy of the individual waveforms $b_p f_p(t)$.

Because the data carried by one basis orthogonal pulse does not interfere with the data on the other carrying pulses and pulses are well separated in terms of energy, the parallel transmission scheme is recognized as an n-dimensional system.

2.2 Hermite Orthogonal Functions

There are a number of candidates for orthogonal function sets used in the n-dimensional system. A good one must exploit the bandwidth efficiently. Some functions, e.g., Legendre polynomial, are orthogonal but are not appropriate for parallel transmission. The Legendre polynomials, defined by [FOL92]

$$p_n(x) = \frac{1}{2^n n!} \frac{d^n}{dx^n} (x^2 - 1)^n , \qquad \textbf{(2.6)}$$

forms an orthogonal set of functions on the argument interval $x \in [-1, 1]$. However, the values at the pulse boundaries do not decay to zero, i.e., $P_n(\pm 1)$ is either 1 or –1. This causes discontinuity at the adjacent pulse boundaries. Because of the boundary transition, the Legendre polynomial waveform is not a good choice for binary transmission.

Note that another class of orthogonality is defined over binary space. The Walsh function, for example, consists of step functions [BEA84]. Since, its values are either high or low, it can be completely described by a binary sequence. Consequently, the Walsh function can be viewed as a binary orthogonal code. In fact, Walsh code can be generated by using the Hamadard matrix [LIN73]. Unusually, the direct sequence (DS) spreading codes used in spread spectrum communications are only near orthogonal. The aim of spreading codes is to have well-behaved periodic cross-correlation properties between the member codes. A good code should look like a random sequence (pseudo noise). Well known Gold codes satisfy the property. Detailed discussion on them can be found in [SAR80]. IS-95, a cellular communication standard, makes use of both orthogonal and near orthogonal codes. A Walsh code is used to denote a particular user channel while a near orthogonal long code is adopted as a DS spreading code [TIA93].

The functions of choice for the parallel transmission system are the functions of a parabolic cylinder, $\psi_j(x)$, which are developed from Hermite polynomials. The functions of a parabolic cylinder form an orthogonal set in $(-\infty, \infty)$ said to be theoretical best in the time-frequency domain [HAR72]. Because of the difficulty of generating their complicated waveforms, applications of the Hermite functions have been few in the past. Today's technology, for example, Digital Signal Processing (DSP), allows us to produce arbitrary waveforms. Thus, complexity is no longer a problem.

The j^{th} function of a parabolic cylinder, $\psi_j(x)$, is defined by

$$\psi_j(x) = \frac{e^{-\frac{1}{4}x^2}}{\sqrt{j!\sqrt{2\pi}}} He_j(x), \tag{2.7}$$

where $He_j(x)$ is Hermite polynomial defined by

$$He_j(x) = e^{x^2/2}\left(-\frac{d}{dx^j}\right)^j e^{-x^2/2}. \tag{2.8}$$

The j^{th} function of the parabolic cylinder is identified as the j^{th} Hermite orthogonal function. Extracting the polynomial defined in (2.8) results in

$$\begin{aligned}
He_0(x) &= 1 \\
He_1(x) &= x \\
He_2(x) &= x^2 - 1 \\
He_3(x) &= x^3 - 3x \\
He_4(x) &= x^4 - 6x^2 + 3 \\
&\vdots
\end{aligned} \tag{2.9}$$

Recursively, the $(j+1)^{th}$ Hermite polynomial can be generated from

$$He_{j+1}(x) = xHe_j(x) - jHe_{j-1}(x) \tag{2.10}$$

Similarly,

$$\psi_{j+1}(x) = \frac{x}{\sqrt{j+1}}\psi_j(x) - \sqrt{\frac{j}{j+1}}\psi_{j-1}(x) \tag{2.11}$$

Figure 2.1 shows first five Hermite orthogonal functions (pulses).

According to Figure 2.1, the pulse widths of higher orders are always greater. However, all Hermite functions, interestingly, contain identical unity energy.

$$\int_{-\infty}^{\infty} \psi_m^2(x) \cdot dx = \int_{-\infty}^{\infty} \psi_n^2(x) \cdot dx = 1 \tag{2.12}$$

for any m and n. This nice property guarantees energy equality in all dimensions.

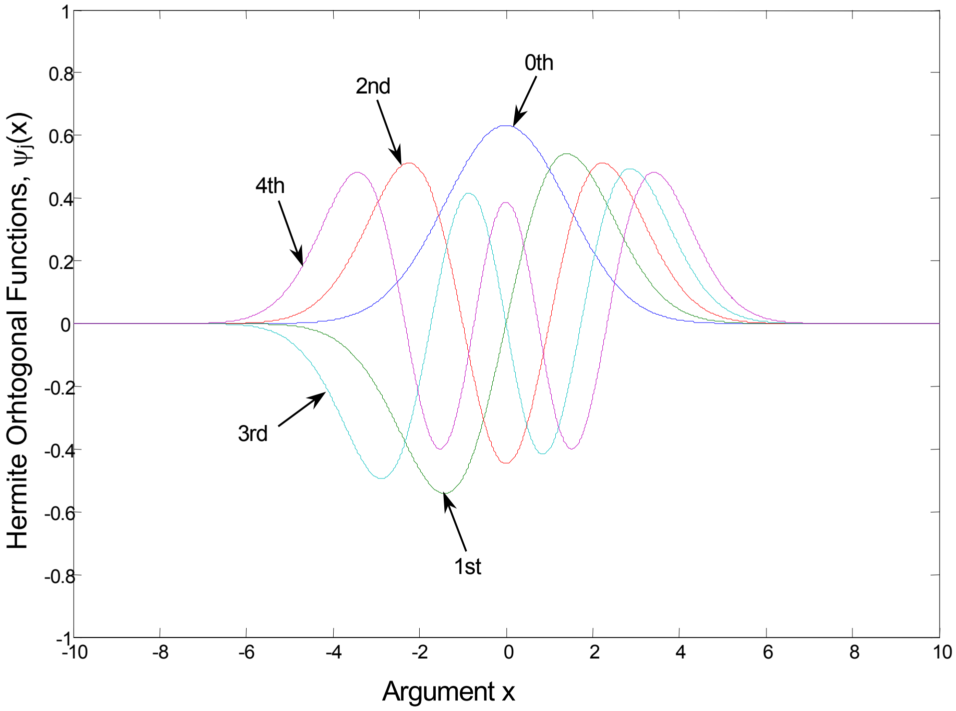

Figure 2.1 First five Hermite orthogonal functions.

2.3 Modification of Hermite Orthogonal Waveforms for a Specific Transmission Rate on an N-dimensional System

The Hermite orthogonal functions discussed in the previous section are not finite time functions. However, their values decay fast and monotonically for larger values of the arguments. Because the Hermite functions are orthogonal in $(-\infty, \infty)$, it is obvious that intersymbol interference (ISI) cannot be completely avoided. To be used as communication symbols, the Hermite functions need to be scaled to fit into a designated symbol period. A sufficient amount of pulse energy must be contained in the symbol period. ISI will be automatically controlled to an acceptable level. This section deals with modifying the Hermite basis functions for an n-dimensional system.

Let us consider the comparability of the serial transmission and the proposed parallel transmission. Let T_b be the bit period of the original serial transmission. A total of n bits are completed in transmission duration of $n \times T_b$. In order to be comparable to the original serial system, all n basis pulses of the n-dimensional system must fit into the $n \times T_b$ as well. Thus, $n \times T_b$ is the symbol period of the n-dimensional system.

Given an n-dimensional system and transmit bit rate of $R_b = 1/T_b$, the goal is to determine an expression for the transmit basic pulse, $f_p(t)$ from the original form Hermite orthogonal function $\psi_p(t)$. Since $\psi_p(t)$ is a time-infinite waveform with unity energy, it is impossible to scale $\psi_p(t)$ to fit into the desired symbol period $n \times T_b$ with 100% of bit energy. Thus, a percentage of the pulse energy that is required to be within the symbol period must be specified.

Let $f_p(t)$ be the p^{th} transmit basis pulse. The transmit pulse is then $f_p(t) = \psi_p(t/T_{n\text{-}scale})$, where $\psi_p(t)$ is the original form of the Hermite orthogonal function and $T_{n\text{-}scale}$ is the to-be-determined scaling factor that forces sufficient energy of $f_p(t)$ to lie within the symbol period. As noted, a high order waveform width is always greater than that of the lower order waveforms. As a result, successfully fitting the largest order basis pulse $\psi_{n-1}(t)$, into $n \times T_b$ guarantees that all lower basis pulses have sufficient energy in the $n \times T_b$ designated period. Thus, the energy criterion is satisfied for all pulses. In summary, it is obvious that the scaling factor $T_{n\text{-}scale}$ depends on the dimension of the system n, the bit rate R_b and the constraint on the energy percentage in the symbol period ρ.

To determine $T_{n\text{-}scale}$, a criterion on energy is introduced. First, consider a truncated version of the basis function $\psi_n(t)$. The pulse width W_n of the n^{th} Hermite orthogonal function, which guarantees ρ percent of energy in [-W_n/2 , W_n/2] satisfies the condition:

$$\frac{\int_{-0.5W_n}^{0.5W_n} |\psi_n(t)|^2 \, dt}{\int_{-\infty}^{\infty} |\psi_n(t)|^2 \, dt} = \frac{\rho}{100} \tag{2.13}$$

For the same ρ, W_n is always greater than W_m for $n > m$. Unfortunately, Hermite functions are in the form of an exponential of negative x squared. Analytical solutions for W_n are not available in practice. Consequently, a numerical method is an appropriate approach to evaluate W_n. The pulse widths W_n for the first 40 Hermite orthogonal pulses at different energy percentage criteria are depicted in Figure 2.2.

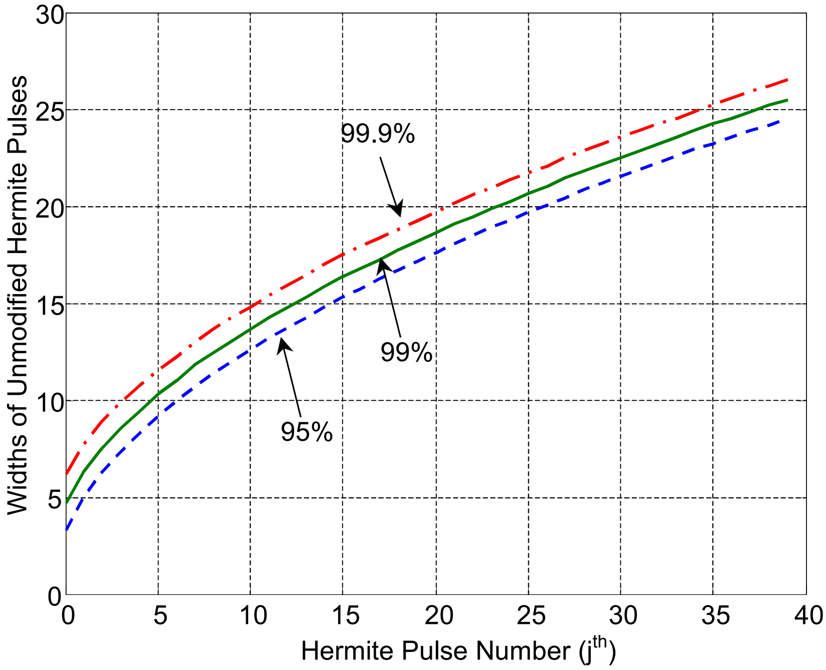

Figure 2.2 Pulse widths of the original Hermite pulses $\psi_j(t)$. Hermite pulse widths are, in fact, infinite. The criteria of 95%, 99% and 99.9% of pulse energy are used to define the pulse widths.

By scaling the Hermite functions by the pulse width W_n, the $\rho\%$ of pulse energy of Hermite pulses $\psi_p(t \times W_n)$ for $p \leq n$ lies in $t \in [-0.5, 0.5]$, a unity interval on the time axis. Our goal is to have n orthogonal pulses fit into $[-0.5nT_b, 0.5nT_b]$, the symbol period. Therefore the transmit basis pulse becomes

$$f_p(t) = \psi_p\left(\frac{t}{nT_b} W_n\right) \quad \textbf{(2.14)}$$

Therefore, the scaling factor $T_{n-scale} = \dfrac{W_n}{nT_b}$.

It is convenient to express the basic pulses using a normalized time. Let τ be normalized time defined by $\tau = t/T_b$, where t and T_b are the actual transmit time and the bit period, respectively. On the normalized time axis, n orthogonal pulses fit into the interval $[-0.5n, 0.5n]$. The interval represents n bit periods, which is the symbol period of the n-dimensional system.

Figure 2.3 shows the first four basis pulses on the normalized time axis when a 99% pulse energy criterion is used. The p^{th} pulse is generated by

$$f_p(\tau) = \psi_p\left(\tau \frac{W_4}{4}\right) \quad \textbf{(2.15)}$$

where W_4 is the original Hermite function pulse width obtained from the numerical method in (2.13). Very little intersymbol interference is observed from the tails of the basis pulses outside the interval [-2, 2].

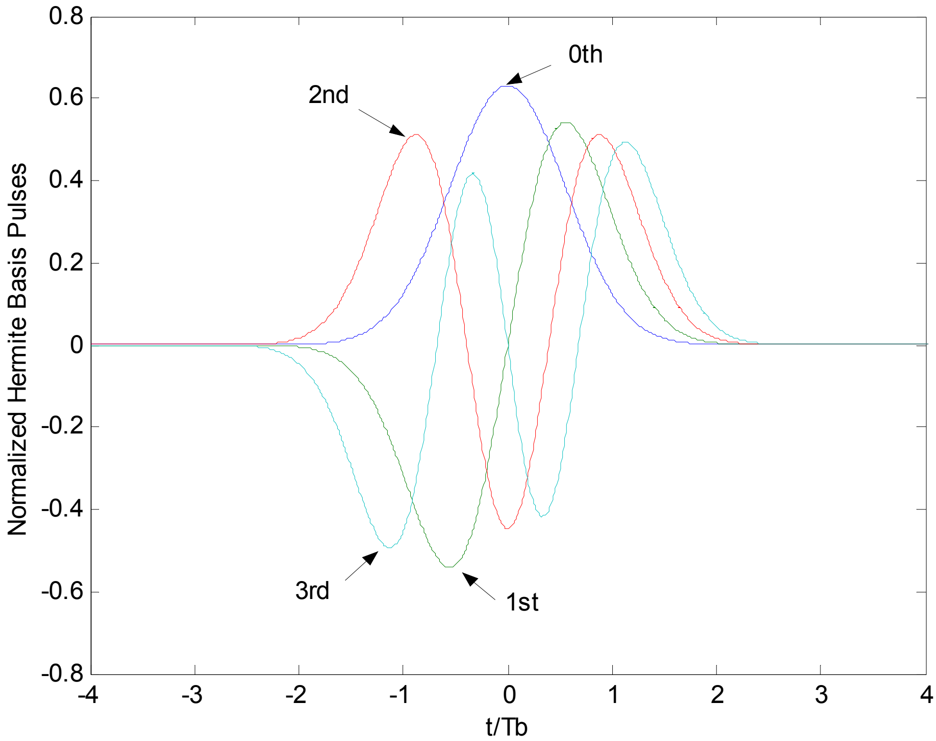

Figure 2.3 Illustration of first four Hermite basis pulses on the normalized time axis. Four waveforms are scaled to fit into four bit periods. All pulses have at least 99.9% of energy within the four bit periods of [-2, 2].

The derivation of the energy in the transmit pulse $f_p(t)$ is based on the pulse width criteria. The original $\psi_p(x)$ is a unity energy waveform but $f_p(t)$, its time scaled version, no longer preserves the property. Energy contained in $f_p(t)$ can be determined as follows.

$$\int_{-\infty}^{\infty} f_p^2(t) \cdot dt = \int_{-\infty}^{\infty} \psi_p^2\left(\frac{t}{T_b} \frac{W_n}{n}\right) \cdot dt \tag{2.16}$$

$$= \int_{-\infty}^{\infty} \psi_p^2(z) \cdot \frac{T_b}{W_n / n} dz \tag{2.17}$$

where $z = \frac{t}{T_b}\frac{W_n}{n}$. Using the unity energy property of Hermite functions, (2.17) is simplified to $\frac{T_b}{W_n / n}$. Therefore, the unity energy basis pulse $\hat{f}_p(t)$ becomes

$$\hat{f}_p(t) = \sqrt{\frac{W_n / n}{T_b}}\psi_p\left(\frac{t}{T_b}\frac{W_n}{n}\right) \tag{2.18}$$

where $0 \le p \le n$.

2.4 Fourier Transform of Hermite Pulses

It can be shown that the Fourier Transforms of the functions also form an orthogonal set. Invariance of orthogonality to the Fourier transform is discussed in [HAR72]. It is interesting that Hermite functions and their Fourier transforms have the same shape [WIE72]. This property implies that infinite time Hermite waveforms are not band-limited signals. However, the identical shape of the time functions and their Fourier transforms allows us to use the numerical results for the pulse width to calculate the bandwidth occupied by these Hermite pulses.

Let $f_p(\theta) = \psi_p(\theta)$, where $\theta = t/T$, is a Hermite time function scaled by a positive time constant T. Its Fourier transform is $g_p(\nu)$, where $\nu = f\,T$, has the same shape and is related by [WIE72]

$$\begin{aligned} g_0(\nu) &= \psi_0(4\pi\nu) \\ g_{2i}(\nu) &= (-1)^i \psi_{2i}(4\pi\nu) \\ g_{2i-1}(\nu) &= -(-1)^i \psi_{2i-1}(4\pi\nu) \end{aligned} \tag{2.19}$$

where $i = 1, 2, \ldots$

It is commonly known that Fourier transform of a Gaussian function preserves its original shape. The $f_0(\theta)$ is indeed a Gaussian shaped function. Its Fourier transform found in (2.19) agrees with that statement. For other orders, the Fourier transforms are signed Hermite functions scaled by 4π. The preserved shapes in the spectral domain allow us to use the results associated with pulse width in the time domain to estimate the pulse bandwidths.

Let us define simultaneous transmission of n orthogonal waveforms as an n-dimensional transmission system. Assume Hermite pulses are adopted as the orthogonal waveforms in the n-dimensional system. The Hermite pulse of the highest order has the widest pulse width and also occupies the widest spectrum. As a result, the bandwidth of the highest order pulse implies the required bandwidth for the baseband transmission.

In a Hermite (n+1)-dimensional system, the basis pulse is defined in (2.14). Using the relationships found in (2.19), the Fourier transform of the n^{th} pulse can be written as

$$F[f_n(\tau)] = F\left[\pm 1 \cdot \psi_n\left(\tau \tfrac{W_n}{n}\right)\right] = \pm 1 \cdot \psi_n\left(\frac{4\pi \cdot \phi}{\frac{W_n}{n}}\right) \quad \textbf{(2.20)}$$

where $\tau = t/T_b$ and $\phi = fT_b$ are the normalized (specifically by the bit period) time and frequency, respectively. Note that Hermite pulse indexing starts from 0.

The bandwidth of the (n+1)-dimensional system on an fT_b scale can be determined as follows. The n^{th} order original Hermite function $\psi_n(\phi)$ needs a pulse width of W_n to keep a designated amount of energy (ρ%) in the truncated pulse, i.e., ρ% of the energy lies in $\phi \in [-0.5Wn, 0.5Wn]$. Thus, the scaled function as in (2.20) will need a pulse width on the ϕ axis of

$$PW_{\phi,n} = \frac{W_n}{4\pi/(W_n/n)} = \frac{W_n^2}{4\pi n} \quad \textbf{(2.21)}$$

to maintain the same energy level in the spectrum. Note that the semi-analytical result requires W_n, which is obtained from a numerical method. Therefore, the bandwidth of the $(n+1)$-dimensional system becomes

$$BW_{\phi,n} = \frac{PW_{\phi,n}}{2} = \frac{W_n^2}{8\pi n}. \quad \textbf{(2.22)}$$

For example, the energy spectral density (ESD) of Hermite pulses used in a 3-dimensional system is shown in Figure 2.4. All pulses have the same energy but the ESD of the 2^{nd} pulse, the highest order, spreads out the most. Hence, its bandwidth reasonably defines the system bandwidth. W_2 is numerically 9.22. Substituting in (2.22), the bandwidth on an fT_b axis is $(9.22^2)/(8\pi\times3) = 1.13$. The bandwidth on the fT_b scale reflects directly the efficiency of using the bandwidth. The normalized bandwidth on the fT_b axis is actually frequency per bit rate. Transmission of a bit rate of R_b bit per second (bps), of which bit period $T_b = 1/R_b$, using the normalized bandwidth of 1.13 requires a de-normalized bandwidth of $1.13R_b$ Hertz (Hz). Thus, bandwidth efficiency can be measured by the ratio of the occupied bandwidth and the transmit bit rate. It is the same value as the bandwidth on the fT_b scale and the unit is in Hz/bps. Figure 2.5 summarizes the bandwidth efficiency (or bandwidth in the normalized scale, fT_b). The calculated bandwidth of the 3-dimensional transmission system is consistent with the plot in the figure. Nulls are observed on the individual energy spectral density. Nevertheless, the overall system ESD does not show nulls. Detailed discussion on the overall system ESD will be made in the next section.

As concluded in (2.22), the relationship between the dimension number and the normalized bandwidth at different energy constraints is illustrated in Figure 2.5. Square waves have the normalized bandwidth (first null) of 1. With a band-limited waveform like a raised cosine pulse, the first null becomes absolute normalized bandwidth.

Theoretically, a zero ISI Nyquist pulse, of which the raised cosine impulse response with a roll-off factor of 0 is one example, can lower the bandwidth down to 0.5 on an $f{\cdot}T_b$ normalized spectrum [ZIE90].

The normalized bandwidths of the Hermite n-dimensional system improve as the system dimension gets large. The asymptotes depend on the percentage of the pulse energy that is selected to lie within the available transmission bandwidth. For 95%, 99% and 99.9% constraints, the normalized bandwidths approach 0.62, 0.66 and 0.71, respectively. Low pass raised cosine filters offer normalized bandwidth of $(1+r)/2$, where r is the roll-off factor. As a consequence, the equivalent roll-off factors for large dimensional Hermite systems with the pulse energy criteria given above are 0.24, 0.33 and 0.42, respectively. A roll-off factor of 0.25 is a practical value. Its occupied bandwidth lies between the bandwidths of the Hermite pulses with the 95% and 99% criteria. Therefore, an n-dimensional Hermite system is not disadvantageous in terms of bandwidth.

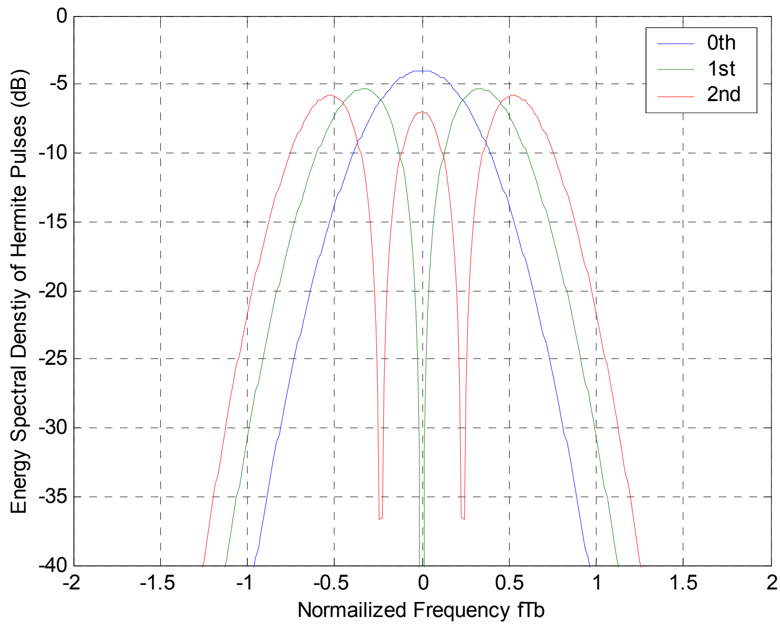

Figure 2.4 Two-sided energy spectral density of the pulses in a 3-dimensional system. A 99.9% energy criterion is used.

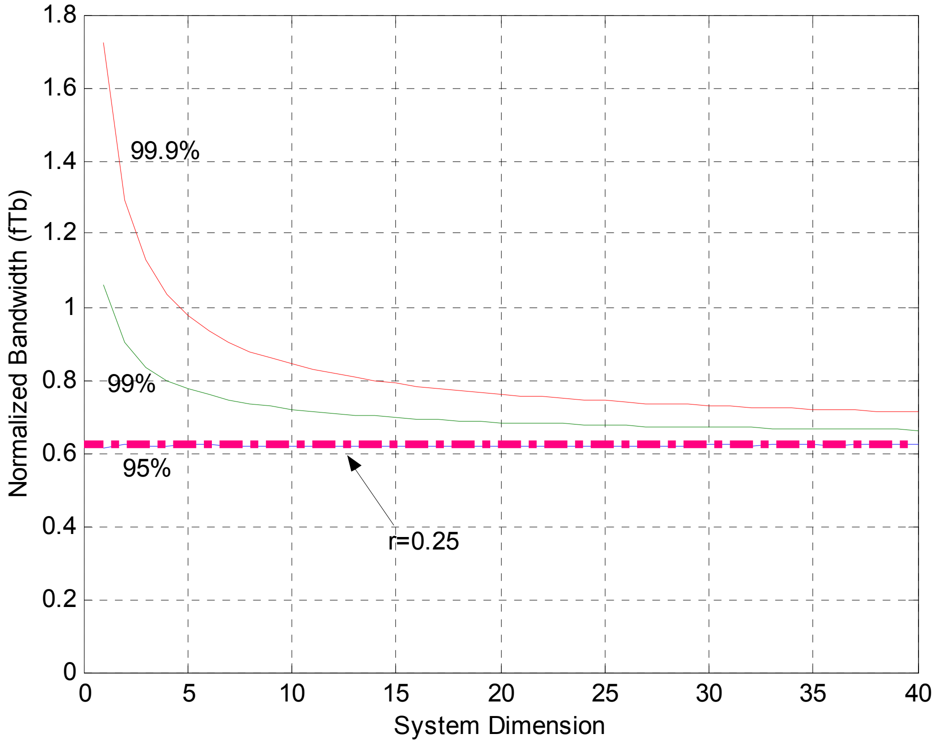

Figure 2.5 Normalized bandwidth of the n^{th} Hermite pulse on fT_b scale versus the system dimension (number of basis pulses used) at the energy criteria of 95%, 99% and 99.9%. It is assumed that the bandwidth of the Hermite pulse of largest order represents the transmit waveform bandwidth. The bandwidth of raised cosine pulse with a practical roll-off factor r = 0.25 lies slightly above the 95% bandwidths.

2.5 Analysis of Power Spectral Density of n-Orthogonal Waveforms

In communication systems, transmit signals are always random. The power spectral density (PSD) for a random process $x(t)$ is given by [COU97]

$$P_x(f) = \lim_{T \to \infty} \left(\frac{\overline{|X_T(f)|^2}}{T} \right) \tag{2.23}$$

where $X_T(f)$ is Fourier transform of the truncated waveform $x(t)$.

Our goal is to determine the PSD of the signal $x(t)$ formed by a linear combination of $h_p(t)$ Hermite basis functions for an n-orthogonal system expressed by

$$x(t) = \sum_{p=0}^{n-1} \sum_{k=-N}^{N} a_{p,k} h_p(t - kT_s), \tag{2.24}$$

where $a_{p,k}$ is a random number whose value is either –1 or 1 and T_s is the symbol period. $X(f)$, the Fourier transform of $x(t)$, is then

$$X(f) = \sum_{p=0}^{n-1} \sum_{k=-N}^{N} a_{p,k} H_p(f) e^{-j\omega kTs} \tag{2.25}$$

The absolute value squared of $X(f)$ is equal to the product of $X(f)$ and its complex conjugate.

$$\begin{aligned} |X(f)|^2 = X(f)X^*(f) &= \left(\sum_{p=0}^{n-1} \sum_{k=-N}^{N} a_{p,k} H_p(f) e^{-j\omega kTs} \right) \left(\sum_{q=0}^{n-1} \sum_{l=-N}^{N} a_{q,l} H_q^*(f) e^{+j\omega lTs} \right) \\ &= \sum_{p=0}^{n-1} \sum_{q=0}^{n-1} \sum_{k=-N}^{N} \sum_{l=-N}^{N} a_{p,k} H_p(f) e^{-j\omega kTs} a_{q,l} H_q^*(f) e^{+j\omega lTs} \end{aligned} \tag{2.26}$$

In (2.26) k and l represent the time indexing while p and q identify the Hermite function numbers. Thus, the PSD for $x(t)$ becomes

$$P_x(f) = \lim_{T\to\infty} \frac{1}{T} \left(\overline{\sum_{p=0}^{n-1} \sum_{q=0}^{n-1} \sum_{k=-N}^{N} \sum_{l=-N}^{N} a_{p,k} H_p(f) e^{-j\omega kTs} a_{q,l} H_q^*(f) e^{+j\omega lTs}} \right) \tag{2.27}$$

Since $a_{p,k}$ and $a_{q,l}$ are random variables concerned with the averaging operator, (2.27) reduces to

$$P_x(f) = \lim_{T\to\infty} \frac{1}{T} \sum_{p=0}^{n-1} \sum_{q=0}^{n-1} \sum_{k=-N}^{N} \sum_{l=-N}^{N} \left(\overline{a_{p,k} a_{q,l}}\right) e^{-j\omega(k-l)Ts} H_p(f) H_q^*(f) \qquad \textbf{(2.28)}$$

Consider the random variables $a_{p,k}$ and $a_{q,l}$. The data for different Hermite basis functions (p and q) are independent. As a result,

$$\overline{a_{p,k} a_{q,l}} = \overline{a_{p,k}} \cdot \overline{a_{q,l}}, \qquad p \neq q \qquad \textbf{(2.29)}$$

Assuming the transmission is symmetric, $a_{p,k}$ and $a_{q,l}$ have an equal probability of being –1 and +1. Their expectations are

$$\overline{a_{p,k}} = \overline{a_{q,l}} = \tfrac{1}{2}(-1) + \tfrac{1}{2}(1) = 0 \qquad \textbf{(2.30)}$$

Therefore

$$\overline{a_{p,k} a_{q,l}} = 0, \qquad p \neq q \qquad \textbf{(2.31)}$$

Moreover, data bits on the same basis function at different times, k and l, are independent causing $\overline{a_{p,k} a_{p,l}} = \overline{a_{p,k}} \cdot \overline{a_{p,l}} = 0$ for $k \neq l$. In the case of $p = q$ and $k = l$, the expectation similarly becomes

$$\overline{(a_{p,k})^2} = \tfrac{1}{2}(-1)^2 + \tfrac{1}{2}(1)^2 = 1 \qquad \textbf{(2.32)}$$

By removing all zero terms from (2.28), the PSD simplifies to

$$P_x(f) = \lim_{T\to\infty} \frac{1}{T} \sum_{p=0}^{n-1} \sum_{k=-N}^{N} | H_p(f) |^2 (1)$$

$$= \sum_{p=0}^{n-1} | H_p(f) |^2 \lim_{T\to\infty} \frac{1}{T} \sum_{k=-N}^{N} 1 \qquad \textbf{(2.33)}$$

Total time required to transmit $2N+1$ symbols is $T_s(2N+1)$ and the transmit time approaches infinity if an infinite number of bits are transmitted. The limit can be rewritten as

$$\lim_{N\to\infty} \frac{1}{T_S(2N+1)} \sum_{k=-N}^{N} 1 = \lim_{N\to\infty} \frac{2N+1}{T_S(2N+1)} = \frac{1}{T_S} \qquad \textbf{(2.34)}$$

Therefore the PSD is as simple as

$$P_x(f) = \sum_{p=0}^{n-1} \left(\frac{1}{T_S} \right) | H_p(f) |^2 \qquad \textbf{(2.35)}$$

If it is a one-dimensional system, the PSD in (2.35) is the PSD of an antipodal signal. Therefore the result in (2.35) concludes that the PSD of n-dimensional antipodal signal as defined in (2.24) is just the sum of the PSDs of the individual one-dimensional signals. The PSD of a one-dimensional system shows nulls but the composite PSD will have the nulls removed. Figure 2.6 illustrates the absence of the nulls.

The PSD for a set of Hermite pulses shows excellent utilization of the available bandwidth. The PSD goes below 30 dB from the maximum PSD by $f = 0.65R_b$. It is very similar to the PSD for a raised cosine pulse with $r = 0.25$. Previously, the predicted transmit bandwidth using the bandwidth of the Hermite pulse of the largest order yields a 99.9% bandwidth of $0.71R_b$, which is equivalent to the bandwidth of raised cosine pulse with $r = 0.42$. Obviously, the prediction method overestimates the transmit bandwidth. The phenomen can be explained by the fact that the PSD of the Hermite pulses of the low orders are packed near DC. When multiple pulses are transmitted, the effective PSD shifts toward DC. As a consequence, the bandwidth of the multiple-pulse signal is lower than the bandwidth of the highest order Hermite pulse.

In a practical system, instead of a regular raised cosine filter, identical square root raised cosine filters are equipped at the transmitter and receiver ends to perform matched filtering with zero-ISI, effectively. The bandwidths of the output signals from the square root raised cosine filters and regular raised cosine filters are identical. Therefore, the spectral performance using the Hermite pulses as a transmit signal is also comparable to that of the practical square root raised cosine filters with $r = 0.25$.

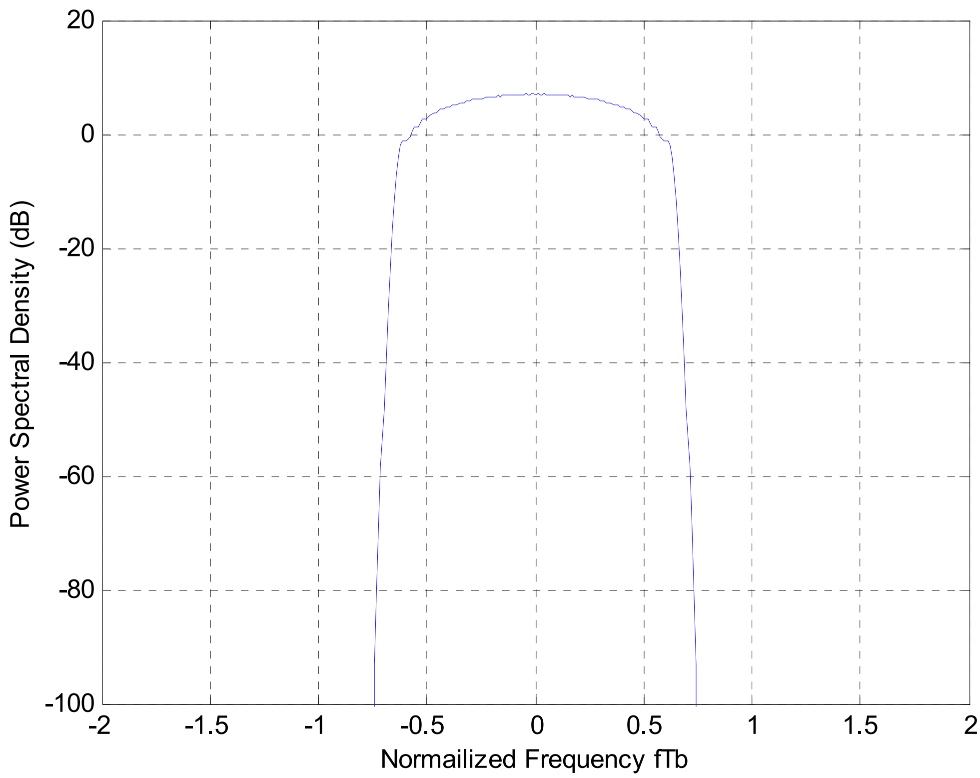

Figure 2.6 PSD of a 40-dimensional Hermite composite waveform. A 99.9% pulse energy criterion is used. The monotonically decreasing PSD is about 30 dB down from the top by *fTb* > 0.65. The bandwidth of the 40-dimensional waveform is close to the bandwidth of a raised cosine pulse with roll-off factor of 0.25.

2.6 Chapter Summary

In this chapter, infinite Hermite functions are investigated. Derived from the Hermite polynomial, Hermite functions can be generated using recursion. Then, Hermite basis pulses are developed from the Hermite functions using criteria for the fraction of the total energy in the pulse that is transmitted by a truncated version. Numerical methods were used to help determine the pulse energy.

The bandwidth of the individual pulses is predicted from a semi-analytical method, which uses the result from the numerical method together with an analytical approach. For ease of comparison, bandwidth is plotted on a normalized fT_b scale. It is found that to maintain 99.9% of pulse energy in the normalized bit period, the asymptotic bandwidth efficiency of the n-dimensional system is equivalent to using raised cosine pulse with roll-off factor of 0.42.

An analysis of the power spectral density of the n-dimensional orthogonal system is carried out. Assuming an antipodal scheme is assigned, the system PSD is just the sum of the PSDs of the individual one-dimensional antipodal signals. As the dimension gets larger, the PSD tends to be smoothed. It is found that the bandwidth of the Hermite n-dimensional waveform is roughly the same as the bandwidth of a raised cosine pulse with roll-off factor of 0.25. The prediction method using the bandwidth of the highest order pulse overestimates the transmit bandwidth.

Chapter 3
N-Dimensional Baseband Transmission and Detection

In this chapter, implementation of the transmission using Hermite orthogonal basis pulses and optimal receivers for the system are discussed. On the transmission end, each bit of binary data either maintains or inverts the transmit pulses forming an antipodal system. The transmit pulse used for each data bit is one of a set of *m* orthogonal Hermite pulses. Since the *m* Hermite pulses are orthogonal, the magnitude and sign of each pulse can be recovered from the additive combined waveform. Therefore, *m* independent bits can be sent at the same time. Therefore, the transmission is viewed as a parallel system.

With the antipodal scheme, *m* Hermite pulses compose 2^m distinct symbols. The transmitter keeps sending symbols after symbols. The receiver needs to know the beginning of the symbols to employ the orthogonality. Symbol synchronization is discussed and a technique for an n-dimensional system is developed. Its performance is then evaluated.

3.1 Transmission System

As discussed in the previous chapter, infinite Hermite pulses can be constrained to be sufficiently orthogonal in a designated period. Thus, a set of orthogonal waveforms for an n-dimensional transmission is formed. Without presence of noise or other interference, the binary data carried on the basis pulses can be perfectly recovered.

In n-dimensional systems, *n* independent data streams are transmitted simultaneously. Typically, the data stream is fed to the modulator on a bit by bit basis. As a result, it is likely that an n-dimensional system will have a serial to parallel data converter. The implementation block diagram of transmission system is shown in Figure 3.1.

According to Figure 3.1, on the transmitter side, the binary data (value is either 1 or –1) changes its basis waveform's polarity. The transmit waveform is a combination of the individual signed waveforms. Let $h_i(t)$ for $i = 0,1,\ldots, n-1$, be the basis Hermite waveforms. The transmit waveform in one symbol period is then written as

$$s_1(t) = \sum_{i=0}^{n-1} a_i h_i(t) \tag{3.1}$$

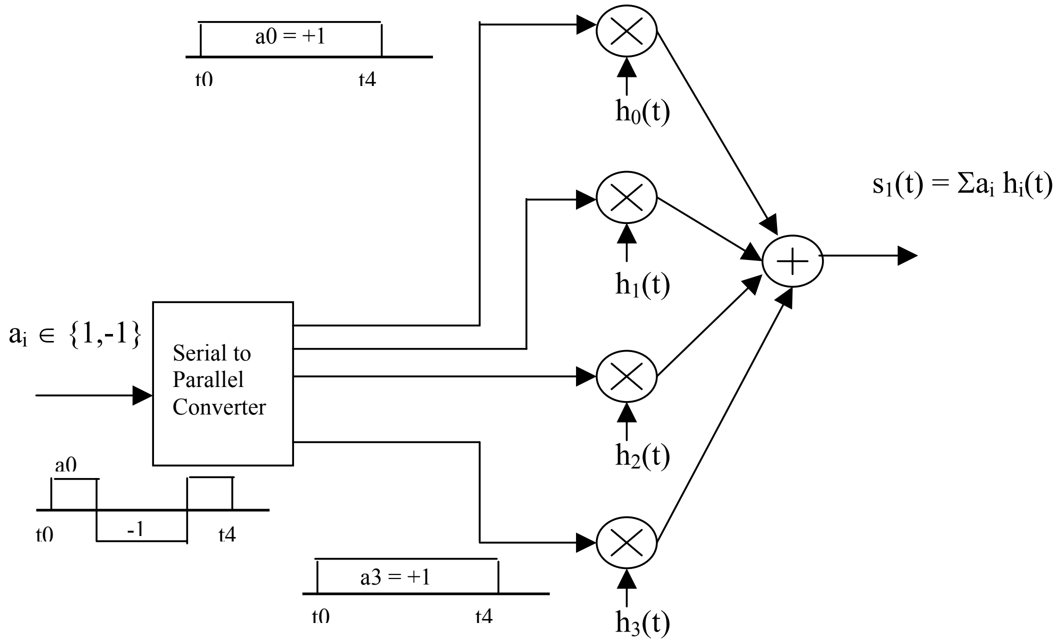

Figure 3.1 Direct implementation of one-symbol transmission in an N-dimensional system. *N*, the dimension of the transmit signal in this illustration, is 4. The $h_i(t)$ are the Hermite waveforms spanning from t_0 to t_4.

Since Hermite waveforms are complicated, generation of the transmit signal is likely to be implemented using an array of discrete time waveform generators as shown in Figure 3.2. According to Figure 3.2, a signed input data pulse train with a rate of R_b is converted to N parallel pulse trains at a slower rate of R_b/N. Each pulse train is then passed through a corresponding discrete-time waveform generator which responds to the pulse train by outputting a sequence $h_i[k]$, where $k = 0, 1, \ldots, (N_{fir} - 1)$. The output sequence of length N_{fir} is a discrete-time version (or sampled version) of the i^{th} Hermite pulse. The output sequence can be viewed as a finite impulse response (FIR) of a digital signal processing system.

Such a discrete-time waveform generator can be implemented using a Finite Impulse Response (FIR) digital filter. An FIR filter of order N_{fir} consists of an array of the coefficients, b_k for k = 0, 1, … , (N_{fir}-1). Its impulse response is exactly the filter coefficients, b_k. Let us set the FIR coefficient with $h_i[k]$, the sampled values of the Hermite waveform. The impulse response of the digital filter will be exactly the discrete-time Hermite waveform. FIR filters are commonly known and widely used in Digital Signal Processing. The desired continuous transmit Hermite waveform can be obtained by using a digital to analog converter (DAC) followed by a proper lowpass filter. Therefore, the complicated Hermite waveforms are practically realizable.

The discrete-time representation of an analog signal can be converted to a continuous waveform without aliasing if the sampling rate is greater twice bandwidth of the analog signal. Let T_{sample} be the sampling time of the waveform generator or the time space between the adjacent samples. The value of the n^{th} sample of the sequence $h_i[k]$ is set to $h_i(t)|_{t = kTsample}$. Thus, the last sample of the sequence, $h[N_{fir-1}]$, represents the value of Hermite pulse at $t = (N_{fir} - 1) \times T_{sample}$. Since the Hermite symbol of an N-dimensional system lasts NT_b, where $T_b = 1/R_b$, the number of sequence samples N_{fir} can be determined from

$$N_{fir} = \frac{NT_b}{T_{sample}} \tag{3.2}$$

The results from Chapter 2 conclude that the power spectral density of the Hermite waveform lies within $0.625R_b$, where R_b is the transmit data rate. The minimum sampling rate that prevents aliasing is twice the bit rate [OPP89]. In this case the minimum sampling rate becomes $1.25R_b$ and the maximum sampling time T_{sample} is $T_b/1.25$. Therefore, the theoretical minimum length of the output sequence, $N_{fir} = 1.25N$, where N is the dimension of the composite Hermite waveform. Since N_{fir} is the order of the FIR generators, it reflects the complexity of digital FIR generator. Thus, the complexity of the Hermite waveform generation using digital approach increases linearly with the dimension N of the transmit Hermite signal.

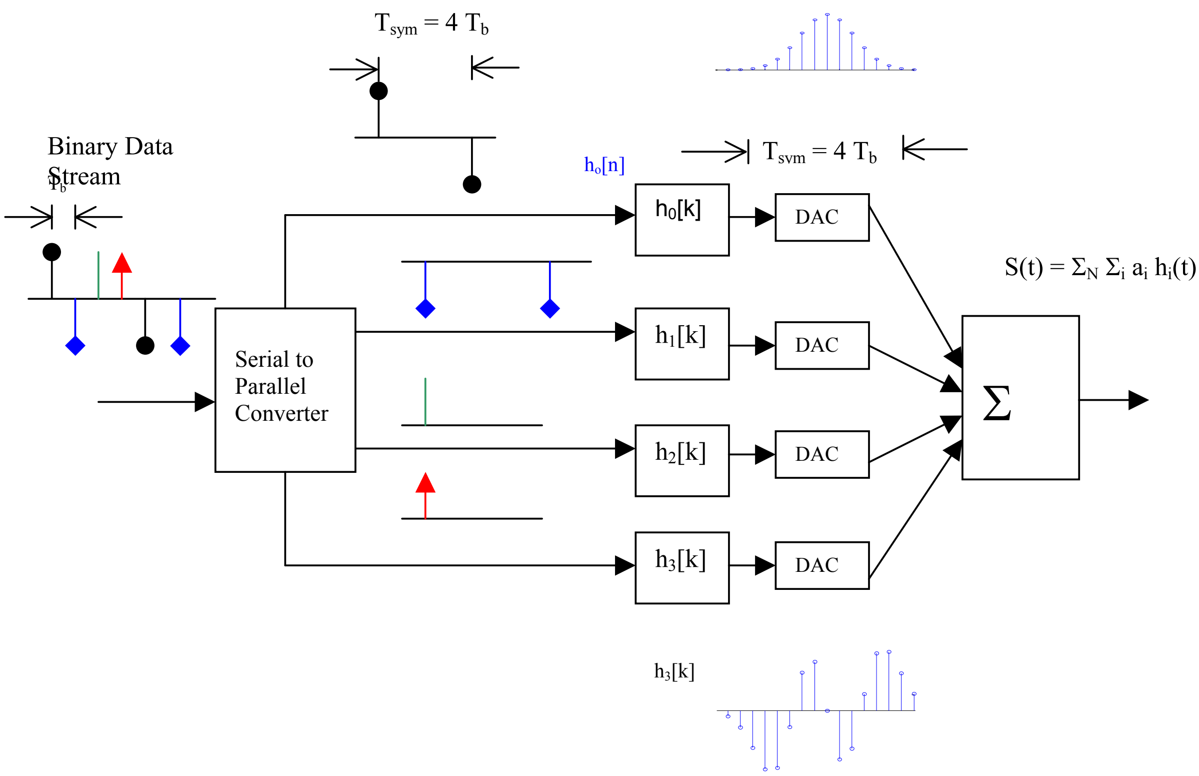

Figure 3.2 Block diagram of a practical implementation using digital FIR filters. Hermite waveforms are generated in discrete time domain. Digital to analog converter and a lowpass filter produce the continuous waveform for the transmission.

3.2 Simple Detector

Theoretically, the binary data carried on the m^{th} basis waveform can be recovered by using a correlation detector with integrate and dump. The method is validated as the follows. Assuming perfect synchronization, the composite signal $s(t)$ is multiplied by $h_m(t)$. Then the product is integrated over the symbol period. Polarity of the integrator output is used to determine which binary data symbol was sent. The integrator output is cleared (dumped) for the next symbol detection. The implementation can be expressed as

$$\int_0^{T_s} s(t)h_m(t) \quad = \int_0^{T_s} \left[h_m(t)\sum_{i=0}^{n-1} a_i h_i(t) \right] \cdot dt \tag{3.3}$$

$$= \sum_{i=0}^{n-1} a_i \int_0^{T_s} h_m(t) \cdot h_i(t) \cdot dt = a_m \delta_{mm}, \tag{3.4}$$

where δ_{kk} is a positive constant.

The orthogonality removes all terms whose $i \neq k$ from the summation. Thus, binary data carried on one basis pulse does not interfere with the detection of the binary data carried on the others.

3.3 Equivalent Receiving System

The integrate-and-dump detector is a powerful tool in data recovery. However, it requires perfect pulse synchronization. Losing the pulse alignment results in inter symbol interference (ISI). Locating the beginning of the symbol on the composite signals of the n-dimensional system is difficult because of the large number of transmit waveform patterns. The number of the patterns increases exponentially as the dimension of the system grows. As a consequence, integrate and dump receivers are not practical for an n-dimensional system.

An alternative way to indirectly implement the integrate-and-dump receiver is to make use of convolution. Consider a linear system with impulse response $h_s(t)$. The response $y(t)$ when the system is driven by a signal $s(t)$ is given by

$$y(t) = \int_{-\infty}^{\infty} s(\tau)h_s(t-\tau)\cdot d\tau \tag{3.5}$$

Assume the input $h_k(t)$ is a time infinite signal whose values are zero outside an interval [0, T_s]. The indefinite integral above becomes a definite integral bounded by lower and upper limits of 0 and T_s, respectively. Let us define the impulse response by

$$h_s(t) = h_m(-t+T_s) \tag{3.6}$$

The output of the system becomes

$$y(t) = \int_{0}^{T_s} s(\tau)h_m(t-[-\tau+T_s])\cdot d\tau \tag{3.7}$$

Thus, at $t = T_s$, the output yields exactly the same results as of the integrate-and-dump receiver.

$$y(T_s) = \int_{0}^{T_s} s(\tau)h_m(\tau)\cdot d\tau \tag{3.8}$$

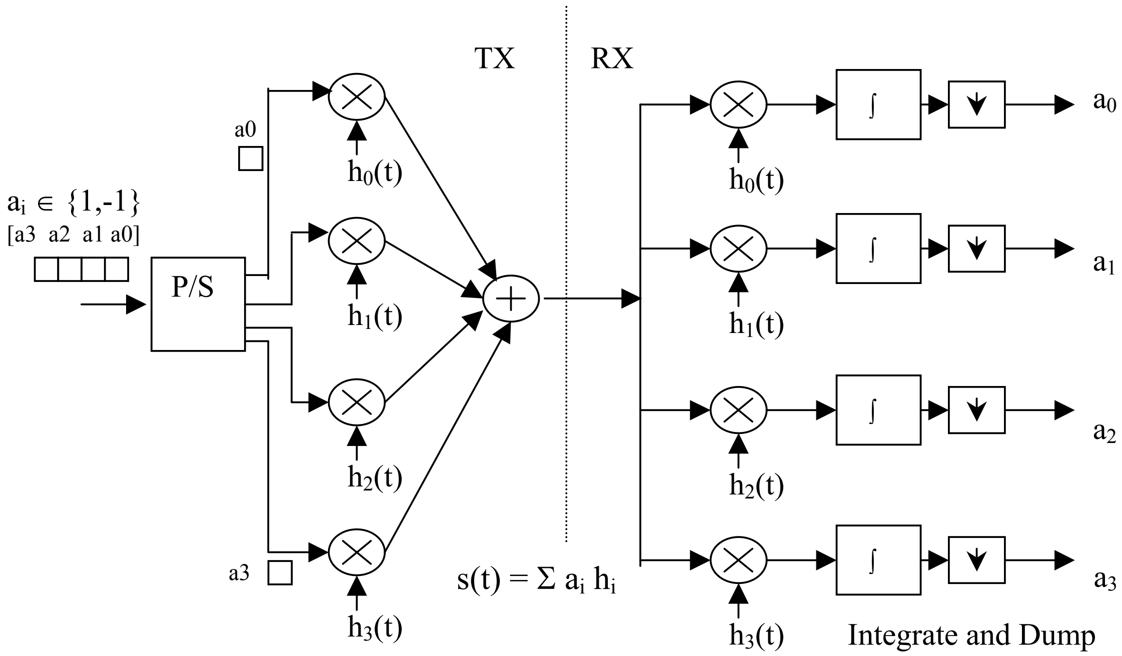

Figure 3.3 Straightforward implementation block diagram of transmitter and receiver. The receivers invokes a correlation detector with an integrate-and-dump (I&D). The received signal is multiplied by Hermite pulses. Then, the resultant waveforms are integrated. The multiplication operation requires that the local Hermite pulses must be synchronized to the transmitted pulses.

Therefore, the integrate-and-dump receiver can be implemented indirectly by passing the signal through a linear time invariant system. The necessary synchronization is only on the output sampling. A straightforward implementation block diagram of the transceiving system using a correlator detector is shown in Figure 3.3. Figure 3.4 illustrates an alternative implementation in continuous time domain of the receiver using matched filters and sampler.

In practice, filters that can produce a Hermite waveform shaped impulse response are unlikely to exist. Again, implementation of the matched filter detector should be done in discrete time domain. The received signal $s(t)$ is first digitized to a sequence $s[k]$ and then digital-filtered by an FIR filter whose discrete impulse response $h[k]$ is the sampled Hermite waveform. Proper sampling of the output sequence yields the same results as using the correlation detector with integrate and dump. For convenience, continuous time notation is used.

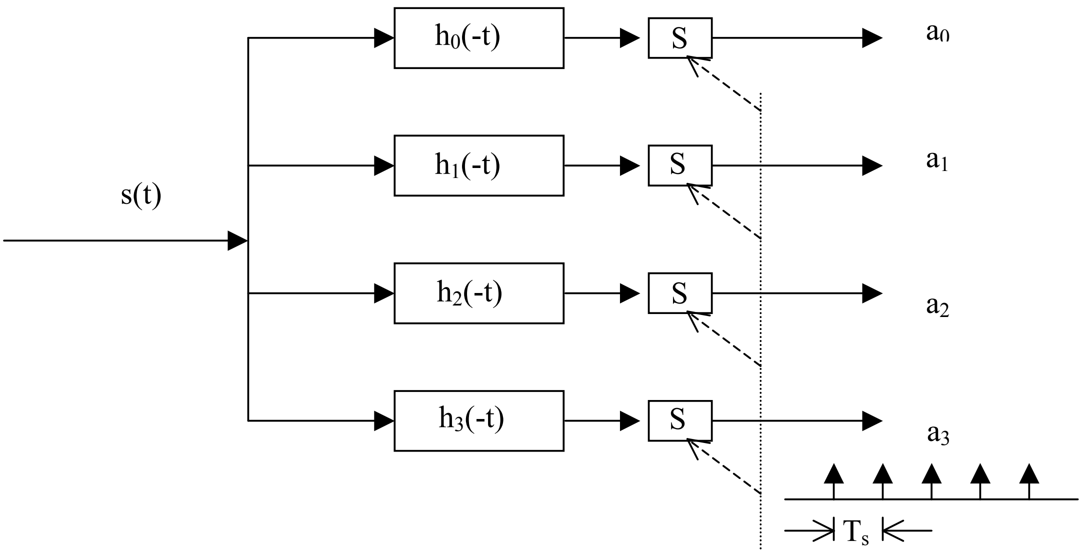

Figure 3.4 An alternative receiver makes use of the matched filters and the samplers. The received signal is passed to the filters for which the impulse responses are Hermite waveforms. Properly sampled filter outputs yield the same values as the synchronized I&D. The illustration is based on continuous time waveform. Practical implementation of the matched filter detector can be realized using discrete-time domain. The transmit signal is digitized first and the matched filters are in fact digital FIR filters.

A demonstration of output invariance of the two receivers is done in the following example. Let [-1 -1 1, 1 1 –1, 1 1 1, 1 –1 –1] be a sequence of 12 data bits to be transmitted using a 3-dimensional Hermite system. The transmission requires 12 bit periods, T_b, to transmit the data sequence. Each 3-dimensional Hermite symbol lasts 3 bit periods, e.g., $T_s = 3T_b$. Figure 3.5 shows the waveforms of each dimension and the combined waveform.

The received signal is detected by both integrate-and-dump (I&D) and filter-and-sample (F&S) receivers. The output waveforms associated with the 1st dimension are shown in Figure 3.6. The I&D dumps the output every $3T_b$ while the F&S takes samples every $3T_b$ as well. The outputs at the multiple of $3T_b$ of both receivers are identical. Hence, the invariance of results of the different approaches is shown.

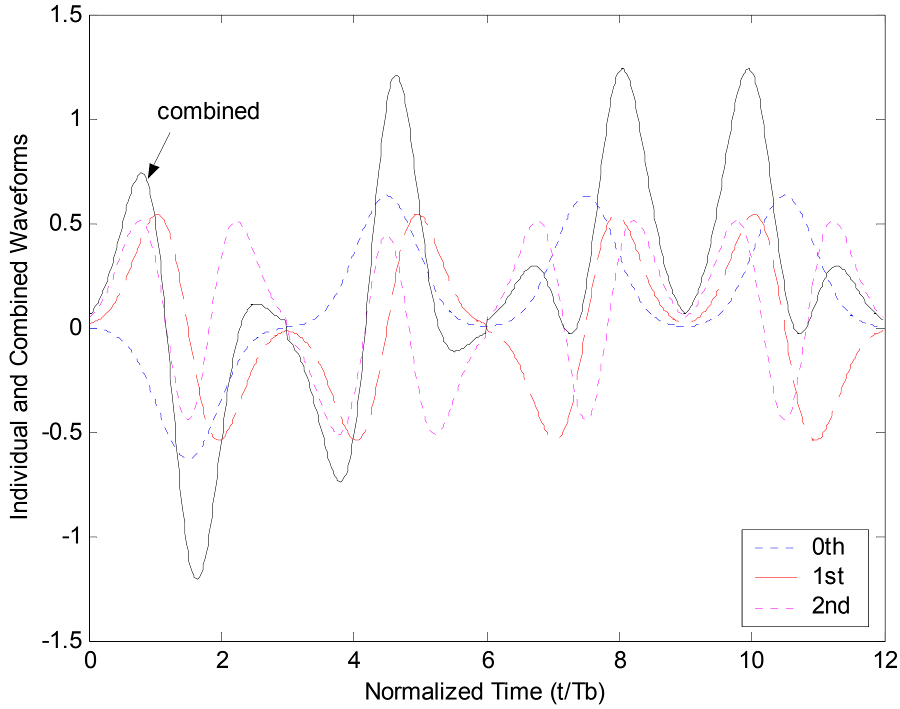

Figure 3.5 Waveforms at the output of each dimension filter and the combined (transmit) waveform of a 3-dimensional system. The 12-bit data sequence is [-1 –1 1, 1 1 –1 1 1 1, 1 –1 1]. The symbol period lasts $3T_b$.

The advantages and disadvantages of the two receivers are as the follows. The integrate-and-dump receiver requires a precise symbol synchronization to multiply the local Hermite pulses with the received waveform. The simulation result shown in Figure 3.6 suggests that the output waveform of the I&D tends to move away from the threshold (zero) before dumping. Therefore, once synchronized, jittering on output sampling is not as critical.

On the other hand, the convolution method is more prone to suffering from sampling jitter because of its relatively high waveform fluctuation. As illustrated in Figure 3.6, both methods yield the same values at the times of sampling. However, slight sampling jitter is more serious with the fluctuating output waveforms of the F&S receiver. Synchronization is an important issue and detailed discussion is in the next section.

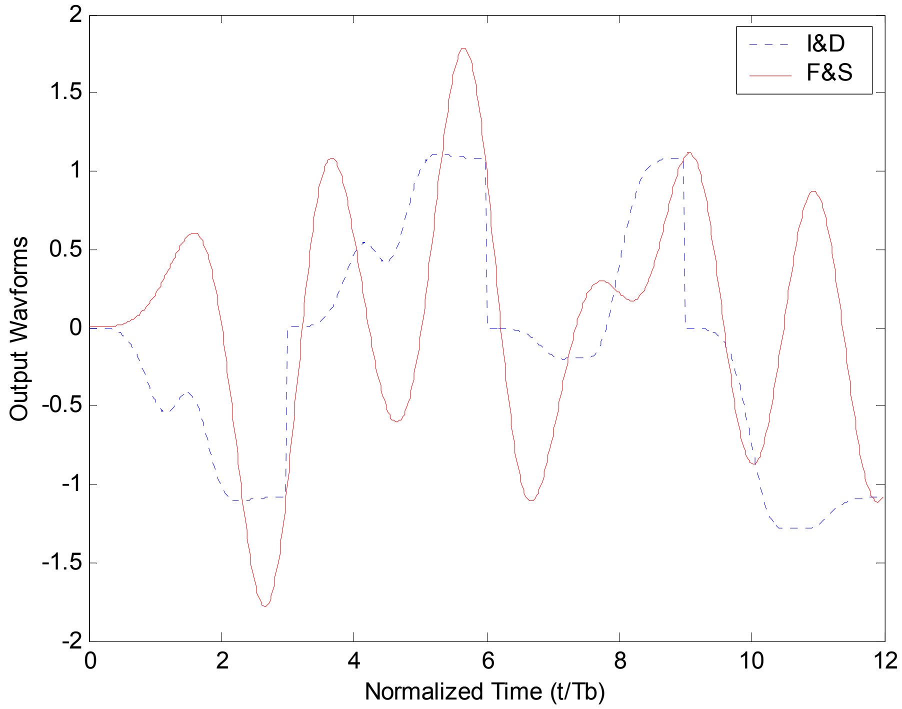

Figure 3.6 Output waveforms corresponding to the 1st dimension of the integrate-and-dump (I&D) and filter-and-sample (F&S) receivers. The I&D dumps the output every symbol period, $3T_b$ while the F&S samples the output every $3T_b$. The transmit data [-1 1 1 -1] is correctly detected.

3.4 Derivation of Synchronization in N-dimensional System

Generally, bit synchronization in a receiver for digital signals can be done by one of the following methods [ZIE90]

1. The transmitter and the receiver share a standard timing.
2. A separate pilot signal is transmitted along with the data signal.
3. Clock is derived from the transmit waveform itself or by self synchronization

Unlike the first two methods, self synchronization does not require additional information. In the case of a one-dimensional system, an implementation of self synchronization employing a maximum *a posteriori* (MAP) estimation is intensively investigated in [LIN73]. Our goal is to extract a synchronization signal from the N-dimensional transmit waveform. Therefore a MAP based self-synchronizer extended for the N-dimensional system is derived. Simplification of implementation is also developed.

Let $s(t)$ be a transmit signal composed from n signed Hermite pulses (an N-dimensional system). The signal $s(t)$ is corrupted by the channel additive white Gaussian noise (AWGN). At the receiver, all possible 2^n expected symbols are known and can be locally generated. However, the local symbol clock is misaligned with the received signal by an epoch ε_o. The unknown epoch ε_o is assumed to be uniformly distributed over the symbol period, $(0, T_s)$. The symbol synchronizer observes the received signal over an interval of K symbol periods and estimates the unknown ε_o. One approach of estimating an unknown parameter in Gaussian noise is using the theory of maximum *a posteriori* (MAP) estimation [VAN67].

Let $h_n(t)$ be the truncated n^{th} Hermite pulses whose values are non-zero only in the symbol interval $[0, T_s]$, where T_s is the symbol period. The N-dimensional transmit signal corresponding to k^{th} symbol period is the sum of the signed Hermite pulses and can be written as

$$s(t; a_{n,k}) = \sum_{n=0}^{N-1} a_{n,k} h_n(t - (k-1)T_s) \qquad \textbf{(3.9)}$$

where $a_{n,k} \in \{-1, 1\}$ is the binary data contained on the n^{th} dimension of the k^{th} pulse.

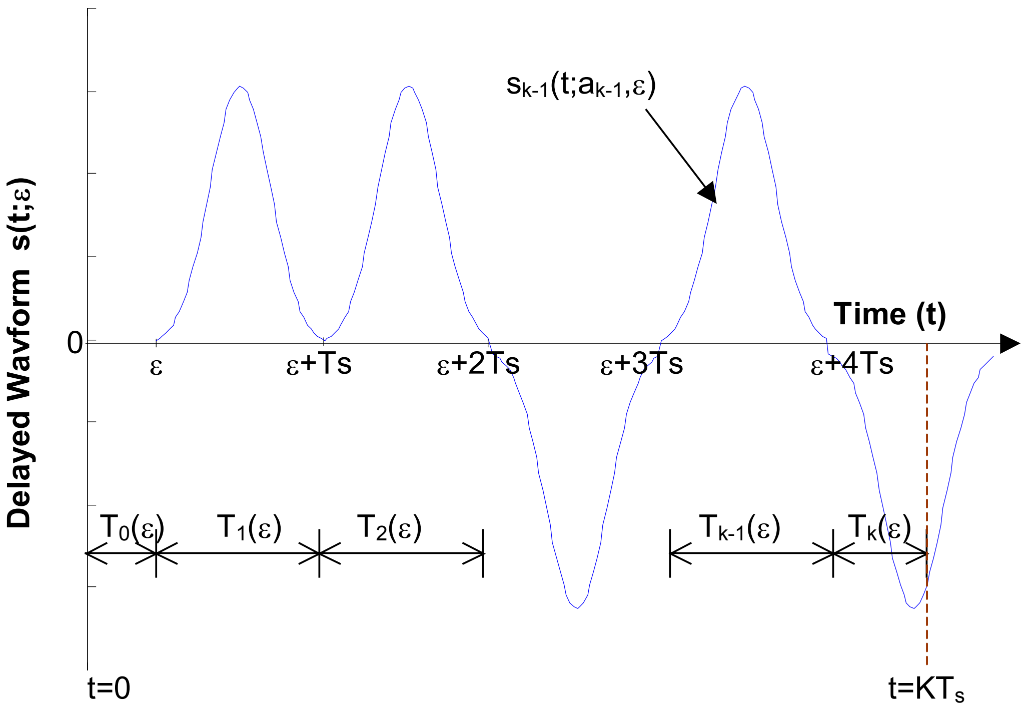

Figure 3.7 Received signal with random delay ε. Symbol synchronization determines ε for the received signal from an observed interval of KT_s.

Let the receiver observe the incoming signal for KT_s. The observed signal $y(t)$ is the transmit signal delayed by ε_o plus the noise, $n(t)$. The delay is actually the misalignment between the locally generated symbol and the received symbols. Observed in the interval $[0, KT_s]$, the received $y(t)$ is characterized by

$$y(t) = \sum_{k=0}^{K} s(t; a_{n,k}, \varepsilon_o) + n(t) \quad \textbf{(3.10)}$$

$$= \sum_{k=0}^{K} \sum_{n=0}^{N-1} a_{n,k} h_n (t - (k-1)T_s - \varepsilon_o) + n(t) \quad \textbf{(3.11)}$$

where $t \in (0, KT)$.

In (3.11), $y(t)$ is partitioned then expressed in the form of a $(K+1)$-fold summation. Indeed, because of the delay, there are $K+1$ symbols appearing in $[0, KT_s]$. The interval associated with $k = 0$ lasting from 0 to ε_o represents the tail from the previous unwanted data bits. Meanwhile, the K^{th} (the last) interval occupies only a fraction of T_s. The incomplete symbol lies in the interval of $[(K-1)T_s+\varepsilon_o, KT_s]$. Let us define $T_k(\varepsilon)$, the k^{th} subinterval, by $T_k(\varepsilon) = (k-1)T_s+\varepsilon \leq t \leq kT_s+\varepsilon$. Note that with the constraint that t is further limited to be in the observation time, i.e., $t \in (0, KT)$, $T_0(\varepsilon)$ and $T_K(\varepsilon)$ are truncated to length of ε and T_s-ε, respectively. Figure 3.7 depicts the definition of the subintervals.

The MAP symbol synthesizer determines the epoch ε_o from the received signal $y(t)$ by choosing ε_o from the epoch under test, ε, that maximizes the conditional probability, $p(\varepsilon|y(t))$. More specifically, $\varepsilon = \varepsilon_o$ does maximize the conditional probability. Strategically, it is more convenient to decompose $y(t)$ to a linear combination of signed orthogonal time signals, keep the coefficients and maximize the associated probabilities which, as a consequence, are not expressed in terms of a time variable.

Let $y_k(t; \varepsilon)$ be the truncated $y(t)$ where $t \in T_k(\varepsilon)$. Thus, for $t \in (0, KT)$, the observed signal $y(t)$ can be written as

$$y(t) = \sum_{k=0}^{K} y_k(t;\varepsilon) \quad \textbf{(3.12)}$$

Moreover, each $y_k(t; \varepsilon)$ is decomposed into a linear combination of an arbitrary set of orthogonal functions, $\{\psi_i(t)\}$. Note that $\{\psi_i(t)\}$ are not necessarily Hermite pulses and the dimension M is not the same as N, the dimension of the transmit signal.

$$y_k(t;\varepsilon) = \sum_{i=1}^{M} y_{i,k}\psi_{i,}(t) \quad \textbf{(3.13)}$$

where

$$y_{i,k} = \int_{T_k(\varepsilon)} y_k(t;\varepsilon)\,\psi_i(t)dt \tag{3.14}$$

Therefore, specifying an orthogonal set $\{\psi_i(t)\}$, $y(t)$ can be completely represented in a matrix form as

$$Y = \begin{bmatrix} y_{1,0} & y_{1,1} & \cdots & y_{1,K} \\ y_{2,0} & y_{2,1} & & y_{2,K} \\ \vdots & & \ddots & \vdots \\ y_{M,0} & y_{M,1} & \cdots & y_{M,K} \end{bmatrix} \tag{3.15}$$

The matrix representation implies that the time subinterval k travels horizontally. Meanwhile, the entries that lined up vertically reflect the coefficients of $\psi_i(t)$.

Thus, the probability $p(\varepsilon|y(t))$ can be alternatively represented by $p(\varepsilon|Y)$. The entries in Y are random variables due to the added noise and also the random data bits, $a_{n,k}$. Note that the set of orthogonal $\{\psi_i(t)\}$ does not need to be related to the Hermite basis pulses, $h_n(t)$. In fact, $h_n(t)$ can be decomposed to a linear combination of $\{\psi_i(t)\}$.

It is not obvious to directly manifest $p(\varepsilon|Y)$. In contrast, the probability of Y can be statistically formed if ε and $a_{n,k}$ are given. As a consequence, compared with $p(\varepsilon|Y)$, the probability $p(Y|\ \varepsilon,a_{n,k})$ is easier to determine. The relationship between $p(\varepsilon|Y)$ and $p(Y|\varepsilon)$ is obtained from Baye's rule [PAP65]

$$p(\varepsilon \mid Y) = \frac{p(\varepsilon)}{P(Y)}\, p(Y \mid \varepsilon) \tag{3.16}$$

The goal is to find ε that maximizes the probability defined in (3.16). Since the epoch is assumed to be uniformly distributed over the interval $(0,T_s)$, the probability $p(\varepsilon)$ is a constant and thus independent of ε. Furthermore, $P(Y)$ reflects the decomposition of the received signal $y(t)$ onto a orthogonal set. Its entries y_{ij} are, of course, a function of ε, $a_{n,k}$ and noise statistics. However, the probability $P(Y)$ is statistically independent of ε. Therefore, ε that maximizes $p(Y|\varepsilon)$ is the same ε that maximizes $p(\varepsilon|y(t))$. In conclusion, the probability to be maximized moves to $p(Y|\varepsilon)$.

To determine $p(Y|\varepsilon)$, let us first model the Y. Assuming the epoch ε is known and no noise is present, the received signal is randomized only by the binary data $a_{n,k}$. Let $w_{n,i,k}(\varepsilon)$ be a weighing metric reflecting the projection of n^{th} Hermite pulse delayed by $\varepsilon+(k-1)T_s$ onto i^{th} dimension of $\{\psi_i(t)\}$.

$$w_{n,i,k}(\varepsilon) = \int_{T_k(\varepsilon)} h_n(t-(k-1)T_s-\varepsilon)\cdot\psi_i(t)dt \tag{3.17}$$

The expected value of the k^{th} subinterval of the transmit signal on the i^{th} dimension for a given ε and a data vector $\mathbf{a'_k} = [a_{0,k}\ a_{1,k}\ \ldots\ a_{N-1,k}]^T$ is then

$$\bar{y}_{i,k}(\varepsilon, a'_k) = \sum_{n=0}^{N-1} a_{n,k} w_{n,i,k}(\varepsilon) \tag{3.18}$$

The data $a_{n,k} \in \{-1,1\}$ is assumed to be equiprobable. Note that $A = [\boldsymbol{a'_0}\ \boldsymbol{a'_1} \ldots \boldsymbol{a'_{K-1}}\ \boldsymbol{a'_K}]$, an $N\times(K+1)$ matrix, represents the entire data transmitted in the interval of observation.

Noise $n(t)$ can also be partitioned and decomposed into the space of $\{\psi_i(t)\}$.

$$n_{i,k}(\varepsilon) = \int_{T_k(\varepsilon)} n(t)\cdot\psi_i(t)dt \tag{3.19}$$

The $n_{i,k}$ is now a random variable. It is still Gaussian distributed with mean and variance preserved under the decomposition onto the orthonormal basis set, $\{\psi_i(t)\}$.

For a given epoch ε and a vector of transmit data $\boldsymbol{a'_k}$, the probability of an entry of Y associated with the k^{th} subinterval can be written as

$$p(y_{i,k} \mid \varepsilon, a'_k) = \frac{1}{\sqrt{2\pi\sigma^2}} \exp\left(\frac{\left[y_{i,k} - \bar{y}_{i,k}(\varepsilon, a'_k) \right]^2}{2\sigma^2} \right) \quad \textbf{(3.20)}$$

$$= \frac{1}{\sqrt{2\pi\sigma^2}} \exp\left(\frac{\left[y_{i,k} - \sum_{n=0}^{N-1} a_{n,k} w_{n,i,k}(\varepsilon) \right]^2}{2\sigma^2} \right) \quad \textbf{(3.21)}$$

$$= \frac{1}{\sqrt{2\pi\sigma^2}} \exp\left(\frac{y_{i,k}^2 - 2\sum_{n=0}^{N-1} a_{n,k} w_{n,i,k}(\varepsilon) y_{i,k} + \sum_{n=0}^{N-1} a_{n,k}^2 w_{n,i,k}^2(\varepsilon)}{2\sigma^2} \right) \quad \textbf{(3.22)}$$

where σ^2 is the noise power associated with the i^{th} dimension. If $\{\psi_i(t)\}$ is orthonormal, it can be shown that σ^2 is identical to $N_o/2$, the two-sided power spectral density (PSD) of the white noise.

Since $p(y_{i,k}|\varepsilon,\boldsymbol{a'_k})$ and $p(y_{j,k}|\varepsilon,\boldsymbol{a'_k})$, for all $i \neq j$, represent the probabilities in different dimension, their added noise is independent. Thus, the joint probability of the received signal at the k^{th} subinterval, $p(y_k|\varepsilon,\boldsymbol{a'_k})$ can be written in a product form of the individual probabilities, $p(y_{i,k}|\varepsilon,\boldsymbol{a'_k})$.

$$p(y_k \mid \varepsilon, a'_k) = \prod_{i=1}^{M} p(y_{i,k} \mid \varepsilon, a'_k) \quad \textbf{(3.23)}$$

Furthermore, the joint probability in the entire observed period becomes

$$p(Y \mid \varepsilon, A) = \prod_{k=0}^{K} p(y_k \mid \varepsilon, a'_k) \quad \textbf{(3.24)}$$

Integrating over A, the conditional probability on both ε and $a_{n,k}$ as in (3.24) reduces to be conditioned by ε only.

$$p(Y \mid \varepsilon) = \int_A p(Y \mid \varepsilon, A) p(A) dA \tag{3.25}$$

$$= \int_A \prod_{k=0}^{K} p(y_k \mid \varepsilon, a'_k) P(A) dA \tag{3.26}$$

Since the data vectors corresponding to the k^{th} subinterval, $\boldsymbol{a'_k}$, are independent of the data in other subintervals, (3.26) can be written in a product form as

$$p(Y \mid \varepsilon) = \prod_{k=0}^{K} \int_{a_k} p(y_k \mid \varepsilon, a'_k) p(a'_k) da'_k \tag{3.27}$$

Now let us evaluate the final form of $P(Y|\varepsilon)$ by expanding each term one at a time. Substituting $p(y_{i,k}|\varepsilon,\boldsymbol{a'_k})$ defined by (3.22) in (3.23), the probability $p(y_k|\varepsilon,\boldsymbol{a'_k})$ in (3.27) can be expanded to

$$p(y_k \mid \varepsilon, a'_k) = \frac{1}{\left(2\pi\sigma^2\right)^{M/2}} \exp\left(\sum_{i=1}^{M} \frac{y_{i,k}^2 - 2\sum_{n=0}^{N-1} a_{n,k} w_{n,i,k}(\varepsilon) y_{i,k} + \sum_{n=0}^{N-1} a_{n,k}^2 w_{n,i,k}^2(\varepsilon)}{2\sigma^2} \right) \tag{3.28}$$

Averaging (3.28) over the pdf of $\boldsymbol{a'_k}$ yields $p(y_k|\varepsilon)$.

$$p(y_k \mid \varepsilon) = \int_{a_{n,k}} p(y_k \mid \varepsilon, a'_k) p(a'_k) d(a'_k) \tag{3.29}$$

Note that the integral with respect to a'_k is, in fact, a summation since the entries of a'_k, $a_{n,k}$, are an independent discrete random variable of which possible values are either –1 or 1. Additionally, $a_{n,k}$ is equiprobable, i.e., $p(a_{n,k} = 1) = p(a_{n,k} = -1) = 1/2$. However, for ease of notation, the integral form is preserved.

$$p(y_k \mid \varepsilon) = \frac{1}{\left(2\pi\sigma^2\right)^{M/2}} \exp\left(\sum_{i=1}^{M} \frac{y_{i,k}^2 + \sum_{n=0}^{N-1} a_{n,k}^2 w_{n,i,k}^2(\varepsilon)}{2\sigma^2} \right) \cdot p(a_{n,k}) \int_{a_{n,k}} \exp\left(\sum_{i=1}^{M} \frac{-2\sum_{n=0}^{N-1} a_{n,k} w_{n,i,k}(\varepsilon) y_{i,k}}{2\sigma^2} \right) d(a_{n,k}) \tag{3.30}$$

The squared $a_{n,k}^2$ is unity and $p(a_{n,k})$ is constant and independent of $a_{n,k}$. Hence, all terms independent of $a_{n,k}$ are factored out as in (3.30). Moreover, the terms $\sum_{i=1}^{M}\sum_{n=0}^{N-1} w_{n,i,k}^2(\varepsilon)$ reflect the sum of the energy of Hermite pulses decomposed to the orthogonal function $\{\psi_i(t)\}$. The epoch ε does not affect the pulse energy. Hence, the summation is independent of ε. Therefore, all terms in front of the integral appear as a constant.

$$p(y_k \mid \varepsilon) = C' \int_{a_{n,k}} \exp\left(\frac{-2}{2\sigma^2} \sum_{i=1}^{M}\sum_{n=0}^{N-1} a_{n,k} w_{n,i,k}(\varepsilon) y_{i,k} \right) d(a_{n,k}) \tag{3.31}$$

The $a_{n,k}$ term is either –1 or 1 with identical probability. Evaluating the integral in (3.31) results in

$$p(y_k \mid \varepsilon) = C' \left[\exp\left(\frac{-1}{\sigma^2} \sum_{i=1}^{M}\sum_{n=0}^{N-1} (-1) w_{n,i,k}(\varepsilon) y_{i,k} \right) + \exp\left(\frac{1}{\sigma^2} \sum_{i=1}^{M}\sum_{n=0}^{N-1} w_{n,i,k}(\varepsilon) y_{i,k} \right) \right] \tag{3.32}$$

$$= 2C' \cosh\left(\frac{1}{\sigma^2} \sum_{i=1}^{M}\sum_{n=0}^{N-1} w_{n,i,k}(\varepsilon) y_{i,k} \right) \tag{3.33}$$

Substituting (3.33) in (3.27) gives $P(Y|\varepsilon)$ in the final form

$$P(Y \mid \varepsilon) = C \prod_{k=0}^{K} \cosh\left(\frac{1}{\sigma^2} \sum_{i=1}^{M}\sum_{n=0}^{N-1} w_{n,i,k}(\varepsilon) y_{i,k} \right) \tag{3.34}$$

Therefore $\hat{\varepsilon}$, the maximum *a posteriori* estimate of ε, is the value of ε that maximizes (3.34). Since the logarithm is a monotonic function of its arguments, alternatively, the value of ε that maximizes the function,

$$\Lambda(P \mid \varepsilon) = \ln\left[\frac{P(Y \mid \varepsilon)}{C}\right] = \sum_{k=0}^{K} \ln\cosh\left(\frac{1}{\sigma^2}\sum_{i=1}^{M}\sum_{n=0}^{N-1} w_{n,i,k}(\varepsilon) y_{i,k}\right) \quad \textbf{(3.35)}$$

is also $\hat{\varepsilon}$.

Let us consider the integral of the product of $y_k(t)$ and $h_{n,k}(t;\varepsilon)$ over $[0, KT_s]$.

$$\int_0^{KTs} y_k(t) h_{n,k}(t;\varepsilon)dt = \int_0^{KTs}\left[\sum_{i=1}^{M} y_{i,k}\psi_i(t)\right]\cdot\left[\sum_{i=1}^{M} w_{n,i,k}(\varepsilon)\psi_i(t)\right]dt \quad \textbf{(3.36)}$$

Since $y_k(t)$ is a truncated version of $y(t)$ and is zero outside the interval $[(k\text{-}1)T_s+\varepsilon,\ kT_s+\varepsilon]$, the expression becomes

$$\int_{(k-1)Ts+\varepsilon}^{kTs+\varepsilon} y_k(t)h_n(t-(k-1)T_s-\varepsilon)dt = \sum_{i=1}^{M}\sum_{j=1}^{M} y_{i,k} w_{n,j,k}(\varepsilon)\int_0^{KTs}\psi_i(t)\psi_j(t)dt \quad \textbf{(3.37)}$$

$$= \sum_{i=1}^{M} y_{i,k} w_{n,i,k}(\varepsilon) \quad \textbf{(3.38)}$$

The orthonormal property of $\{\psi i(t)\}$ eliminates all $i \neq j$ terms. Substituting the integral form of $\sum_{i=1}^{M} y_{i,k} w_{n,i,k}(\varepsilon)$ into (3.35) transforms the function to be maximized, $\Lambda(Y|\varepsilon)$, to a realizable form,

$$\Lambda(Y \mid \varepsilon) = \sum_{k=0}^{K}\ln\cosh\left(\sum_{n=0}^{N-1}\frac{1}{\sigma^2}\int_{(k-1)Ts+\varepsilon}^{kTs+\varepsilon} y_k(t)h_n(t-(k-1)T_s-\varepsilon)dt\right) \quad \textbf{(3.39)}$$

For each subinterval, the final form multiplies the received signal $y_k(t)$ by a flipped and delayed (by ε) version of a Hermite pulse and integrates the product over the subinterval. The procedure is repeated for all Hermite pulses. Then the outputs of all dimensions are summed up. The final quantity $\Lambda(Y|\varepsilon)$ is obtained from accumulation over K symbols periods of the logarithm of the hyperbolic cosine of the sum.

The block diagram depicted in Figure 3.8 shows the big picture of the straightforward implementation of the MAP synchronizer. Figure 3.9 details the functional block to evaluate the quantity $\Lambda(Y|\varepsilon)$ for the hypotheses $\{\varepsilon_1, \varepsilon_2, \varepsilon_3, \ldots, \varepsilon_p\}$. The ε which maximizes $\Lambda(Y|\varepsilon)$ is said to be the best estimate out of the candidate ε.

The limitation of the straightforward implementation is that only a finite number of the hypotheses $\{\varepsilon_1, \varepsilon_2, \varepsilon_3, \ldots, \varepsilon_p\}$ can be the candidates. A more accurate solution comes at cost of computational complexity increased by a larger number of hypotheses. Although numerous candidates are allowed, they are theoretically still quantized hypotheses. An improved version in terms of continuity is discussed in the next section.

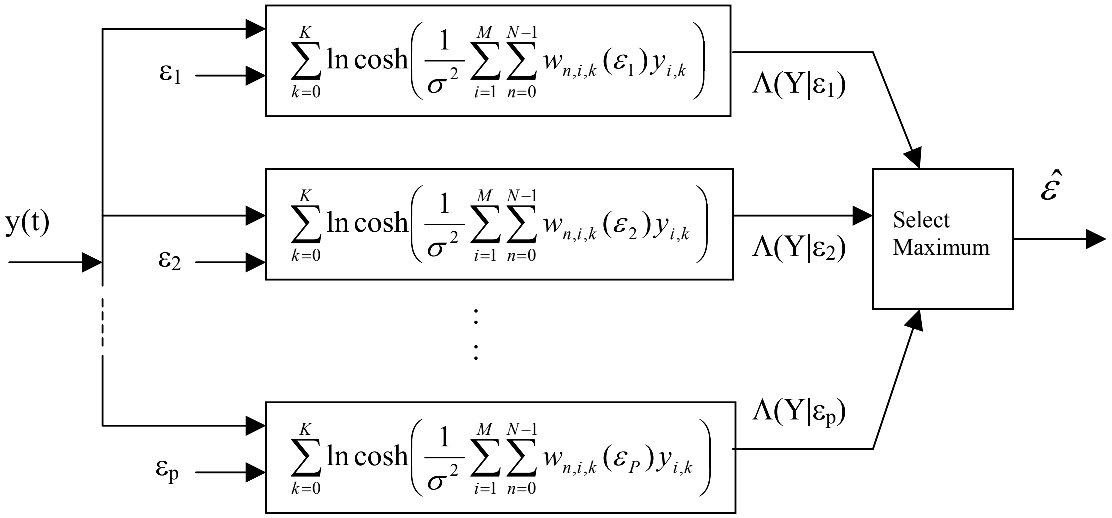

Figure 3.8 Realization of the maximum *a posteriori* probability (MAP) symbol detector. The maximum likelihood is tested among p hypotheses, $\{\varepsilon_1, \varepsilon_2, \varepsilon_3, \ldots, \varepsilon_p\}$.

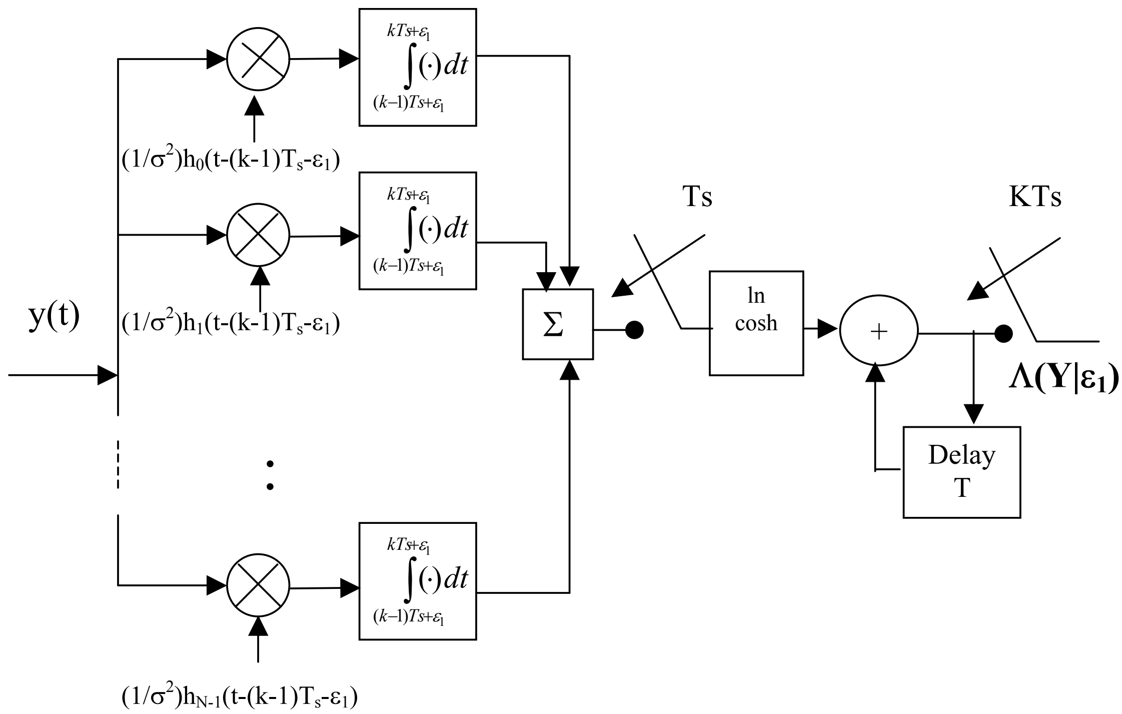

Figure 3.9 Inside each hypothesis block in Figure 3.8. The output of the implementation block is the quantity to be maximized, $\Lambda(Y|\varepsilon)$.

3.5 Implementation of MAP Synchronization

As discussed earlier, the integrate-and-dump detector can be replaced by a matched filter and a proper sampler. The relationship is re-expressed by

$$\int_{(k-1)Ts+\varepsilon}^{KT+\varepsilon} y(t)h_n(t-(k-1)T_s-\varepsilon)dt = y(t)\otimes h_n(T-t)\,|_{t=(k-1)T+\varepsilon} \tag{3.40}$$

where $h_n(t) = 0$ for $t \notin (0,T_s)$ and $\otimes$ denotes convolution. As a consequence, the desired metric $\sum_{i=1}^{M} y_{i,k} w_{n,i,k}(\varepsilon)$ can be continuously produced for arbitrary k^{th} subintervals and ε from the output of the matched filter. The desired metric is then represented by the convolution output at $t = (k-1)T_s+\varepsilon$.

$$y(t)\otimes h_n(T-t)\,|_{t=(k-1)+\varepsilon} = \sum_{i=1}^{M} y_{i,k} w_{n,i,k}(\varepsilon)\,. \tag{3.41}$$

Furthermore, ln cosh(x) is approximated by

$$\ln\cdot\cosh(x) \cong \begin{cases} 0.5\,|\,x\,| & |\,x\,| >> 1 \\ 0.5x^2 & |\,x\,| << 1 \end{cases} \tag{3.42}$$

This approximation suggests replacing the ln cosh( ) function block by either a square law or absolute device. A block diagram of the synchronizer with the simplification of the ln cosh( ) function is shown in Figure 3.10. Fortunately, the Hermite matched filters are already available as a functional block in the detector. The synchronizer can make use of the existing filter banks. The complete receiving system is shown in Figure 3.11. Since no extra information is needed to generate the synchronization signal, the system is categorized as a self-synchronized system.

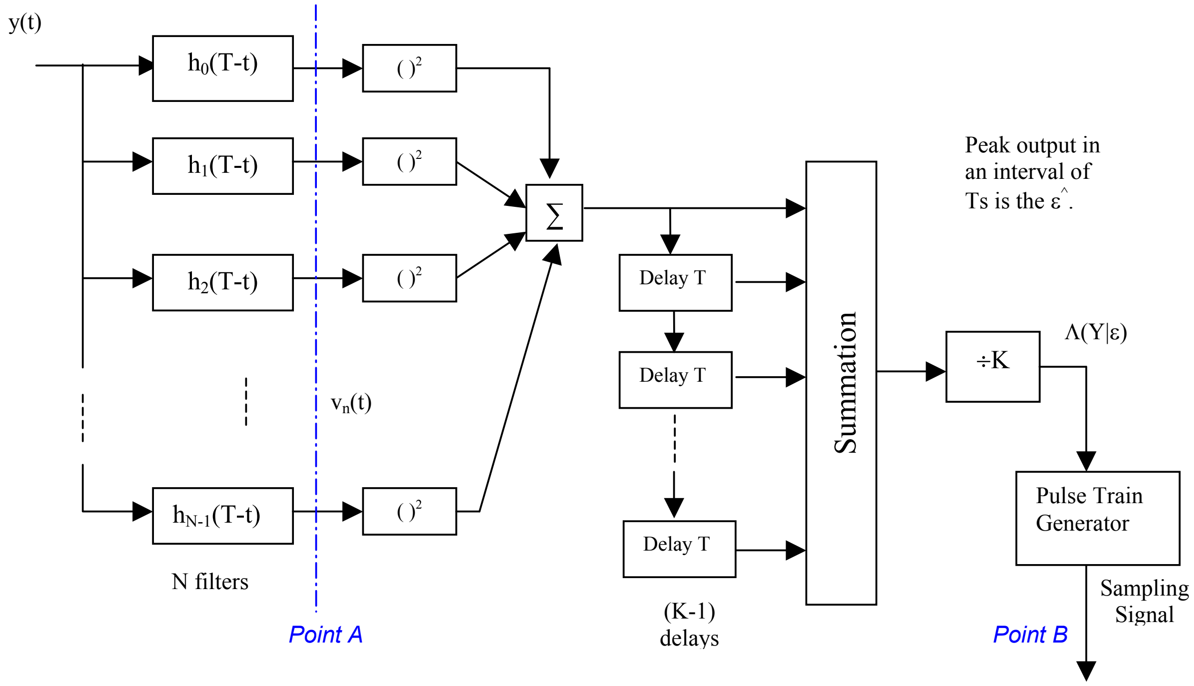

Figure 3.10 A stepless implementation of MAP synchronizer. Note that the matched filters can be shared with the Hermite detector.

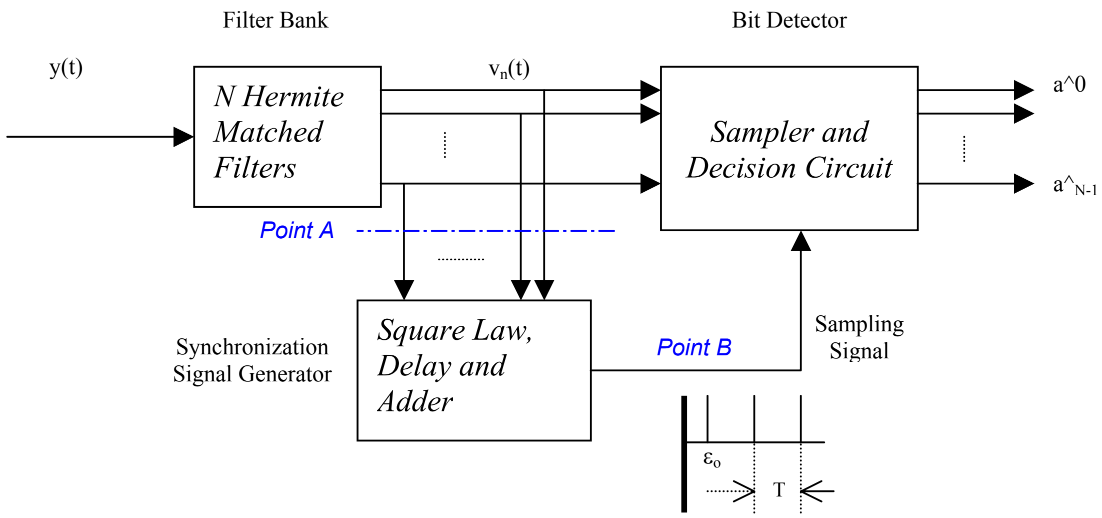

Figure 3.11 The flow of the signal in the overall system. The outputs of the Hermite matched filters are fed to the synchornizer and the detector. Points A and B locate the associated signals in Figure 3.10.

3.6 Effects of Basic Pulse Cross Correlation on the MAP Synchronizer

The MAP synchronizer observes the received signal for K symbol periods and estimates the epoch ε by maximizing the probability of the received signal for given hypothetical epochs. Based on the limited observation of the signal corrupted by AWGN, the estimate is the best. However, the MAP synchronizer suggests neither the minimum observation symbol periods nor the probability of false estimation.

Let us select a counterexample for synchronization failure. Let an alternating sequence [1 1 1 1, -1 1 -1 1, 1 1 1 1, -1 1 -1 1] be the data bits transmitted by the Hermite system. In this demonstration, noise is assumed to be absent. The MAP synchronizer is supposed to be capable of accurately estimating the epoch. Assume the transmit signal $s(t)$ arrives at the receiver exactly at a multiple of the symbol period. A successful synchronizers will produce peaks at $t = kT_s$, where k is an integer.

The received signal $y(t)$ is passed to the filter bank as in Figure 3.10. The received signal $y(t)$ and the outputs of the matched filter bank $v_n(t) = y(t)\otimes h_n(T\text{-}t)$ versus normalized time are graphed in Figure 3.12. Let the MAP synchronizer observe the received signal over only one symbol period ($K = 1$) before generating the metric $\Lambda(Y|\varepsilon)$. The outputs of the synchronizer versus the time are shown in Figure 3.13. For ease of locating the correct sync time, the time axis is normalized by the pulse period T_s, which is 4 times the bit period T_b in the 4-dimensional system.

According to Figure 3.13, with $K = 1$, the MAP synchronizer produces maxima in the middle of the correct sync times (multiples of T_s). Evidently, the synchronizer fails to detect the epoch by using such a short observation period when the particular sequence is transmitted.

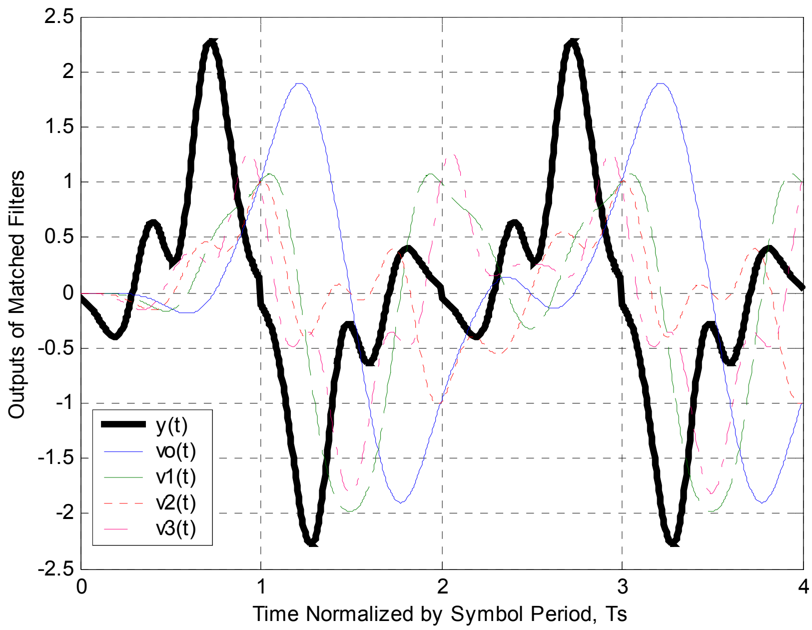

Figure 3.12 A 4-dimensional received signal $y(t)$ for the bit sequence [1 1 1 1, -1 1 -1 1, 1 1 1 1, -1 1 -1 1] and the waveforms at the outputs of the matched filters $v_n(t)$. In absence of interference, the output of the matched filters at $t = kT_s$, $v_n(kTs) \in \{-1, 1\}$.

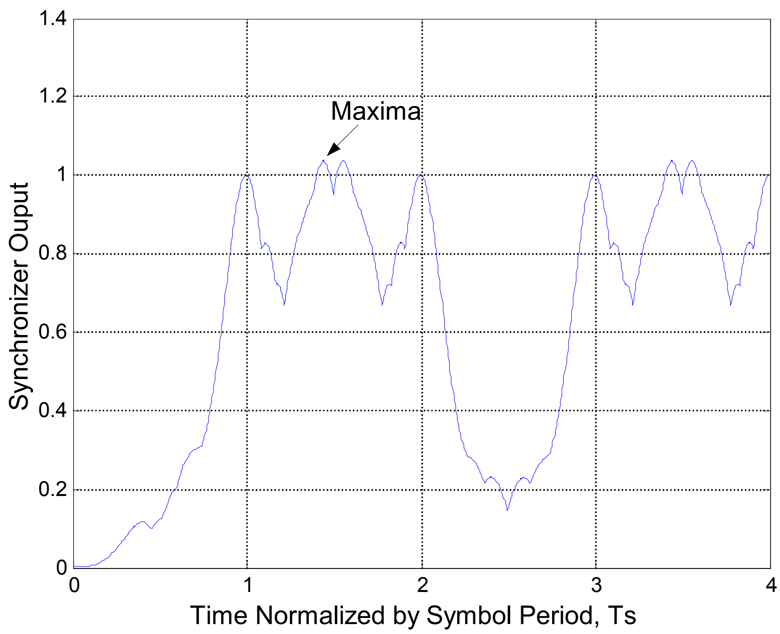

Figure 3.13 The estimation metric $\Lambda(\varepsilon|Y)$ at the output of the synchronizer for the bit sequence [1 1 1 1, -1 1 -1 1, 1 1 1 1, -1 1 -1 1], as in Figure 3.12, versus time. The signal is assumed to arrive exactly at the multiple of symbol period T_s. Maxima detected are in the middle of pulse period. The synchronizer fails to detect the epoch.

An explanation of this phenomenon is as follows. The estimation metric $\Lambda(Y|\varepsilon)$ is computed by multiplying $y(t)$ by $h_{m,k}(t;\varepsilon)$, $m = 0, 1, \ldots, N\text{-}1$ and integrating the product over the interval of the Hermite pulses, $T_s = NT_b$. The values associated with all m are then added. Since the received signal $y(t)$ is a delayed (by ε_o) version of a linear combination of signed Hermite pulses, the computation on each $h_m(t)$ is equivalent to evaluating the sum of cross correlation functions of m^{th} Hermite pulse and the n^{th} pulse, $n = 0, 1, \ldots, N\text{-}1$.

$$\int_{(k-1)Ts+\varepsilon}^{kTs+\varepsilon} h_{m,k}(t;\varepsilon)\cdot y(t)dt = \int_{(k-1)Ts+\varepsilon}^{kTs+\varepsilon} h_m(t-(k-1)T_s-\varepsilon)\sum_{n=0}^{N-1} a_{n,k}h_n(t-(k-1)T_s-\varepsilon_o)dt \tag{3.43}$$

$$= \sum_{n=0}^{N-1} a_{n,k}R_{mn}(\varepsilon-\varepsilon_o) \tag{3.44}$$

where $R_{mn}(\,)$ is the cross correlation of m^{th} and n^{th} Hermite pulses. Assuming $\varepsilon = \varepsilon_o$, the cross correlation function becomes $R_{mn}(0)$. For $m \neq n$, there is no guarantee that $R_{mn}(0)$ is maximum. Therefore, there possibly exists $R_{mn}(\varepsilon\text{-}\varepsilon_o)$ greater than $R_{mn}(0)$. With proper signs of $a_{n,k}$, $\left|\sum_{n=0}^{N-1} a_{n,k}R_{mn}(\varepsilon-\varepsilon_o)\right|$, at some ε not equal to ε_o, becomes a maximum. As a consequence, the MAP synchronizer fails. It is interesting that in one-dimensional systems, the MAP synchronizer does not encounter this kind of problem. Since only one pulse is signed, the cross correlation does not exist. Auto-correlation function, $R_{xx}(\tau)$ always has a maximum at $\tau = 0$.

Nevertheless, the usability of the derived MAP synchronizer is not lost by this counterexample. From the counterexample, it can be concluded that observing the received signal for only one single symbol period does not guarantee synchronization success even though noise is not present. Now, let us observe the signal longer. For $K = 2$ and $K = 3$, the outputs of the synchronizer are shown in Figure 3.14. The longer observation times eliminate the unwanted peaks as found in the counter example ($K = 1$).

However, as shown in Figure 3.14, longer observation time is a tradeoff of improved accuracy and speed of acquisition.

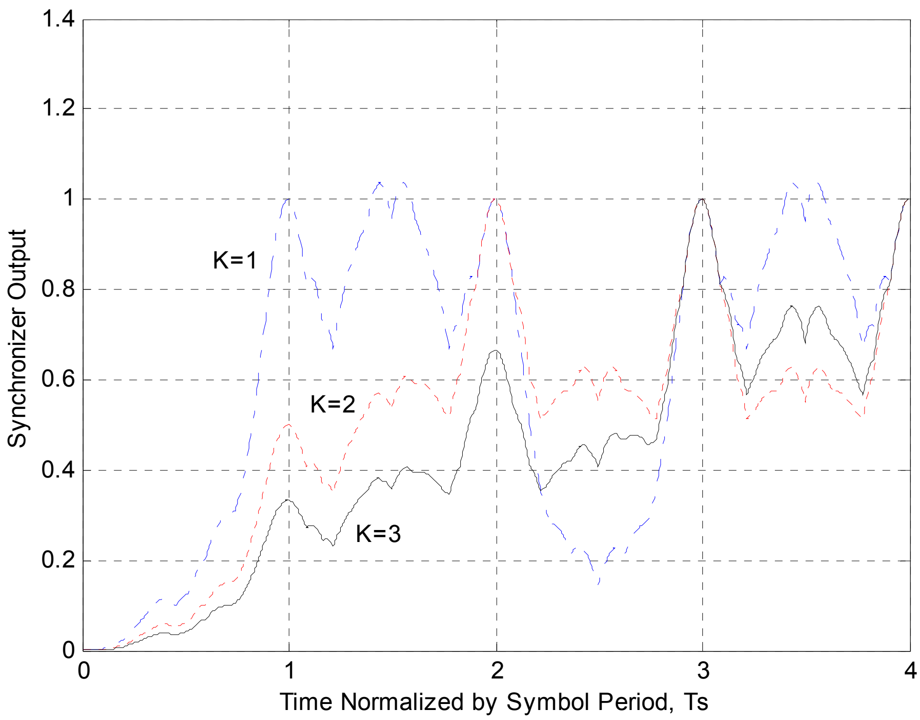

Figure 3.14 Outputs of the synchronizer when longer observation times are used. With K = 1, the synchronizer fails to estimate the epoch. Observing longer symbol periods (K = 2 and K = 3) improves the estimation accuracy. However, the outputs are ready by $t = 2T_s$ and $t = 3T_s$, respectively. The reliablity comes at cost of speed of acquistion time.

3.7 Performance of MAP Synchronizer in Low Signal to Noise Ratio

The derivation of the MAP estimator shows an optimal method to generate synchronization from a limited observation of noise-corrupted received signal. Nevertheless, the theory does not suggest noise immunity performance of the synchronization technique at all. This section investigates the performance of the MAP synchronizer at low signal to noise ratio (SNR).

Lost synchronization or false epoch estimation occurs when the output of the synchronizer produces peaks in between the symbol period or in the interval $[\varepsilon_o+(k-1)T_s\ ,\ \varepsilon_o+kT_s]$, where ε_o is the correct epoch. An example of the missed synchronization is the early illustration with $K = 1$. An analytical result of the probability of false estimation is complicated since full knowledge of all Hermite pulse cross correlation functions must be known along with their probabilities of occurrence. As a consequence, simulation is an alternative if the relationship between the probability of false detection and the SNR is needed.

Assuming synchronization is perfect, typical communication systems with a bit energy to noise power spectral density ratio (E_b/N_o) less than 3 dB suffer from unacceptable BER. Although BER performance of Hermite system has not yet been discussed, let us assume that at E_b/N_o = 3 dB, the Hermite transmission system cannot deliver an acceptable BER. Therefore as long as the MAP synchronizer survives an E_b/N_o of 3 dB, the overall system performance is bounded by the BER, not the synchronization.

The investigation is carried out through simulation. The simulation invokes a random sequence of 48 bits. The data bits modulate the signs of Hermite pulses in a 4-dimensional system. As a result, the transmit duration spans 12 symbol periods. The receiver observes the transmit signal plus white noise at an E_b/N_o of 3 dB. The transmit signal and the noisy received signal (before any filters) are shown in Figure 3.15. Figure 3.16 shows the outputs of the first two matched filters on the receiver side. The waveforms are at Point A in Figure 3.10. Because of the added noise, the absolute values of the output waveforms sampled at $t = kT_s$ are not unity.

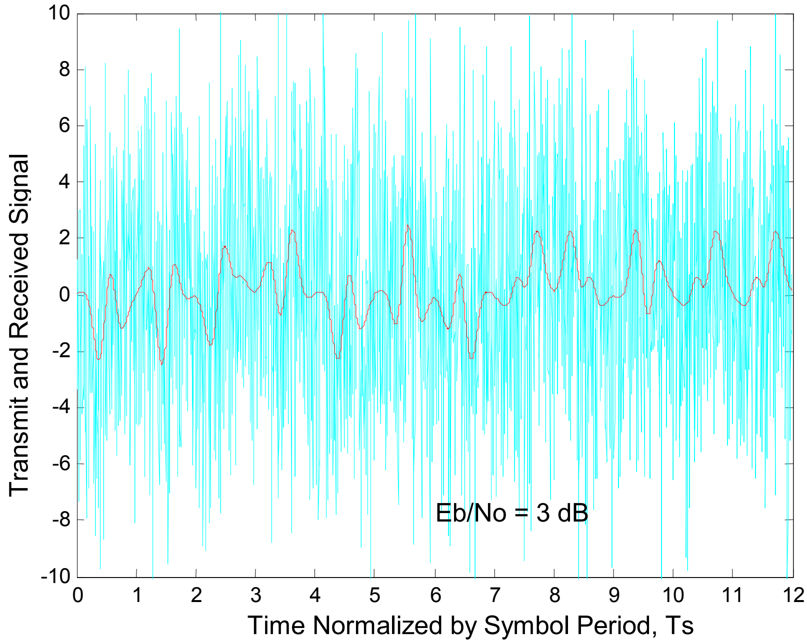

Figure 3.15 A 4-dimensional Hemite transmit signal. A total of 4x12 = 48 data bits are carried on the waveform. The received signal is corrupted by wideband AWGN which causes an effective E_b/N_o of 3 dB. The plot shows the received signal before any filtering.

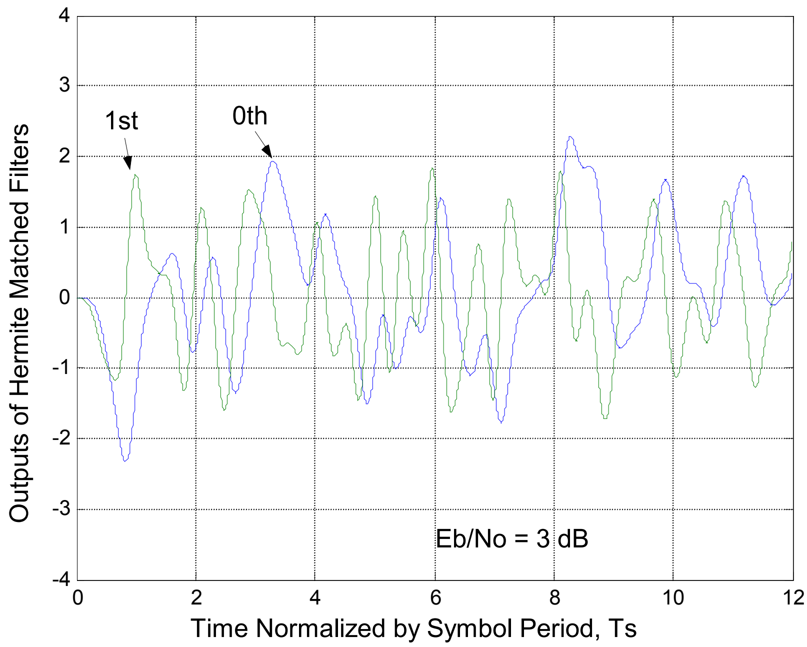

Figure 3.16 First two outputs (out of four) of the Hermite filter bank. The absolute values of output waveforms at $t = kT_s$, where k is an interger, deviate from unity because of the noise.

If noise is removed, as illustrated in Figure 3.17, the tested sequence does not introduce false synchronization for an observation period of three symbol periods ($K = 3$). For the same observation period, the added noise causes a false synchronization. The incorrectly generated output waveform of the MAP synchronizer for the E_b/N_o of 3 dB is illustrated in Figure 3.18. According to Figure 3.18, a peak shows up in the interval of 8th and 9th symbol periods. The false peak on the output waveform fails the MAP synchronizer.

The false synchronization is eliminated by lengthening the observation period. Figure 3.19 shows the output of the MAP synchronizer with $K = 6$. The unwanted peak is eliminated. Thus, better synchronization is achieved by the longer observation time. However, the drawback is that the first synchronization pulse is completed after 6 symbol periods. The speed of acquisition is lowered.

The number of symbols used by the MAP synchronizer to acquire symbol synchronization as shown in Figure 3.19 is not considered excessive. In transmission of data bursts in Time Division Multiple Access (TDMA) system, information bits are preceded by a group of bits known as preamble. The first portion of the preamble is a Carrier and Bit timing Recovery (CBR) sequence which is used to lock the receive station to the carrier frequency and also recover bit timing of the burst. A typical structure of TDMA satellite bursts, as shown in [CAM83], consists of a 176-bit CBR sequence. If three quarters of the CBR time are used for carrier recovery, there are 42 bits for the bit timing. Moreover, high-bit-rate TDMA, e.g., 120 Mbps, requires a longer CBR sequence of 300-400 bits [HA90]. Therefore, six symbol periods of the 4-dimensional Hermite system, which are equivalent to 24 bit periods, is comparable.

It is beyond the scope of this thesis to finalize or reshape the output of the synchronizer for practical use. Also, its performance in terms of false synchronization rate for various K and E_b/N_o is outside the area of interest since the MAP synchronizer shows promise to survive in such a low E_b/N_o. In conclusion, the Hermite transmission system is not limited by the capability to synchronize the symbol at such a low E_b/N_o.

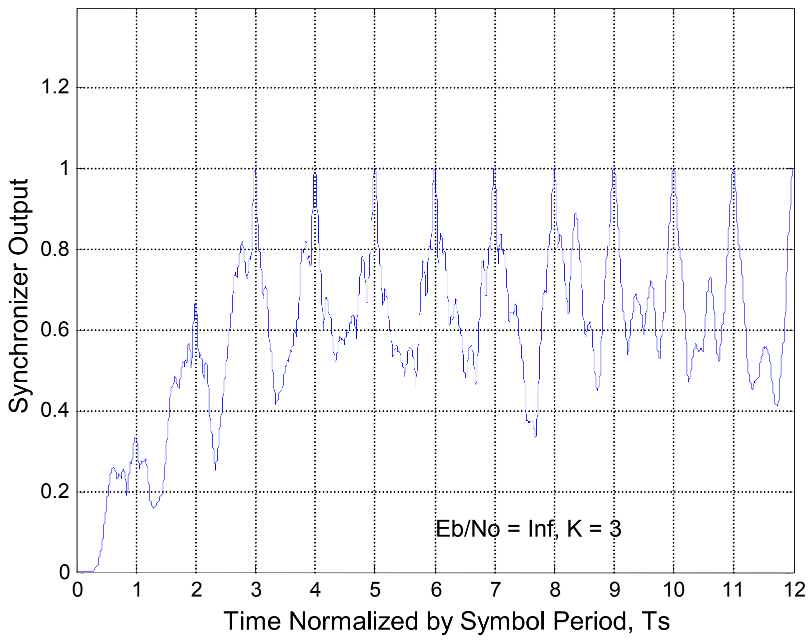

Figure 3.17 The output of the sychronizer without the presence of noise. The test data bits do not introduce the effects of Hermite pulse cross-correlation with an observation interval of $3T_s$ (K = 3).

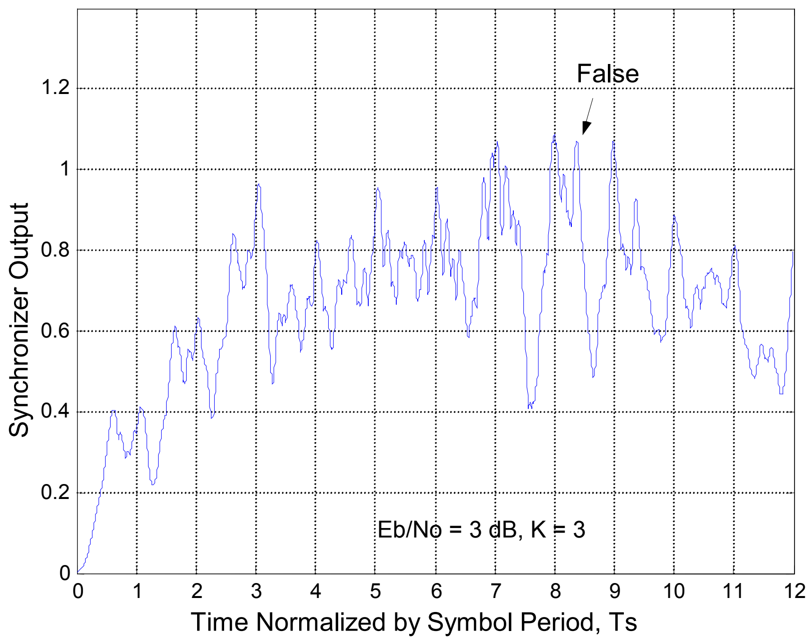

Figure 3.18 In presence of noise at an E_b/N_o of 3 dB, output of the synchronizer with an observation period of $3T_s$ culminates at wrong times. A false maximum is found in the interval of ($8T_s$, $9T_s$).

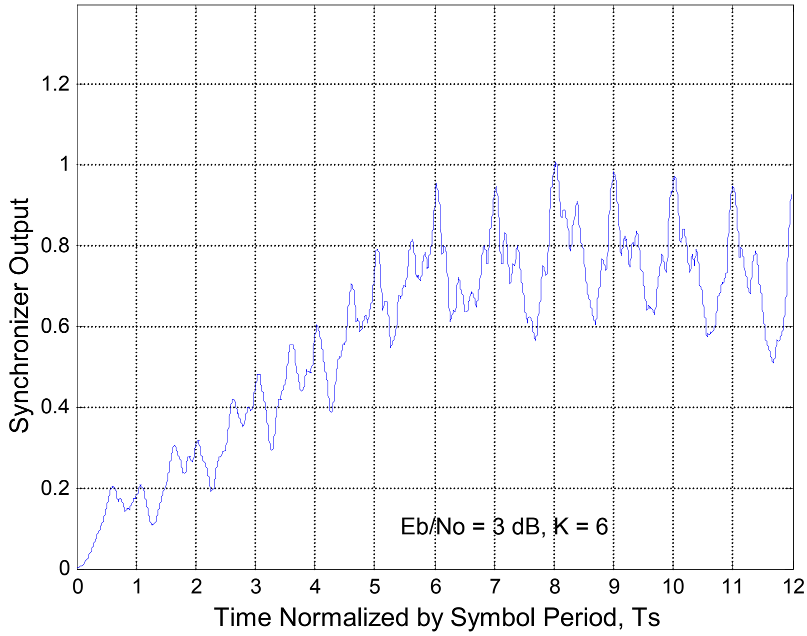

Figure 3.19 Output of the synchronizer with a longer observation period of $6T_s$ ($K = 6$). The false maximum found earlier in the interval of ($8T_s$, $9T_s$) with $K = 3$ disappears. The drawback is on the speed of acquisition. The synchronization is not ready until $t = 6T_s$.

3.8 Chapter Summary

This chapter first proposes a method to generate N-dimensional transmit waveforms. The generation is implemented by passing a signed impulse train to a discrete waveform generator with impulse responses that are sampled Hermite basis pulses. The generator can be realized using a finite impulse response (FIR) digital filter.

At the receiver end, it is shown that a bank of correlators with proper sampling circuit can completely replace the need for integrate-and-dump receivers in the detection of data carried on the orthogonal waveform. Again, the correlators are implemented in discrete-time domain.

Since symbol synchronization is critical for the correlator receiver, a synchronization method using maximum a posteriori (MAP) estimation is derived. The MAP estimator extracts synchronization from the received signal, observed for some short symbol periods. It is shown that the MAP synchronizer can be constructed by making use of the output of the detecting Hermite correlators. A synchronizer block diagram is proposed. The simulation shows that the MAP synchronizer can extract the synchronization at E_b/N_o as low as 3 dB.

Chapter 4
BER Performance of Baseband and Linear Modulated Hermite N-Dimensional Systems

In the two previous chapters, bandwidth efficiency and synchronization methods are discussed. In this chapter, the performance of the Hermite N-orthogonal systems in terms of power efficiency is evaluated by simulation. The simulation focuses on immunity in an additive white Gaussian noise (AWGN) environment. The performance is evaluated by bit error rate (BER). The simulation for a bandpass signal makes use of complex envelope, which is a carrier-free representation. This allows simulation of bandpass signals to be implemented indirectly by their complex baseband representations.

4.1 Theoretical Performance of Baseband Signals in AWGN

Intangible data symbols are converted into material form before they can be physically transmitted. Very often, the symbols are mapped to electrical pulses. Direct transmission of the electrical pulses over some media, e.g., wire or cable, is said to be baseband communication and transmit signal is a baseband signal. Typically, the spectrum of the transmit pulse is concentrated about zero.

In an antipodal scheme, the waveform representing Binary 0 is a sign reversed form of the waveform representing Binary 1. In AWGN, a matched filter, which is an alternative to a correlator receiver, is the optimal receiver in the sense that the signal to noise (SNR) at the output of the receiver is maximized. The output SNR of the receiver is simply the ratio of signal bit energy to the two-sided noise power spectral density, $E_b/(N_o/2)$ [PRO95]. Assume that the binary states 0 and 1 are equi-probably sent. The optimal bit-by-bit detection with a zero decision threshold yields the probability of error

$$P_b = Q\left(\sqrt{\frac{2E_b}{N_o}}\right) \tag{4.1}$$

The probability is independent of the shape and duration of the symbol.

Now, let us consider an N-dimensional system. Based on the discussion in Chapter 3, a method used to retrieve the data carried on Hermite pulses already falls into a form of matched filter. An extended version of the matched filter used in an N-dimensional system is shown in Figure 4.1. Furthermore, the analysis in Chapter 3 shows that in an N-dimensional orthogonal system, the output SNR of each matched filter is also $E_b/(N_o/2)$, which is exactly the same as the results in the case of one-dimensional antipodal systems. Therefore, the bit error rates of either a single or an N-dimensional system are theoretically identical.

Note that in an N-dimensional system, 2^N symbols are possible in one symbol period. In a strict-sense, a total number of 2^N filters are needed to implement matched filtering. This implementation only matches the received signal dimension-wise to reduce complexity. The strict-sense matched filtering doubles the number of filters used for each additional dimension. In contrast, the complexity of the dimension-wise scheme increases linearly. Therefore, the alternate receiver, which matches the received signal dimension-wise, is more practical.

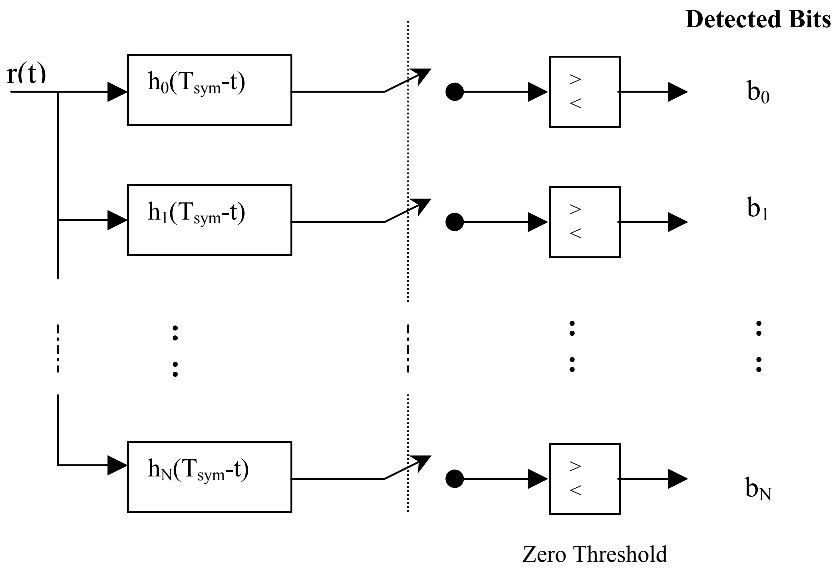

Figure 4.1 Matched filters for N-dimensional antipodal systems. The received signal, impulse response of the Hermite i^{th} filter, and the detected bits (-1 or 1) are denoted by $r(t)$, $h_i(t)$ and b_i, respectively.

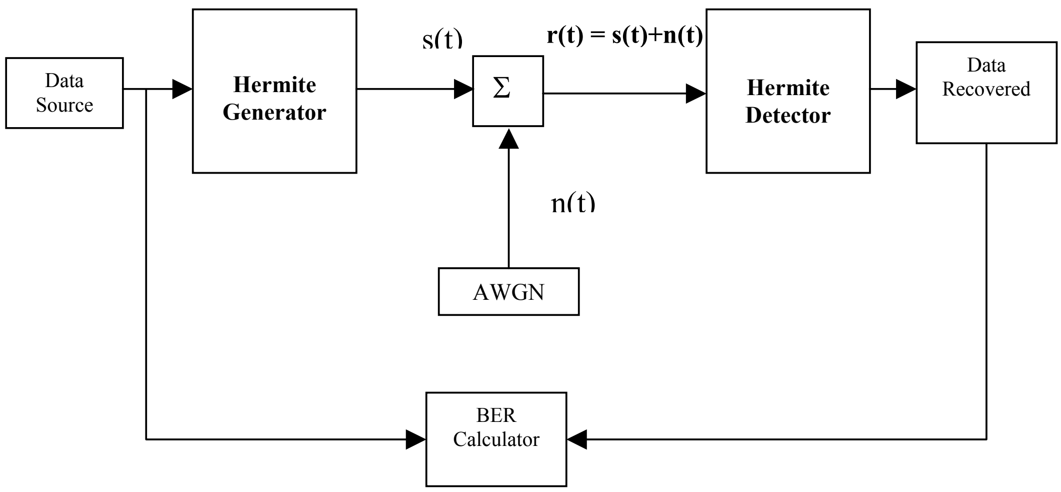

Figure 4.2 Transmitter and receiver model for the simulation of BER performance in AWGN. The transmit signal $s(t)$ is corrupted by $n(t)$, the AWGN. The received signal $r(t)$ is the sum of the transmit signal and the noise.

4.2 Simulation Results of Baseband N-dimensional Systems

The analytical discussion in the previous section concludes that the BER performance of a dimension-wise detection scheme is identical to the BER of a receiver using matched filters for a one-dimensional antipodal scheme. The theoretical result is compared to a simulation result in this section.

The baseband signal is very often an electrical pulse train. Generally, the received pulse is a distorted version of the transmit pulse. Possibly, the received signal suffers from intersymbol interference (ISI) caused by filters or the limit of allowed bandwidth. Equalizers are a tool to mitigate such interference. More or less, thermal noise causes interference with the received pulses. Thermal noise has a flat spectrum (white). Typically, the receiver filters out the white noise by a matched filter. Weak signals will be affected by the noise severely. The system is modeled here with white noise as the only interferer.

As a matter of fact, the simulation is implemented solely on digitized versions of both transmit signal and noise. In this simulation, the transmit waveform is sampled at least of 50 samples per one bit. The sampling rate F_s is then $50R_b$, where R_b is the bit rate. The sampling interval $T_s = 1/F_s = 1/(50R_b)$. The discrete time representation of the signal is reliable (no aliasing) if the signal bandwidth is less than one half of the sampling rate; in this case it is $25R_b$. The bandwidth of $25R_b$ is far greater than the Hermite signal bandwidth, which is, according to the results in Chapter 2, $0.625R_b$.

To constrain to unity bit energy, the transmit signal is scaled so that the sum of the squared values of the signal samples times the sampling interval $1/(50R_b)$ is one. Note that, since power is the rate of transmitting energy (energy divided by observing time), the average of the squared sample values is simply the signal power. The power can be calculated directly from the sample values without the knowledge of sampling rate [OPP89].

Noise is generated by independently randomizing a number for each signal sample. Typically, most software packages, including Matlab, provide a zero-mean and normal-distributed random number generator with unity power; the average of samples generated from the random generator is zero and the average squared values is one. The generated numbers can be scaled to meet specific noise power. For a given sampling rate, the noise power spectral density (PSD) is white from DC to one half of the sampling rate. In the case with a sampling rate F_s of $50R_b$, the generated noise PSD is flat from DC to $25R_b$. The noise power calculated by the average of the squared samples is equal to $N_o \times Fs/2$, where N_o is one-sided noise power spectral density. Therefore, given an N_o and the sampling rate F_s, the corresponding noise power can be determined by the relationship. The value of the noise power is then used to scale the unity-power noise samples generated from the Gaussian random generator. Therefore, in this simulation a broadband noise is added to the transmit signal. The noise spectrum is flat from DC to one half of the sampling rate.

For example, an E_b/N_o of 10 dB is desired in a simulation with sampling rate $F_s = 50R_b$. First F_s is used to constrain unity energy of E_b. For the 10 dB and unity pulse energy, N_o is 1/10. Thus, the broadband noise power becomes $(1/10) \times 25R_b$. Thus, the output samples from the normal distributed generator need to be multiplied by $1/\sqrt{(250R_b)}$ before being added to the signal. The sum achieves an E_b/N_o of 10 dB.

The system model to evaluate BER performance by simulation is illustrated in Figure 4.2. The transmit signal $s(t)$ is constrained to have unity bit energy. The Hermite pulses are truncated using a 99.9% energy criterion as discussed in Chapter 2. The signal is corrupted by channel AWGN. In this simulation, it is assumed that neither fading of any kind nor co-channel interference affects the received signal. The style of simulation is based on Monte Carlo simulation. BER is determined by the ratio of incorrectly detected bits to the total number of trial bits.

Simulation is carried out at various E_b/N_o and number of Hermite pulses used (dimension). For each E_b/N_o, the transmission of at least 4 million bits of data is simulated. Four million simulated data bits were used to ensure that the BER can be reliably estimated down to at least 4×10^{-5} by using the criterion of a minimum of 10 bit errors. The results then establish reliable statistics of the BER. Figure 4.3 dimensional-wise lists the BER of a 4-dimensional system. Simulated BERs on all dimensions are identical. Figure 4.4 compares the overall BER when different numbers of Hermite pulses are used. According to the simulation results, the BER are independent of the number of dimensions. Moreover, the simulated and the theoretical results are consistent. Therefore, N dimensional matched filters can replace the strict-sense 2^N filters without losing BER performance in AWGN.

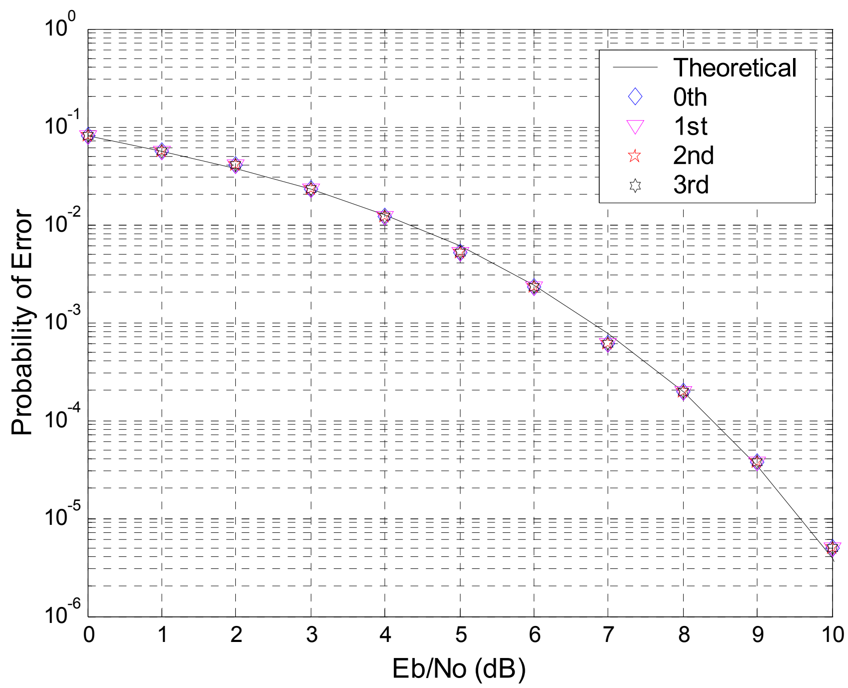

Figure 4.3 BER versus E_b/N_o listed by dimensions of a 4-dimensional Hermite system. The received signal is interfered by AWGN only. The receiver invokes matched filters and ideal synchronization is assumed. The BER is uniformly distributed over all dimensions.

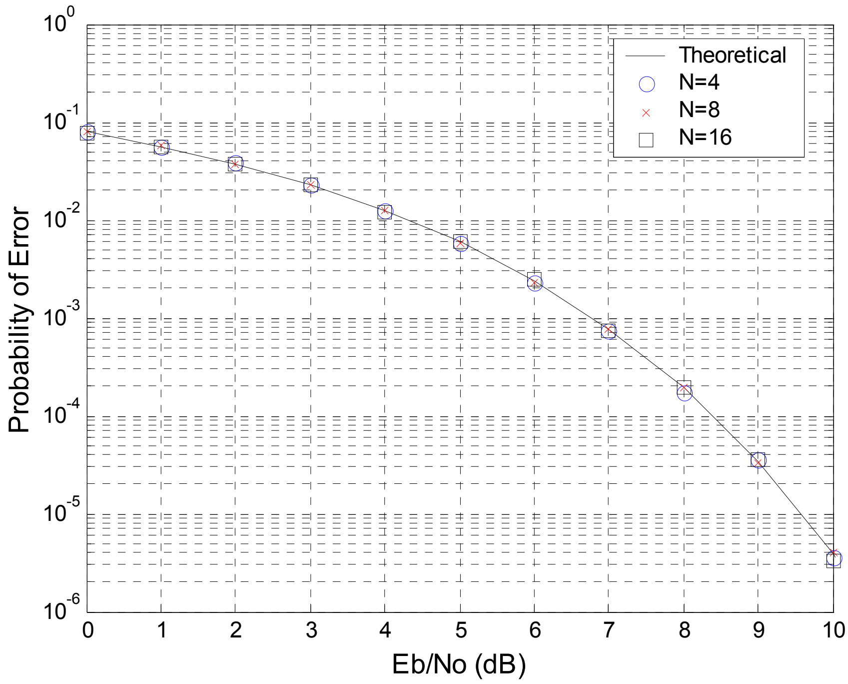

Figure 4.4 Overall BER versus E_b/N_o of different dimensional systems. The same system as the previous figure is assumed. The dimension does not affect the overall BER. For the same bit energy, the Hermite BER is identical to the baseband polar pulse. Pulse shape does not matter.

4.3 A Brief Review of Bandpass Transmission Representation

There are two common methods to carry baseband signals over radio channels. One is using the baseband signal to modulate the sinusoidal carrier amplitude (AM) and the other is to modulate the carrier phase or frequency (PM/FM). Each of these methods relocates the spectrum to an RF band centered about the carrier frequency. Direct simulation of bandpass signals requires a sampling rate more than twice the carrier frequency (Nyquist rate) to avoid aliasing [OPP89]. Compared with the sampling capability of the computer, the carrier frequencies are high, generally. Additionally, the range of carrier frequencies varies dramatically from kilohertz to gigahertz. For ease of computer simulation, representation of the bandpass signals in a complex baseband format is developed.

Bandpass signals can be described by [COU97]

$$s(t) = \text{Re}\{R(t)e^{j\phi(t)}e^{jw_c t+\theta}\}, \tag{4.2}$$

where $Re\{\cdot\}$ denotes the real part. Having the imaginary part removed, $s(t)$ can be rewritten in terms of bandpass real signals as

$$s(t) = x(t)\cos(w_c t + \theta) - y(t)\sin(w_c t + \theta), \tag{4.3}$$

where $R(t) = \sqrt{x^2(t) + y^2(t)}$ and $\phi(t) = \tan^{-1}\frac{y(t)}{x(t)}$. The random carrier phase delay θ is generally assumed to be uniformly distributed over [-π, π].

$R(t)e^{j\phi(t)} = x(t)+jy(t)$ is a complex baseband signal and it is called the complex envelope of the bandpass signal. Furthermore, $x(t)$ and $y(t)$ represent the inphase and quadrature components of the signal. Signal power of the bandpass signal $s(t)$ defined in (4.3) is calculated by

$$\left\langle s^2(t) \right\rangle = \tfrac{1}{2}\left\langle | R(t) |^2 \right\rangle \tag{4.4}$$

where $\langle\cdot\rangle$ denotes time average.

Bandpass noise is assumed to be a wide sense stationary (WSS) process [COU97] and can similarly be decomposed to

$$n_{bp}(t) = n_c(t)\cos(w_c t) - n_s(t)\sin(w_c t) \tag{4.5}$$

where $n_c(t)$ and $n_s(t)$ are zero-mean Gaussian distributed real baseband processes. The power of bandpass noise can be determined either from the power of the inphase or of the quadrature components.

$$\overline{n_{bp}^2(t)} = \overline{n_c^2(t)} = \overline{n_s^2(t)} \tag{4.6}$$

Double Sideband Suppressed Carrier (DSB-SC), a linear modulation technique, keeps the modulating signal in the inphase component $x(t)$, and nothing is in $y(t)$. While in single sideband (SSB) modulation, one of the sidebands is removed by forcing the quadrature component $y(t)$ to be the Hilbert transform (90° phase shift) of $x(t)$. In fact, two independent baseband signals can be transmitted using carriers with the same frequency; one is on the inphase channel and the other is on the quadrature channel. Quadrature Phase Shift Keying (QPSK) is an example of maximizing spectrum efficiency using this approach.

For angle modulation, $\phi(t)$ is a function of the baseband modulating signal $m(t)$. The constant envelope property of angle modulation is achieved because $R(t)$ is constant. One advantage of angle modulation is that the bandwidth of the bandpass signal is adjustable. Another advantage of angle modulation over amplitude modulation is that its instantaneous and average powers are identical.

4.4 Transmission of N-dimensional Signals on Carrier's Amplitude

It is commonly known that the bandwidth of an AM modulated signal is twice that of its baseband modulating signal. The result in Chapter 2 concludes that bandwidth efficiency of a baseband Hermite N-dimensional system is about
0.7 Hz/bps. It implies that if AM is used as the modulation technique, the spectrum efficiency becomes 1.4 Hz/bps. However, the spectrum efficiency can be improved by making use of both inphase and quadrature components.

4.4.1 Transmitter Implementation

Making use of both inphase and quadrature carriers can be done by first splitting the data stream into two channels. The bit rate in each channel is dropped to one half of the original. Each half-rated bit stream is passed to a Hermite baseband generator. The outputs of the first and second Hermite generators are then used to amplitude modulate a cosine wave and its π/2 phase-shifted sine wave, respectively. The implementation block diagram is illustrated in Figure 4.5.

According to Figure 4.5, the transmit signal can be written as

$$s(t) = H_i(t)\cos(\omega_c t) - H_q(t)\sin(\omega_c t) \tag{4.7}$$

where $H_i(t)$ and $H_q(t)$ are baseband Hermite signals containing the binary information. The complex envelope representation of $s(t)$ is then

$$g(t) = H_i(t) + jH_q(t) \tag{4.8}$$

The inphase component, $H_i(t)$, can be written as

$$H_i(t) = \sum_{k=0}^{K}\sum_{n=0}^{N-1} a_{n,k} H_n(t - kT_s) \tag{4.9}$$

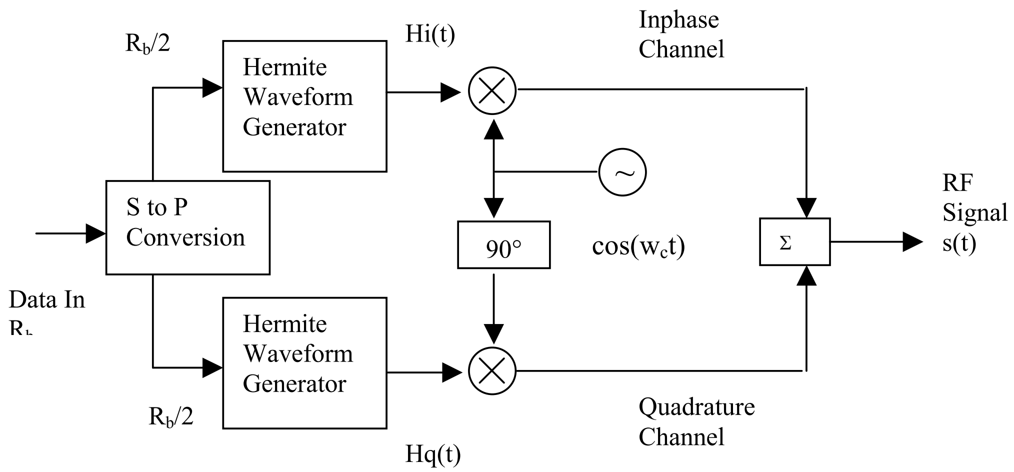

Figure 4.5 Transmission of an N-dimensional signal over an RF channel by using an amplitude modulation technique. Utilizing both inphase and quadrature components helps maximizing spectrum efficiency.

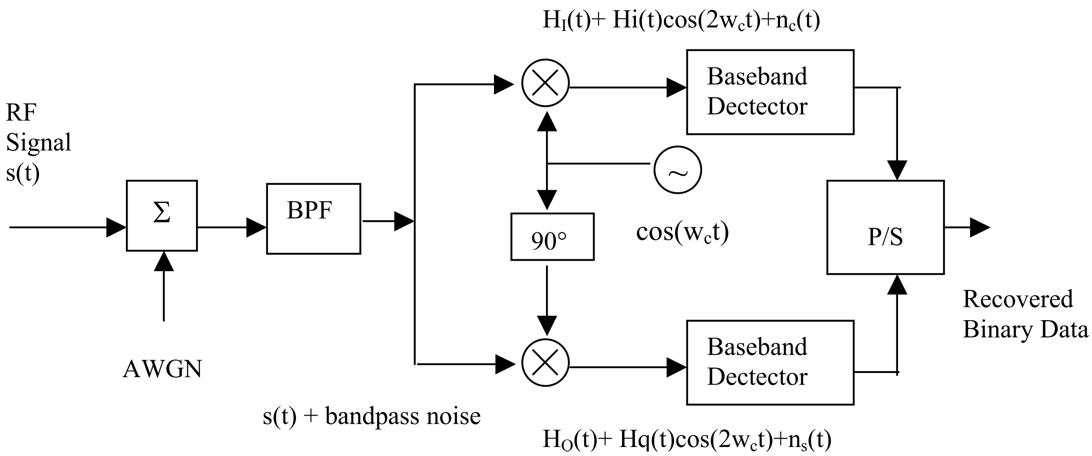

Figure 4.6 A model of an AM coherent demodulator in an AWGN channel. The baseband detector consists of an array of Hermite matched filters. The block P/S in the figure performs parallel to serial conversion.

where $H_n(t)$ is the n^{th} Hermite pulse with symbol period T_s and binary data $a_{n,k} \in \{-1, 1\}$. A similar expression can be written for the quadrature component $H_q(t)$.

Assume the system is symmetric meaning the inphase and quadrature powers are identical. One can use (4.4) and the property or the orthogonality to show that the RF transmit power is equal to $\sum_{n=0}^{N-1} \left\langle H_n^2(t) \right\rangle$. Receiver block diagram and BER performance for this RF transmission technique are discussed next.

4.4.2 **Receiver Structure and Discussion on BER Performance**

A model for AM Hermite receivers is shown in Figure 4.6. The RF transmit signal $s(t)$ is corrupted by channel AWGN right before the bandpass filter (BPF). In an ideal system, the intersymbol interference (ISI) caused by the pre-detection BPF is negligible. Assuming perfect carrier recovery, the outputs of the mixers contain both the wanted baseband signal and the high frequency components, $H_i(t) + H_q \cdot \cos(2w_c t+\theta)$. Generally, a lowpass filter is needed to remove the carrier double frequency components. However, a Hermite detector already consists of Hermite filter banks, which coincidentally behave as lowpass filters (LPF). Therefore, an additional LPF is theoretically not necessary. Finally, the two detected bit stream are combined by the parallel to serial converter.

Let us consider the output of the mixer. Assuming the high frequency component is removed, calculation of the BER is reduced to the case of baseband transmission. Therefore, the BER performance of this amplitude modulation is identical to the baseband case. For example, filtered binary phase shift keying (BPSK) signal can be viewed as an AM modulated signal of which the modulating signal is a raised cosine pulse train. The BER performance of the raised cosine pulse reflects the performance of BPSK. In fact, BER performance of any AM-based modulation techniques can be determined from the performance of the baseband modulating signal. The results of the AM Hermite system are as expected.

Using complex envelope representation, the received signal can be written as

$$y_{CE}(t) = H_i(t) + jH_q(t) + n_c(t) + jn_s(t) \tag{4.10}$$

Since the inphase (real part) and the quadrature (imaginary part) signals can be treated independently, the BER calculation can be derived from the noise immunity of the baseband signals $H_i(t)$ and $H_q(t)$. Note that complex bandpass noise $n_c(t) + jn_s(t)$ is not white throughout the entire spectrum. Nevertheless, with an ideal BPF, its spectrum is flat over the bandwidth of $H_i(t)$ and $H_q(t)$. It does not affect the BER evaluation.

4.5 Peak to Average Power Ratio

Modulated signals with non-constant envelopes undergo excessive peak to average signal ratios. The Hermite system is not an exception. Although the amplitudes of all basis pulses are constant (Walsh codes, for example), summing them up results in a waveform with amplitude variations. Hence, a non-unity peak to average power is observed. Peak to average power ratio is a common quantitative measure to determine the degree of envelope fluctuation.

Although, Hermite pulses can be fully described mathematically, the random binary data carried on the pulses makes analysis of the peak power complicated. Alternatively, a hybrid of analysis and simulation can be used to predict the peak power. In the worst case, all Hermite pulses are combined in additive fashion. Instead of adding the actual Hermite pulses, their absolute values are summed. Then the maximum of the sum is searched over the pulse period. The peak power is then determined from the square of the maximum. This approach delivers a semi-theoretical bound of the system peak to average power ratio (PAR).

Figure 4.7 illustrates the absolute value of the all Hermite pulses in a 4-dimensional system and their sum. Using this approach, the peak to average power ratio is predicted to be approximately 6, or 7.8 dB. The accuracy of the predicted method is validated by comparing the predicted peak to average power ratio with the values from simulation. The simulation monitors the peak on a long generated waveform. The results are compared in Figure 4.8. According to the results, the prediction method and the simulation results are consistent for all numbers of Hermite pulses used. Furthermore, the peak to average power ratio increases linearly as the number of Hermite pulses increases. In the 8-dimensional system, the peak to average power ratio reaches approximately 10 dB.

The simulated data suggests that the relationship between PAR and the dimension conforms to linearity. Applying Minimum Least Square Error (MLSE) technique to the simulated data, the linear relationship is modeled as

$$PAR = 1.08N + 1.68 \tag{4.11}$$

where N is the number of Hermite pulses used or the system dimension. The relationship is valid up to $N = 10$, and PAR is a linear ratio, not in decibels.

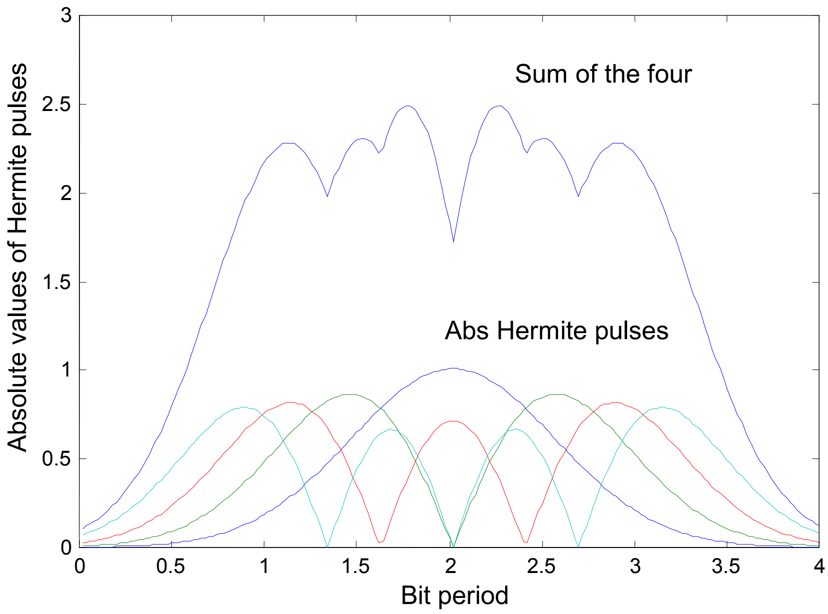

Figure 4.7 Absolute values of the first four Hermite pulses and their combination.

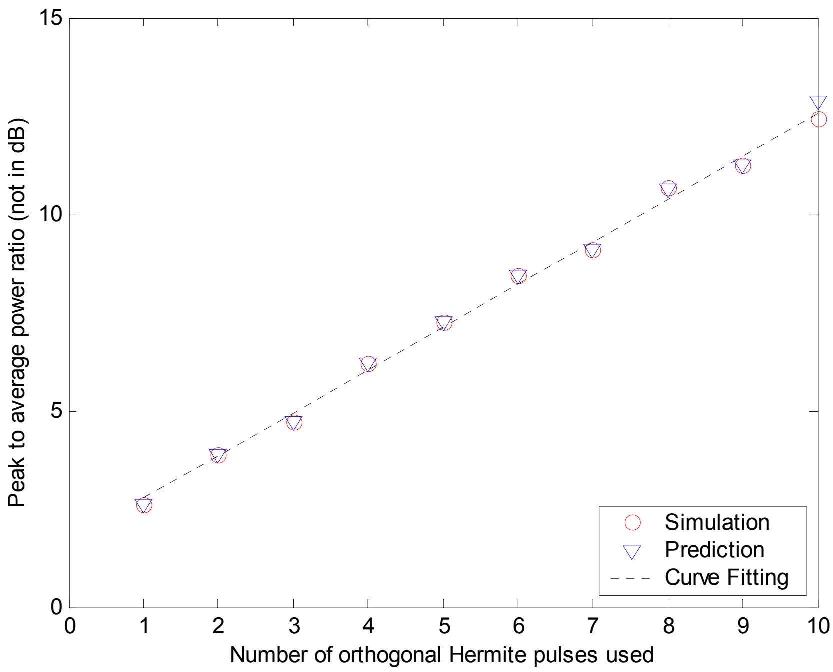

Figure 4.8 Comparison of the predicted peak to average power ratio (PAR) in linear ratio and the ratio monitored on a long transmit waveform. The dashed line is the linear estimation of the relationship between PAR and Hermite dimension (*N*).

In the antipodal Hermite N-dimensional system, N Hermite pulses span over N bit periods of the rectangular NRZ pulses. Each bit energy in Hermite system is distributed over N bit periods. N orthogonal pulses are overlaid. Thus, the added dimension extends the symbol period but the added dimension does not improve the spectral efficiency (bps/Hz). At the same time, the additional dimension introduces a peaky transmit waveform. Nevertheless, using additional dimensions does not require additional energy per bit to maintain a specific BER. The results are as shown earlier. In summary, increasing the number of pulses neither improves the bandwidth efficiency nor worsens the BER. Both spectral efficiency and BER in AWGN are independent of the number of dimensions. A longer symbol period is linearly gained from the larger dimension at the cost of higher PAR.

The idea of dimension in Hermite waveforms is different from the case of M-ary Quadrature Amplitude Modulation (QAM). In QAM, if a higher bit rate is needed, the QAM signal constellation allows more signal levels on the inphase and quadrature components. The spectral efficiency is improved by the multi-level scheme. The signal dimension of QAM is strictly 2: inphase and quadrature components, independent of the signal constellation. The drawback is that, for a fixed occupied spectrum, doubling the bit rate requires roughly 6 dB of additional energy per bit to maintain the bit error rate [ZIE92]. For example, given a fixed symbol rate, the bit rate of a 16-QAM scheme (4 bits/symbol) is 4 times that of QPSK (2 bits/symbol). For the same symbol rate, both occupy the same transmit bandwidth. However, an extra energy per bit of roughly $6\times2 = 12$ dB is needed to maintain the same BER. It is a bandwidth and power tradeoff. PAR of QPSK and 16-QAM is as high as 7 dB and 8 dB, respectively [MUR00]. Note that the symbol period of M-ary QAM does not change as M increases.

4.6 Chapter Summary

The BER performance of Hermite baseband systems was simulated. The results are consistent with the analysis. A linear modulation to carry the Hermite baseband signal over an RF channel is proposed. Complex envelope representation is briefly reviewed. Then simulation of the modulated signal is implemented using the complex envelope representation. It is found that the BER of the modulation scheme is identical to the baseband case. Peak to average power ratio of Hermite system is discussed. The chapter ends with a model of the linear relationship of PAR and the system dimension.

Chapter 5
Constant Envelope Transmission of Hermite Signals

In the previous chapter, the combination of Hermite pulses introduces a high peak to average power ratio (PAR). Using the waveform to amplitude-modulate the RF carrier does not affect the bandwidth efficiency. However, the high PAR is disadvantageous. In this chapter, the Hermite waveform is carried in the phase of the carrier. Bandwidth efficiency and BER performance in AWGN are simulated.

5.1 Relation to Existing Modulation Schemes

Many attempts have been proposed to reduce the degradation in system performance caused by the envelope fluctuations that occurs in many digital modulation formats when Nyquist filtering is employed. Offset quadrature phase shift keying (OQPSK), for example, is a successful attempt to reduce the envelope fluctuation, and improved BER performance is gained [GUN94]. Furthermore, linearly modulated signals require linear RF amplifiers. In contrast, non-linearity of the amplifiers does not seriously affect the information contained in the phase or frequency of the carrier. Thus, constant envelope modulation is power efficient in these systems[SAL94].

Minimum shift keying (MSK), one of the most popular constant envelope modulations, can be viewed as a special case of frequency shift keying (FSK). In MSK, the frequencies for mark and space are separated by one half of the bit period. MSK generation can be implemented by applying a non-return-to-zero (NRZ) waveform to an FM modulator. In conventional FSK, the FM modulator produces only two frequencies for each modulating signal level. However, the sharp transition from one to another frequency (discontinuous phase) introduces strong side lobes in the power spectral density of the signal. Continuous phase FSK and MSK are two ways to avoid this problem.

Gaussian Minimum Shift Keying (GMSK) filters the NRZ baseband waveform by a Gaussian shaping filter before applying it to the FM modulator [MUR81]. The frequency transition is smoothed and continuous phase is maintained. As a result, spectral side lobes are well suppressed. Varieties of demodulation techniques for GMSK are reported. The techniques range from a low complexity non-coherent limiter/discriminator [VAR91], multiple-symbol differential detection [ABR95] to coherent detectors [ISH84].

Instead of using a Gaussian-filtered waveform as an FM modulating signal, the baseband combined Hermite pulses are used. Let us name this system Hermite Keying (HK). There is a relation between HK and GMSK. Let us consider the 0^{th} Hermite pulse.

$$\psi_0(t) = \frac{1}{\sqrt[4]{2\pi}} \exp\left(-\tfrac{1}{4}t^2\right) \tag{5.1}$$

and the impulse response of the Gaussian lowpass filter as used in GMSK

$$h_G(t) = \frac{\sqrt{\pi}}{\alpha} \exp\left(-\frac{\pi^2}{\alpha^2} t^2\right), \tag{5.2}$$

where B_{3dB} is the 3-dB bandwidth of the filter defined by $B_{3dB} = \frac{\sqrt{\ln(2)/2}}{\alpha}$.

Obviously, both impulse responses are in the same form. From that result, Hermite pulses can be viewed as a dimensionally extended version of the Gaussian pulse. However, the generation methods of GMSK and constant-envelope Hermite signals are slightly different. In GMSK, the NRZ waveform is filtered by a Gaussian filter to form a modulating signal for the FM modulator, while in a HK system, the NRZ waveform and a single filter are replaced by impulse trains driving a bank of Hermite waveform generators. Hermite waveforms are likely to be synthesized digitally in practice. A digital to analog converter is required to convert the discrete-time waveform to a continuous-time waveform for the input of an FM modulator. Figures 5.1 and 5.2 illustrate block diagrams of GMSK and HK generations, respectively.

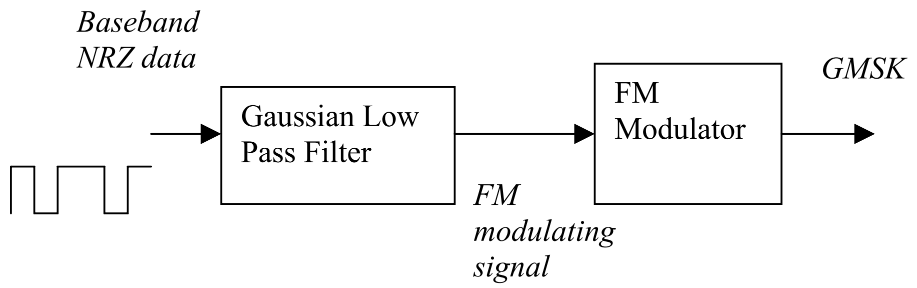

Figure 5.1 Generation of GMSK using an FM modulator. The Gaussian filter is bypassed if an FSK signal is desired.

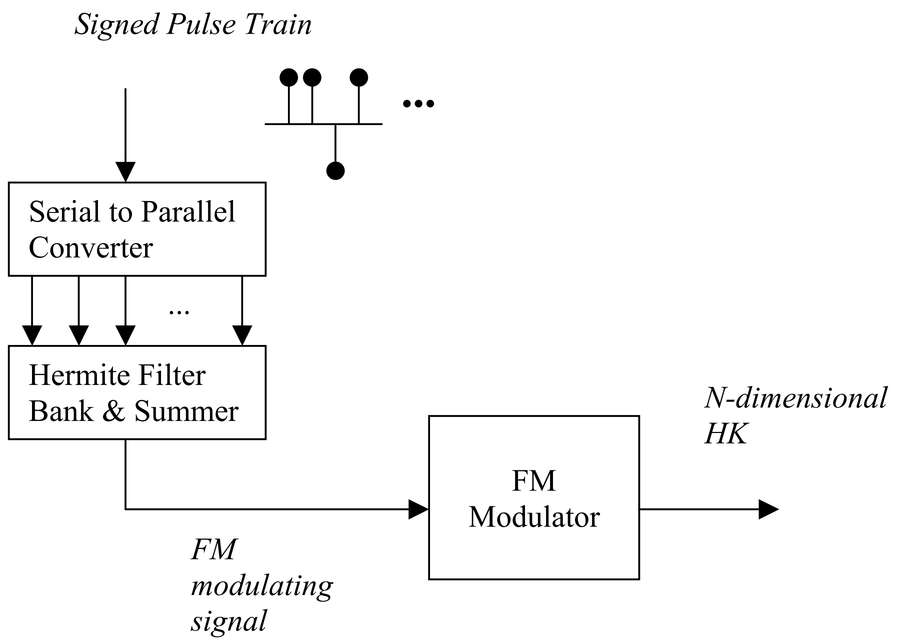

Figure 5.2 Block diagram of constant-envelope Hermite system (Hermite Keying).

5.2 Bandwidth of Constant-Envelope Hermite System

By Carson's rule, FM bandwidth is bounded by

$$B_{Tupper} = 2(\Delta f_{pk} + f_{\max}) \tag{5.3}$$

$$B_{Tlower} = 2 \cdot \Delta f_{pk} \tag{5.4}$$

where Δf_{pk} and f_{max} are the maximum frequency deviation and the bandwidth of the modulating signal, respectively. However, for the deviation ratio D defined by the ratio of Δf_{pk} and f_{max} less than one, the bandwidth is effectively restricted within $2f_{max}$ and FM modulation is categorized as narrow band. The deviation ratio can be referred to as an FM modulation index. A common notation for the FM modulation index is β_{fm}. The subscript fm implies that the modulating signal is an analog signal. .

In an MSK modulation scheme, the frequencies for spaces and marks are separated by $R_b/2$. Effectively, the maximum frequency deviation $\Delta f = R_b/4$. For the bit rate of R_b, a minimum baseband bandwidth of $R_b/2$ is required to satisfy the Nyquist criterion of zero intersymbol interference (ISI) without a multi-level scheme [NYQ28]. The digital modulation index for MSK is 0.5 [PRO95]. As in the analog case, the modulation index can also be determined from the ratio of Δf_{pk} and f_{max},

$$\beta_{digital} = \frac{(R_b/4)}{(R_b/2)} = 0.5 \tag{5.5}$$

Compared with the NRZ pulse of MSK, the pulse width of the Gaussian shaped modulating signal of GMSK is broader. The effective baseband bandwidth to drive the FM modulator decreases. Therefore, for the same maximum frequency deviation, the occupied bandwidth of GMSK is reduced. The penalty is that the narrower the bandwidth, the more ISI is introduced. BER performance deteriorates. It is a bandwidth efficiency tradeoff.

The results from Chapter 2 suggest that the bandwidth of the Hermite pulses that keeps 95% of energy in the symbol period is equal to the bandwidth of the raised cosine pulse with a roll-off factor of 0.24. At most, 5% of the leaking bit energy interferes with the adjacent symbols. Therefore, Hermite pulses should be a bandwidth-favor modulating signal for the FM transmitter. Nevertheless, Carson's rule suggests that the FM transmit bandwidth could increase if the maximum frequency deviation gets large. Unfortunately, the waveform consisting of Hermite pulses is peaky.

As discussed in Chapter 4, the Hermite waveform peak to average power ratio increases linearly with the dimension of the system. The peak of the modulating signal implies a larger maximum frequency deviation Δf_{pk} and tends to broaden the FM bandwidth. It is hope that the peaking effects on the FM spectrum are minimized with proper arrangement.

Given the carrier frequency f_c, the instantaneous phase of an FM signal in radians is written as

$$\phi(t) = 2\pi f_c t + 2\pi f_m \int_{-\infty}^{t} g(\tau)d\tau \quad \textbf{(5.6)}$$

where f_m is the maximum frequency deviation and $g(\tau)$, whose maximum absolute value is typically set to unity, is the modulating signal.

The derivative of the instantaneous phase yields the instantaneous frequency.

$$f(t) = f_c + f_m g(t) \quad \textbf{(5.7)}$$

In MSK, a special case of FM modulation, the modulating signal $g_{MSK}(t)$ is an NRZ waveform. Its instantaneous frequency, depending on the binary state transmitted, is either f_c+f_m or f_c-f_m, where $f_m = R_b/4$, one quarter of the bit rate. GMSK has a Gaussian-shaped modulation signal, $g_{GMSK}(t)$. One approach to compare the occupied bandwidth of the two is to set the maximum frequency deviation of both cases identically.

Between MSK and HK, the approach concerning Δf is not appropriate since the Hermite modulating signal is peaky. An alternative method is the constraint on identical energy per bit (E_b) in the NRZ baseband signal of $g_{MSK}(t)$, the MSK waveform and $g_{HK}(t)$, the Hermite modulating signal. This method is based on the assumption that after an FM demodulator, both systems have the same power and the BER can be fairly compared. The $g_{HK}(t)$ baseband waveform will force the carrier frequency to deviate more than the NRZ baseband waveform used to generate MSK signals. However, the high peaks of the HK modulating signal occur occasionally only in short periods. In addition, the baseband bandwidth of $g_{HK}(t)$ is narrower than that of the NRZ waveform for the same bit rate. Therefore it cannot be justified that the bandwidth efficiency of HK is worse.

The power spectral density (PSD) of an MSK waveform is described in a closed form in [GRO76]. In contrast, the PSD of a GMSK waveform is obtained from either simulation or empirical results. The spectrum depends on the 3-dB bandwidth of the Gaussian filter. In the case of HK, more parameters are involved: the dimension of HK and the constraint on the percentage of the energy in the symbol period. The former directly influences the modulating signal peak while the latter affects the bandwidth of the modulating signal (f_{max}).

The PSD of an MSK, GMSK, 4-dimensional HK and 16-dimensional HK are compared in Figure 5.3. The 3-dB bandwidth of the GMSK Gaussian filter is set to 0.5887 on the normalized scale (BT). At this 3-dB bandwidth, degradation caused by the ISI is said to be minimum [ISH80]. Both HK modulating signals are generated under a 99% symbol energy criterion. The absolute bandwidth of each participating modulation scheme is infinite. Table 5.1 lists the bandwidths in which some specific percentages of power are contained.

According to Figure 5.3, the spectrum of HK is monotonically decreasing. The overall shape looks like a triangle without both nulls and sideband ripples. Spectral superiority between MSK and HK depends on how the occupied bandwidth is defined. According to Table 5.1, the 4-HK is spectrally superior for the 90%, 95% and 99.9% energy criteria. However, if 99% is the criterion, MSK becomes preferable. GMSK is the best in terms of bandwidth efficiency among the three. In fact, GMSK bandwidth can even be lowered but it comes at the cost of higher BER due to ISI [MUR81].

Using the formula (4.11), the peak amplitude of a 16-HK modulating signal is predictably about 8 times that of the 4-HK waveform. However, the higher amplitude dynamic range of the modulating signal does not significantly expand the RF bandwidth. The bandwidths of the 16-HK and the 4-HK are trivially different. Increasing the dimension does increase the peak to average power ratio but does not change the RF bandwidth significantly.

GMSK bandwidth efficiency improves significantly if the 3-dB bandwidth of the Gaussian filter is decreased. Such a filter allows more ISI. Similarly, ISI is introduced in the Hermite system as well if the constraint on the pulse energy is relaxed. The gain is that the bandwidth of the modulating signal is lowered. The Hermite modulating signal with ISI does improve the occupied RF bandwidth but it is not as large an improvement as in the case of GMSK. Figure 5.4 illustrates the PSD of HK at various pulse energy constraints and dimensionality (the number of dimensions used). Table 5.2 summarizes the RF occupied bandwidth of the HK shown in Figure 5.4.

Modulation	Percentages of RF Power			
	90%	95%	99%	99.9%
0.59-GMSK	0.72	0.84	1.06	1.67
MSK	0.78	0.90	1.20	2.75
99% truncated 4-HK	0.79	1.02	1.55	2.17
99% truncated 16-HK	0.84	1.07	1.54	2.21

Table 5.1 Occupied RF bandwidth ($B_{RF}T$) containing at least the given percentages of the RF power. The bandwidth is normalized by R_b reported in units of BT, bandwidth-bit period product.

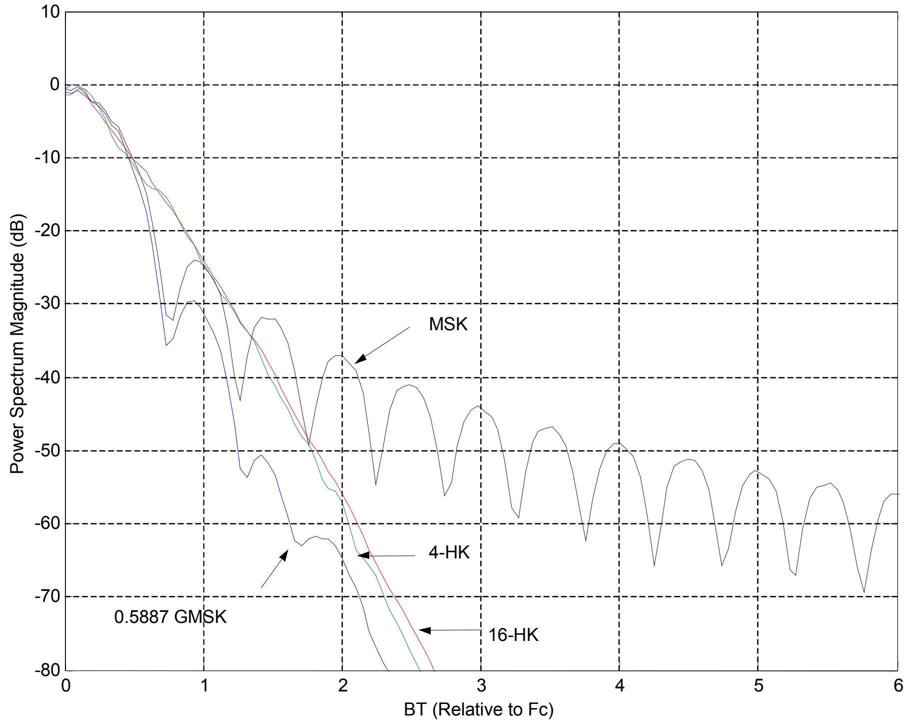

Figure 5.3 Comparison of power spectral densities of an MSK, GMSK, 4- and 16-dimensional HK. Only the upper side spectrum above the carrier frequency is shown. The abscissa is normalized by the bit rate.

Modulation	Percentages of RF Power			
	90%	95%	99%	99.9%
90% truncated 4-HK	0.82	1.02	1.40	2.00
90% truncated 16-HK	0.81	1.03	1.47	2.14
99.9% truncated 4-HK	0.79	1.07	1.66	2.40
99.9% truncated 16-HK	0.82	1.08	1.59	2.35

Table 5.2 Comparison of HK occupied RF bandwidth ($B_{RF}T$) at various constraints on percentage of pulse energy and dimensions. The bandwidth is normalized by R_b and reported in units of BT, bandwidth-bit period product.

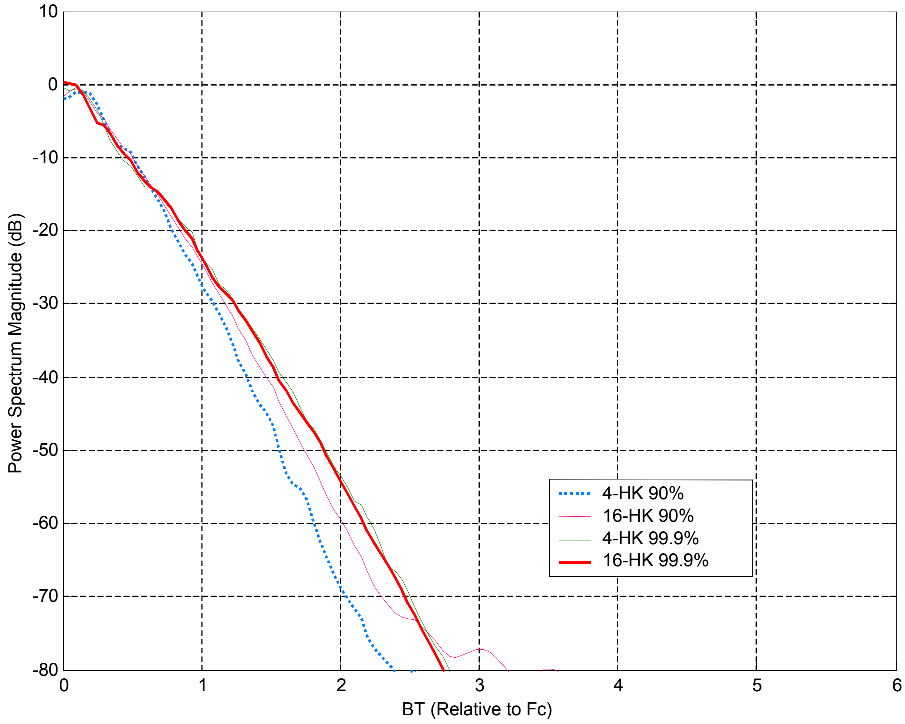

Figure 5.4 Power spectral densities of HK at various pulse energy criteria and dimensions. Only the upper side spectrum above the carrier frequency is shown. The abscissa is normalized by the bit rate.

5.3 Detection of Constant-Envelope Hermite System Signals

Matched filters are the optimal digital receiver for which the output signal to noise ratio is maximized. The minimum number of matched filters required by the optimal receiver is equal to the dimension of the system [PRO95]. Although, the dimension of a Hermite modulating signal is known, the dimension of a Hermite Keying (HK) transmit RF waveform is not obvious. Therefore it is not practical to use matched filter receivers in this case. A non-optimal but robust receiver is discussed in this section.

The complex envelope representation of an FM signal can be written as

$$s_{CE}(t) = \exp(j\phi(t) = \exp\left(j2\pi f_m \int_{-\infty}^{t} g(\tau)d\tau \right) \quad \textbf{(5.8)}$$

In an HK system, the modulating signal is described by

$$g(t) = \sum_{k=-\infty}^{K} \sum_{n=0}^{N-1} a_{n,k} H_n(t - KNT_b), \quad \textbf{(5.9)}$$

where $a_{n,k} = \pm 1$.

Consider the first symbol period in a causal system ($t \geq 0$). The complex envelope representation is reduced to

$$s_{CEsym}(t) = \exp\left(j2\pi f_m \int_0^t \sum_{n=0}^{N-1} a_n H_n(\tau)d\tau \right), \text{ for } 0 \leq t \leq NT_b \quad \textbf{(5.10)}$$

There are 2^N possible symbols of $s_{CEsym}(t)$ spanning over one symbol period, which is equal to N bit periods. Thus, the number of filters required in a matched filter receivers is 2^N, the number of possible symbols. The complexity increases by power of 2 for each additional dimension. This is a disadvantage of angle modulation compared to baseband or linear modulation, whose number of filters is linearly increased by an added dimension, i.e., N matched filters are needed for an N dimensional system.

A widely used non-coherent FM receiver is shown in Figure 5.5. The receiver makes use of a combination of a limiter and a discriminator followed by a post-detection processor. Of course, the receiver is not optimal, but it is robust. In the absence of noise, the limiter and discriminator extract the derivative of the phase, which exactly is the FM modulating signal. The post processor for the HK signal is a Hermite baseband detector. It consists of a bank of Hermite corrlelators and a sampling circuit. Note that this block diagram works with MSK as well but the Hermite detector can simply be replaced by an integrate-and-dump circuit.

If the input to the FM detector is white noise, the output of the FM discriminator is no longer white [ZEI90]. The noise at the input of the post-processor is colored. The post-processor, which is a matched filter receiver designed for AGWN, is hence not optimal. Some degradation of BER is expected.

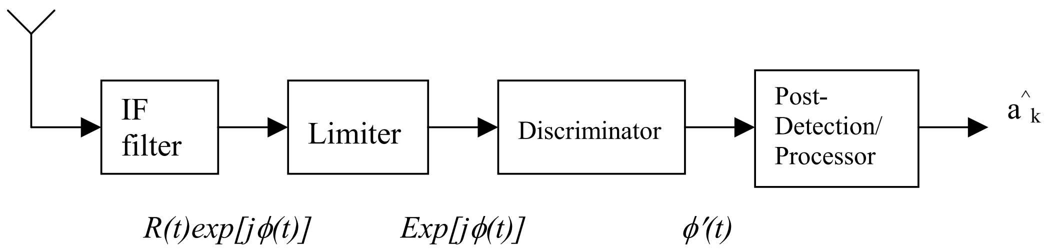

Figure 5.5 Limiter and Discriminator receiver with post processor. The signal represented in the complex envelope is italicized.

5.4 Discriminator Noise for Hermite Keying

Let $s(t) = \cos(\omega_c t + \phi(t))$ be a transmitted FM signal. The FM signal is corrupted by AWGN in the channel. The received signal at the output of the IF filter is the sum of the signal and the bandpass noise, $n(t) = n_c(t)\cos(\omega_c t) + n_s(t)\sin(\omega_c t)$.

$$r(t) = A(t)\cos(\omega_c t + \phi(t)) + n_c(t)\cos(\omega_c t) + n_s(t)\sin(\omega_c t) \quad \textbf{(5.11)}$$

where $A(t)$ is the possibly non-constant amplitude of the IF carrier . The noise terms can be rewritten as

$$n(t) = x(t)\cos(\omega_c t + \phi(t)) - y(t)\sin(\omega_c t + \phi(t)) \quad \textbf{(5.12)}$$

where

$$x(t) = n_c(t)\cos(\phi(t)) + n_s(t)\sin(\phi(t)) \quad \textbf{(5.13)}$$

and

$$y(t) = n_s(t)\cos(\phi(t)) + n_c(t)\sin(\phi(t)) \quad \textbf{(5.14)}$$

The newly rewritten form expresses the noise components relative to the modulated phasor. Thus, $r(t)$ becomes

$$r(t) = R(t)\cos(\omega_c t + \phi(t) + \theta(t)) \quad \textbf{(5.15)}$$

where

$$R(t) = \sqrt{[A(t) + x(t)]^2 + y^2(t)} \quad \textbf{(5.16)}$$

and

$$\theta(t) = \tan^{-1}\left(\frac{y(t)}{A(t) + x(t)}\right) \quad \textbf{(5.17)}$$

Assuming no fading and no effects from the IF filter, $A(t)$ is a constant. However, $R(t)$ still fluctuates because of the noise components. The derivative of the received signal is the desired signal plus frequency noise.

$$\dot{\theta}(t) = \frac{[A + x(t)]\dot{y}(t) - y(t)[\dot{x}(t)]}{R^2(t)} \tag{5.18}$$

The relative inphase and quadrature components of the noise, $x(t)$ and $y(t)$, and their derivatives are Gaussian and independent [RIC63]. The probability density function (pdf) of the frequency error is difficult to evaluate, but it looks Gaussian, especially for high signal to noise ratios or large values of the received signal amplitude A [CAS99]. This can be validated as the follows. For a large signal to noise ratio and the carrier unmodulated, i.e., $\phi(t) = 0$, A >> $x(t)$ and $y(t)$,the $\theta(t)$ and $\dot{\theta}(t)$ can be estimated by

$$\theta(t) \approx \frac{y(t)}{A} \tag{5.19}$$

$$\dot{\theta}(t) \approx \frac{K_D}{A}\frac{dn_s(t)}{dt} \tag{5.20}$$

The power spectral density (PSD) of the frequency noise is just the PSD of the derivative of the white noise process $n_s(t)$. The transfer function of the differentiator $H_{diff}(f)$ is $K_D f$. Thus, the PSD of the frequency noise, which is the output of the differentiator, becomes

$$S_{nF}(f) = \frac{K_D^2}{A^2} N_o f^2 \tag{5.21}$$

where N_o is the PSD of $n_s(t)$. Therefore, the PSD of noise from any FM demodulators is proportional to the baseband frequency squared.

Occasionally, $x(t) < -A$ and $y(t)$ goes through zero. This causes the phasor to encircle the origin rapidly. The instantaneous phase, $\phi(t) + \theta(t)$, jumps by either 2π or -2π, depending on the direction of the encirclement. The discriminator output responds to the phase jump with a spike. This phenomenon is called an FM click. Integrating the spike in the short period returns an area of $\pm 2\pi$.

In a digital FM receiver, a non-coherent detector makes use of a limiter/discriminator (L/D) and is followed by either integrate-and-dump (I&D) or sampling-and-hold (S&H) bit detection. The I&D circuit reintegrates the output of the discriminator over the bit period. The output of the S&H, on the other hand, simply takes the instantaneous frequency at the center of the bit interval. Detailed analysis can be found in [PAW88].

An MSK time waveform with bit rate of R_b can be written as

$$s_{MSK}(t) = \cos\left(2\pi(f_c \pm \frac{R_b}{4})t\right) \tag{5.22}$$

The received signal in a complex envelope form is represented by

$$s_{CE,MSK}(t) = R(t)\exp\left(\pm j2\pi\frac{R_b}{4}t + \theta(t)\right) \tag{5.23}$$

The wanted phase is $\phi(t) = 2\pi(R_b/4)t$. In the absence of noise, integrating the output of the L/D detector over the bit period $T_b = 1/R_b$ returns either $\pi/2$ or $-\pi/2$. Noise changes the output values and this is called phase noise. If strong noise is present, an FM click is likely to occur. The $\theta(t)$ quickly jumps by 2π and thus integrating $\dot{\theta}(t)$, the derivative of $\theta(t)$, over T_b or even a short period of time causes an additional $\pm 2\pi$ added to the output of the L/D with an I&D. Thus, in addition to the continuous phase noise, the clicks aggravate the BER performance. It has been concluded that for a digital modulation index of 0.7, the phase noise and the click equally contribute to the BER. The click effect dominates the BER for higher modulation indexes and the influence of the click can be neglected for lower modulation indexes [PAW99].

Click rate is a helpful too in evaluating the BER of digital FM. In Hermite Keying (HK) detection, analysis of FM clicking effects on BER is more complicated. The output of the L/D must be multiplied by a proper Hermite pulse first then I&D is performed. Assuming there is a click from the output of the L/D detector, multiplying the Hermite pulse weighs the spike. Hence, the integral of the weighed spike is not always $\pm 2\pi$. Depending on its location, the spike could be cancelled out by a zero in the multiplying Hermite pulses or amplified by the pulse. Although the click rate can be determined, it is still complicated to evaluate the BER degradation due to the click on HK system. Nevertheless, there are various FM threshold extension methods to combat the clicks [POL88].

Because of the linearity of Hermite correlators, the pdf of the noise at the output of the correlator preserves the Gaussian distribution property. The PSD of the input noise is not white and is described by (5.21). The PSD of noise at the output of the n^{th} Hermite correlator becomes

$$S_{o,n}(f) = |H_n(f)|^2 \, S_{nF}(f) \tag{5.24}$$

$$= |H_n(f)|^2 \, \frac{K_D^2}{A^2} N_o f^2 \tag{5.25}$$

where $H_n(f)$ is the transfer function of the n^{th} Hermite correlator.

The integral of $S_{o,n}(f)$ over frequency yields the noise output power, which directly affects BER. Although the output powers of all Hermite correlators driven by an impulse (flat spectrum) are equal, the inputs to the filters are not white - they exhibit the classical baseband frequency squared dependence of all FM demodulators. The output noise power of one Hermite correlator differs from another Hermite filter. Therefore the BER observed for different dimensions is not identical. Note that in the linear modulation discussed in Chapter 4, BER is independent of dimensionality.

An ideal transfer function to minimize the noise output should have an amplitude response of the transfer function packed about zero (DC), where the input noise power density is minimum. The 0^{th} order Hermite correlator matches that requirement. Unfortunately, the higher the order of the filter, the more the transfer function is distributed away from DC. As a result, more noise is present at the output of the FM demodulator for the higher order filters. Therefore the BER corresponding to a high order waveform is worse than that of the lower orders. Dimensionality plays an important role in BER of angle modulated Hermite system.

5.5 Power Spectral Density in Hermite Keying Systems

Rather than attempting an analysis, simulation is used as a tool to evaluate BER performance of Hermite Keying (HK) in AWGN. First, the relationship between signal to noise ratio (S/N) and bit energy to white noise density ratio (E_b/N_o) is discussed. Then, an investigation addresses FM noise power and spectra at the input and output of the Hermite filters (the post processing unit). Finally, system performance is evaluated by simulation of BER versus E_b/N_o. The results are then compared to the BER performance of the linear modulation.

5.5.1 Relationship between Power to Noise Ratio and Bit Energy

Signal power and bit energy are related by

$$S = \frac{E_b}{T_b} \tag{5.26}$$

where T_b is the bit duration.

If AWGN is filtered by a brick-wall IF bandpass filter with bandwidth B, noise power at the output of the filter becomes

$$N = BN_o \tag{5.27}$$

Hence, the signal to noise ratio and bit energy are related by

$$\frac{S}{N} = \frac{E_b / T_b}{BN_o} \tag{5.28}$$

In the cases of raised-cosine filtered BPSK and QPSK, noise equivalent bandwidth is equal to the transmit symbol rate, independent of signal bandwidth or the roll-off factor of the raised-cosine filter. The S/N is simplified to E_b/N_o and $2E_b/N_o$ for BPSK and QPSK, respectively [PRA86].

Assume a brick-wall RF bandpass filter with a cut-off frequency of kR_b is used in the Hermite FM system. Using (5.28), the relationship between E_b/N_o and S/N becomes

$$\left(\frac{E_b}{N_o}\right)_{HK} = k\frac{S}{N} \tag{5.29}$$

Since the absolute bandwidth of the HK waveform is infinite, the percentage of the signal power in the band is used to define HK bandwidth. The parameter k is determined from the percentage used to define the HK bandwidth. For example, assume 99.9% of signal power is used as the bandwidth constraint. From Table 5.1, signal bandwidth for 4-HK is $1.55R_b$. The constant k in (5.29) is then 1.55. Compared with BPSK/QPSK, the noise bandwidth of an FM Hermite system is quite broad. In this particular setup, S/N is not completely described without specifying what the corresponding IF bandwidth is. On the other hand, E_b and N_o are independent of the filter. Consequently, E_b/N_o is employed to compare BER throughout this chapter.

5.5.2 **Noise Power at Post Processing Outputs**

A demonstration of how FM noise power unequally distributes and unevenly affects the dimensional BER of a Hermite system is as follows. As shown in Figure 5.6 with the switch is set to A, an unmodulated carrier is sent to an AWGN channel. At the receiver end, an IF filter and limiter/discriminator (L/D) are chosen as an FM demodulator. The signal from the FM demodulator is then passed to a Hermite post-processing unit. If noise is non-existent, the L/D returns zero and so do the Hermite correlators. In the presence of noise, the noise PSD at the output of the L/D follows a square law and its power is reciprocal to the carrier power. Since there is no information carried in the carrier, the output of the post-processing unit is due to the noise only. The noise power levels at the output of different Hermite filters are then compared.

Switching to Position B, the desired signal without noise is received. The output from the FM detector is the linear combination of signed Hermite pulses. The transmitted data bits are obtained by sampling the outputs of the post-processing unit. The system gain is set so that the noise-free sampled output values are unity. Fixing the system gain, with the switch at Position A, noise power at the output of the Hermite signal detector is computed from the time average of the squared output. The output signal to noise ratio (SNR) of the Hermite filter outputs is defined by the ratio of the unity signal power and the noise power.

Figure 5.7 (a) and (b) illustrate the PSD of the FM noise at the output of the L/D detector for an unmodulated FM signal corrupted by AWGN at E_b/N_o of 3 dB and 10 dB, respectively. Comparing Figure 5.7 (a) and (b), the PSDs are similarly shaped but the PSD corresponding to E_b/N_o of 10 dB is further suppressed (less power) and looks less white than the PSD corresponding to E_b/N_o of 10 dB. Also shown in the figures, the noise PSD at the outputs of filters are shaped differently, depending on the Hermite correlator transfer functions. The low order noise powers are less than the power of the higher orders. For example, the PSD level at the output of the 0^{th} filter is less than that of the 3^{rd} and 7^{th} filters. The results are emphasized when the E_b/N_o get large, e.g., 10 dB. The simulation results agree with the analytical prediction discussed earlier in the section.

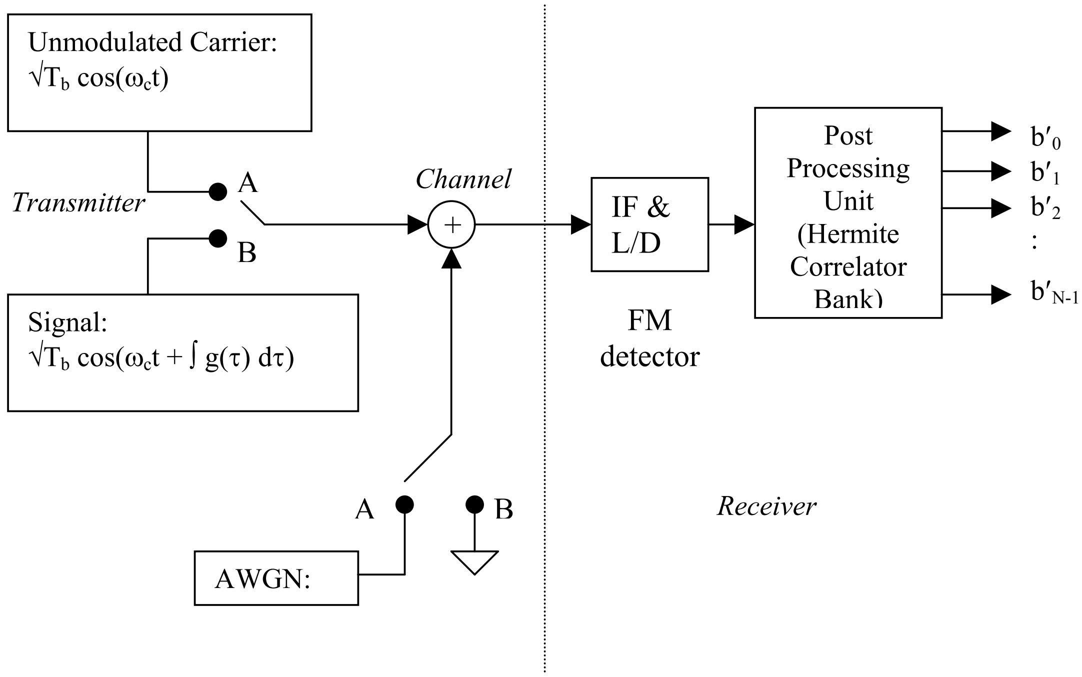

Figure 5.6 Block diagram to examine the noise PSD at the output of the FM limiter and discriminator (L/D) detector and at the output of the post-processing Hermite filters. Switch A allows unmodulated carrier plus AWGN to be passed to L/D detector. Switch B passes the HK modulated signal without noise to the receiver. The signal powers in both case are T_b. With this setup, unity bit energy, E_b, is constrained.

At low E_b/N_o, the input to the L/D is almost noise only. The noise PSD at the L/D output preserves the flat spectrum. High E_b/N_o de-whitens the PSD at the output of the L/D. Transfer functions of distinct Hermite correlators frequency-selectively react to the input colored noise. As a result, the differences of the noise power at the outputs of distinct Hermite correlators are emphasized. Figure 5.8 compares the SNR at the outputs of an 8-dimensional Hermite post-processor for some E_b/N_o. At low E_b/N_o, 0 dB, for instance, the SNR at the output of the 0^{th} and the 7^{th} correlators are almost identical. However, at 13-dB E_b/N_o, the difference between the two is as high as 12 dB. Note that the simulation turns the noise off when an HK signal is being transmitted. The noise at the correlator outputs is determined based on transmission of an unmodulated carrier at the same power as the HK signal.

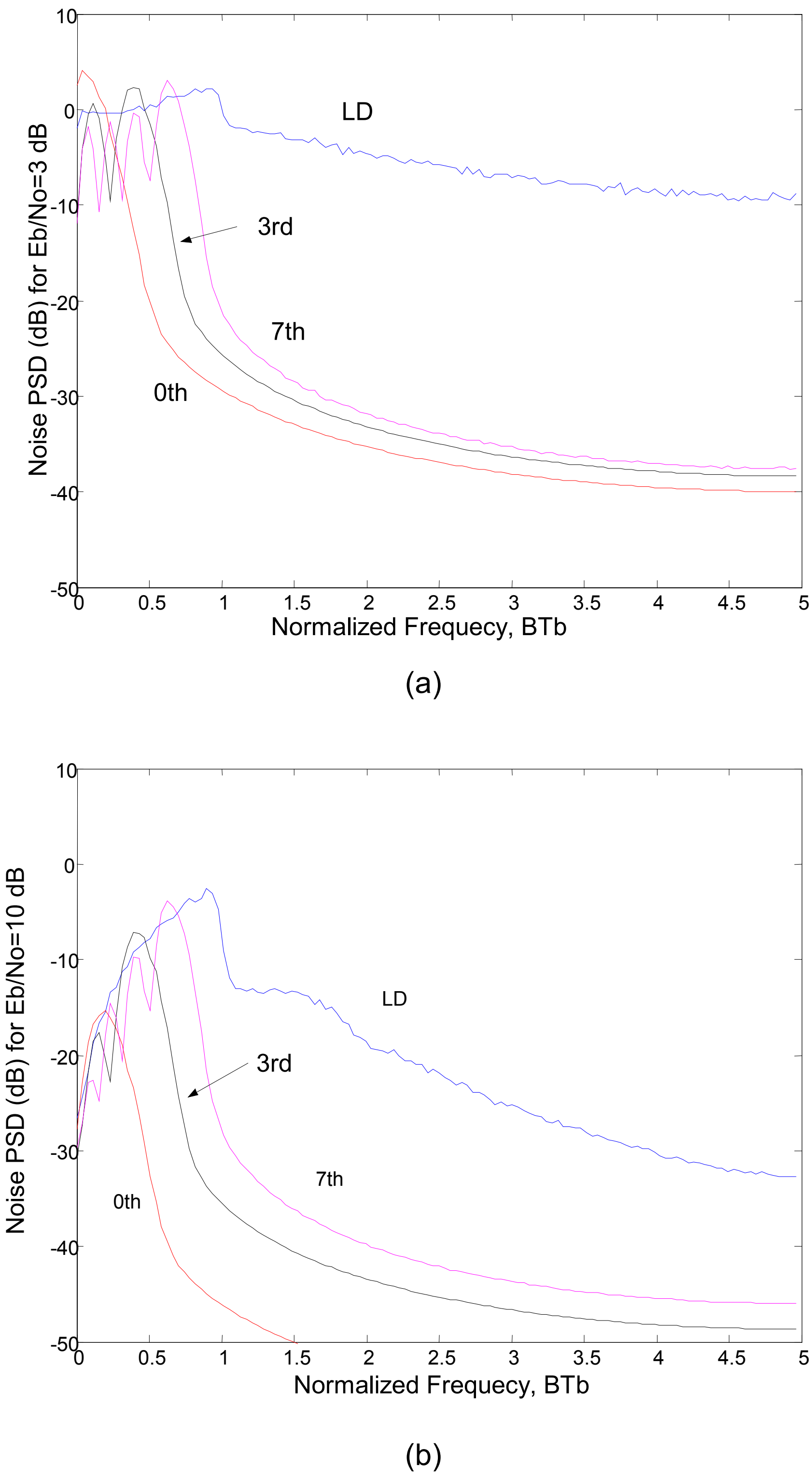

Figure 5.7 Noise PSD at the output of L/D detector and at the outputs of 8-dimensional Hermite detecting correlators given E_b/N_o of (a) 3 dB and (b) 10 dB.

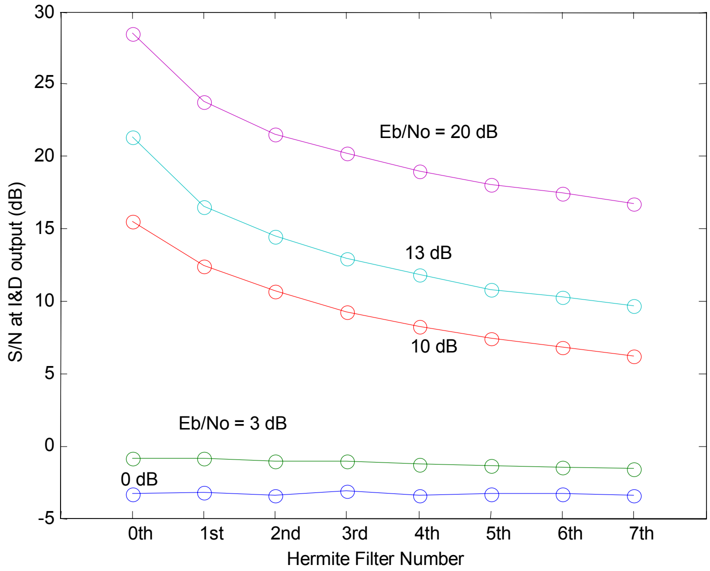

Figure 5.8 Signal to noise ratio at the output of the Integrate-and-Dump (I&D) detectors listed dimension-wise at various input E_b/N_o. The setup is as shown in Figure 5.6.

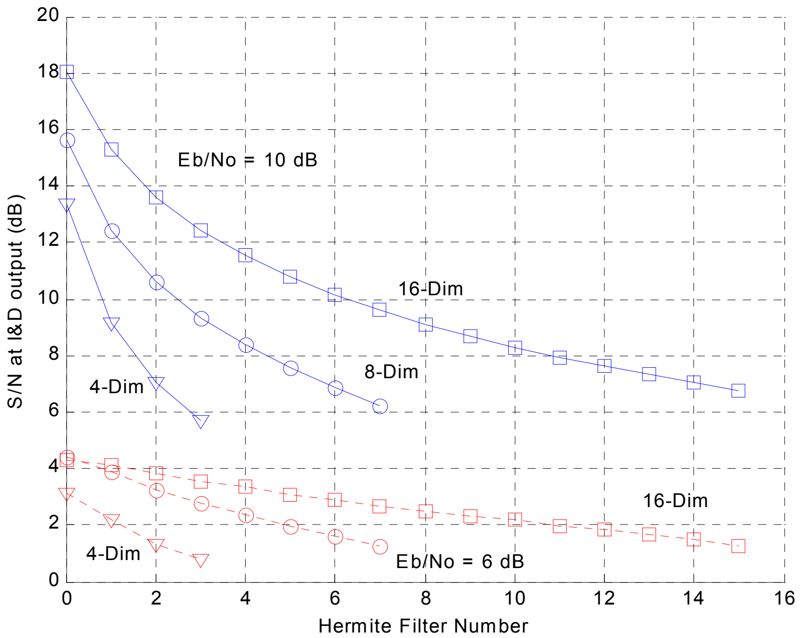

Figure 5.9 Comparison of the I&D output SNR for 4-, 8- and 16-dimensional systems. For the same transmit E_b/N_o, the highest orders of the system (3^{rd}, 7^{th} and 15^{th} for 4-, 8- and 16-dimensional, respectively) share almost identical output receiver E_b/N_o.

Figure 5.9 compares the SNR at the outputs of the Hermite correlators for 4-, 8- and 16-dimensional systems. The simulated results suggest that for the same transmit E_b/N_o, the highest order correlators for all systems deliver about the same output SNR. For example, at E_b/N_o of 10 dB, the output SNR of the 3rd correlator in the 4-dimensional system and the ratio of the 7th correlator in the 8-dimensional system are about the same.

5.6 BER of Hermite Keying System

In the previous section, noise at the output of the limiter/discriminator detector is colored. More specifically, the noise PSD increases proportional to the frequency. Hermite matched filters, optimal receivers for AWGN, are no longer optimal filters in this colored noise. Consequently, the analytical relationship between BER and the input SNR derived for AWGN, as in Chapter 4, does not apply. Nevertheless, the noise power present at the output of high order Hermite filters is greater than at lower order outputs. Therefore, BER on higher order dimensions is expected to be larger.

A configuration of an HK transmission system is shown in Figure 5.10. The diagram also includes an optional preemphasis and deemphasis circuits, which can be implemented either in continuous or discrete domain. The block diagram suggests alternative points where the digital/analog conversion can be placed. In simulation for BER, all signals are converted to complex envelope representation to avoid sampling at the double the carrier frequency. The noise is also represented by a band-limited baseband complex signal, whose PSD is brick-wall like. BER is determined and recorded dimension-wise. The results are shown in Figure 5.12 and Figure 5.13.

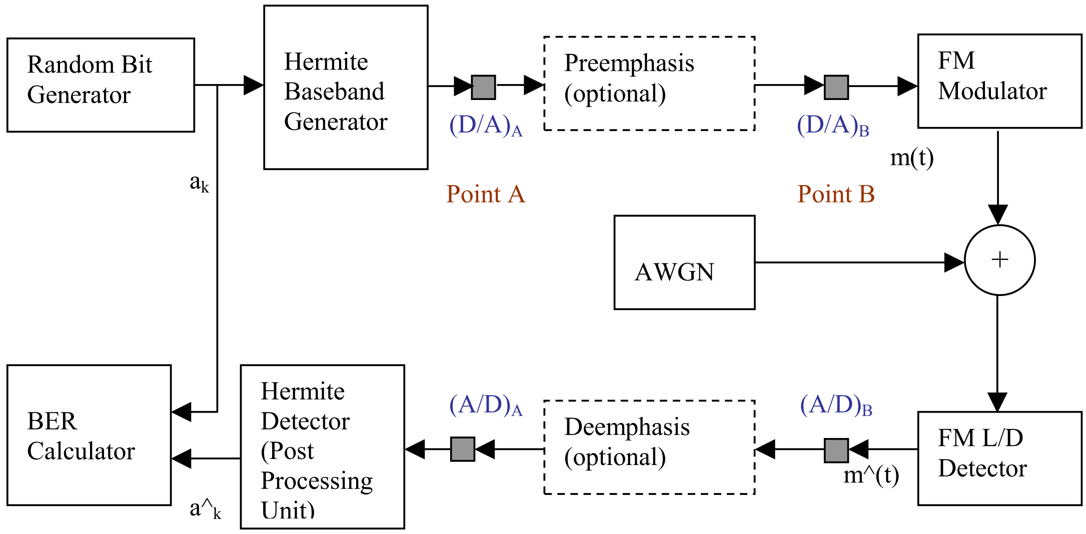

Figure 5.10 An implementation block diagram of Hermite Keying system with BER evaluation. The preemphasis and deemphasis are optional and can be implemented either in continuous (D/A at Point A) or discrete (D/A at Point B) domain.

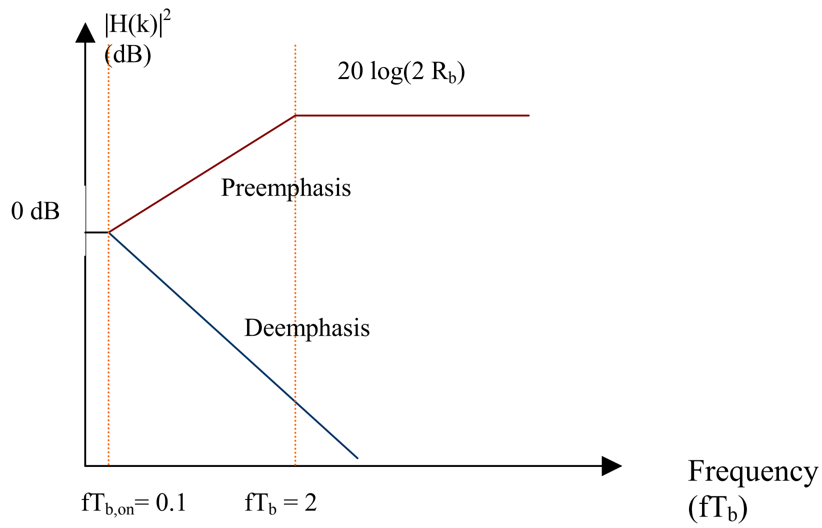

Figure 5.11 Amplitude responses of discrete-time preemphasis and deemphasis filters. The cut-off frequency chosen at $fT_b = 2$ is well above the Hermite modulating signal bandwidth. With digital filter allows placing the cut-on frequency arbitrarily close to DC ($fT_b = 0$).

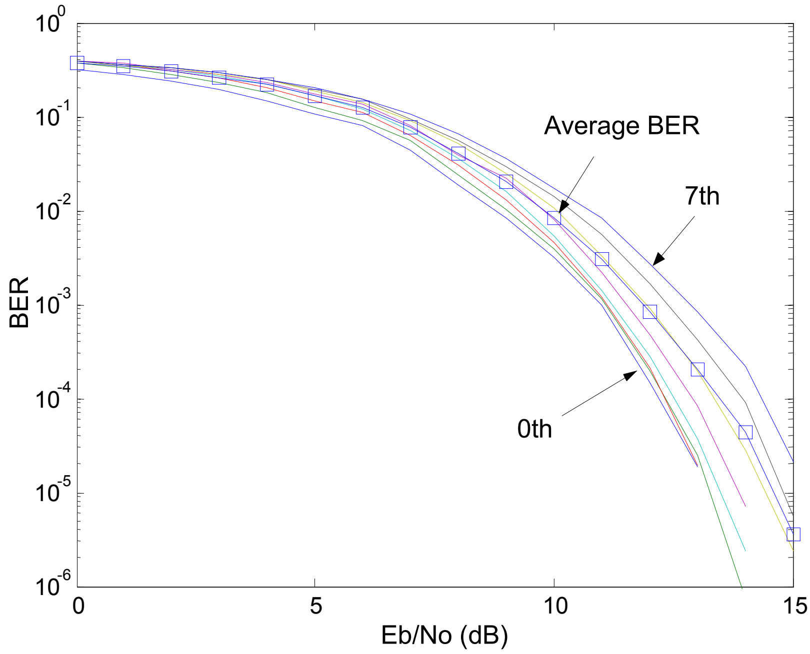

Figure 5.12 BER of an 8 dimensional HK. The higher order dimensions yield worse BER. To achieve a BER of 10^{-6}, the 0^{th} dimension requires E_b/N_o less than 14 dB while the 7^{th} dimension needs about 17 dB. The required powers are different by 3 dB. The system does not invoke pre/deemphasis.

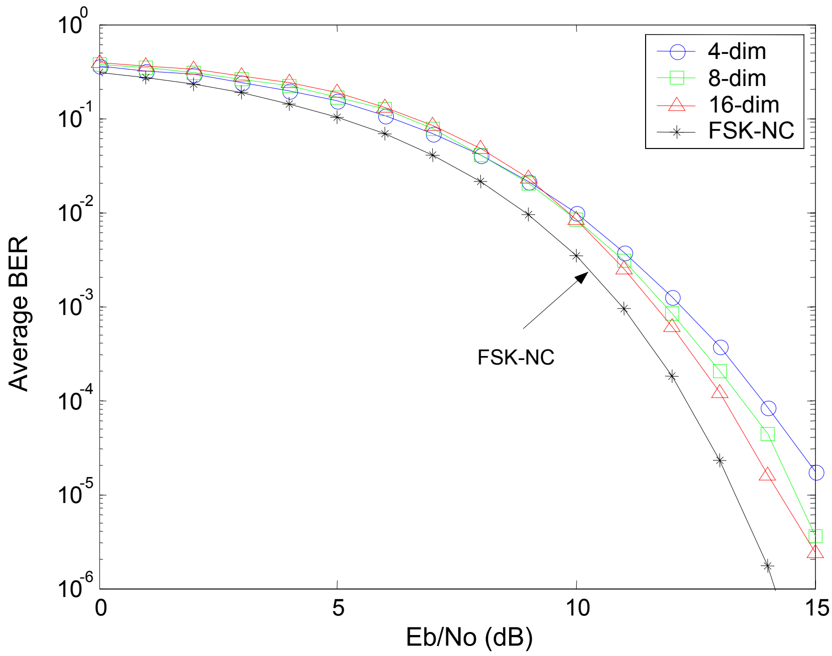

Figure 5.13 Average BER of different dimensional system compared to non-coherent FSK. To achieve a BER of 10^{-6}, the 8- and 16-dimensional Hermite Keying systems require about 2 dB more power than the FSK does. The average BER of the 4-dimensional system is the worst. Compared with the FSK, additional power of 3-4 dB is needed**.**

Figure 5.12 shows BER of an 8-HK transmit signal versus E_b/N_o. In this simulation, the system does not invoke preemphasis. It is assumed that the RF bandwidth is $2R_b$, which certainly covers almost 99.9% of the signal bandwidth. No other effects of the RF filter are taken into account in this simulation. In fact, the simulator represents the filtered AWGN by a baseband complex envelope representation. Effectively, the cut-off frequency is R_b. According to Figure 5.12, the BER of the 7th dimension is the highest as anticipated. The average BER conforms to the BER of the 5th dimension.

Figure 5.13 compares the average BER of 4-, 8- and 16-HK. At E_b/N_o under 10 dB, the simulated BER of all HK systems are roughly the same. When E_b/N_o gets larger, dimensionality starts to improve the BER. A BER of 10^{-5} is achieved by an E_b/N_o of 14 dB and 15 dB on the 16- and 4-dimensional systems, respectively.

BER of non-coherent FSK is written as [COU93]

$$P_{e,FSK-NC} = \tfrac{1}{2}\exp\left(-\tfrac{1}{2}\frac{E_b}{N_o}\right). \qquad \textbf{(5.30)}$$

Compared with the HK, non-coherent FSK outperforms HK for all E_b/N_o simulated. However, the HK is simulated without preemphasis/deemphasis. An improved HK system is investigated in the next section.

5.7 BER Improvement by Preemphasis/Deemphasis

In analog FM, signal to noise ratio at the output of the detector can be improved if preemphasis and deemphasis are used [COU93]. Deemphasis is basically a lowpass filter at the output of the FM demodulator, which suppresses the large amount of high frequency FM noise. A filter with a transfer function proportional to $1/f$ exactly neutralizes the increasing noise power with frequency. A side effect is that the deemphasis also lowers high frequency components of the wanted signal as well. The problem can be cured by pre-distorting the modulating signal by using a proper highpass filter so that there is no net effect on the signal after the deemphasis process. A typical preemphasis and deemphasis magnitude response pair is illustrated in Figure 5.11. The filters can be simply implemented by RC circuits [ZIE90]. However, it is recommended to implement the preemphasis/deemphasis digitally since the Hermite filters are in digital format already.

BER performance improvement gained from the pre/deemphasis for an 8-dimensional HK is illustrated in Figure 5.14. Comparing to Figure 5.12, the BER associated with the low order dimensions are hardly improved. In contrast, considerable improvement is gained on the high order dimensions. The pre/deemphasis narrows the differences of BER among the dimensions. The average BER of the systems with pre/deemphasis and the analytical BER of non-coherent FSK are compared in Figure 5.15. The pre/deemphasis considerably reduces the required E_b/N_o for BER = 10^{-5}, up to 1 dB in the 4-dimensional system. The improvement obtained from the pre/deemphasis on the 8- and 16-dimensional system are not as much as on the 4-dimensional system. Nonetheless, the simple pre/deemphasis system brings the BER of HK system close to the BER of the non-coherent FSK.

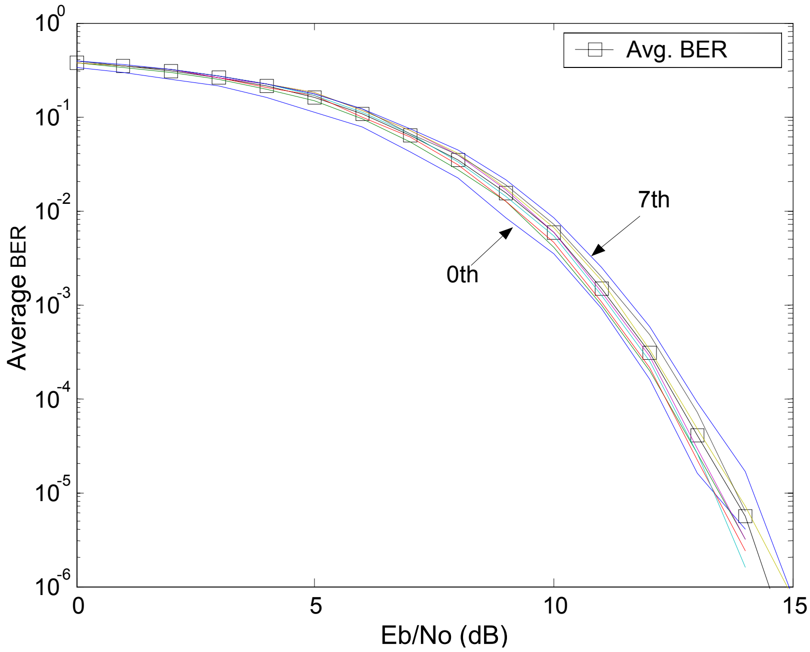

Figure 5.14 BER of 8-HMSK with pre/deemphasis listed in dimension order. Little BER improvement is found on the 0^{th} dimensional BER but the 7^{th} dimensional BER is significantly improved. The gap between the two is considerably narrowed.

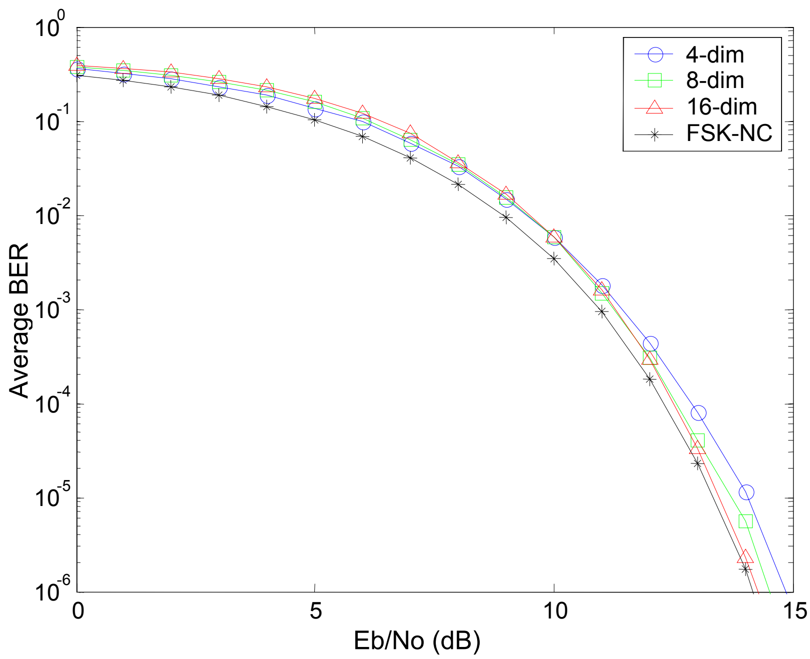

Figure 5.15 Comparison of average BER when pre/deemphasis are used. BER of HK comes close to that of non-coherent FSK. BER of noncoherent GMSK depends on the constraint on the BT bandwidth. The best performance is about the same as that of FSK [ELT89].

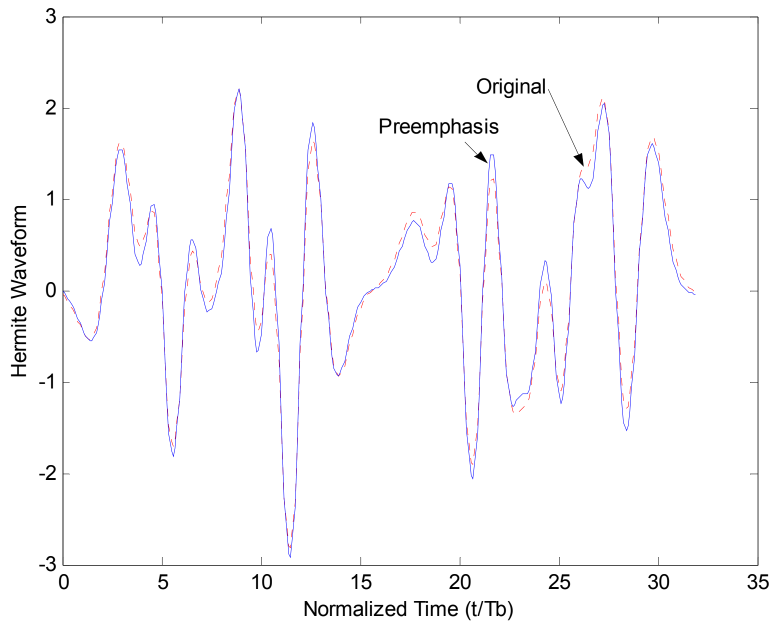

Figure 5.16 Comparison of Hermite baseband waveform (dotted) and pre-emphasized waveform (solid). The pre-emphasized waveform is attenuated so that both waveforms share an identical power. Signal powers after the FM demodulator in both cases are equal.

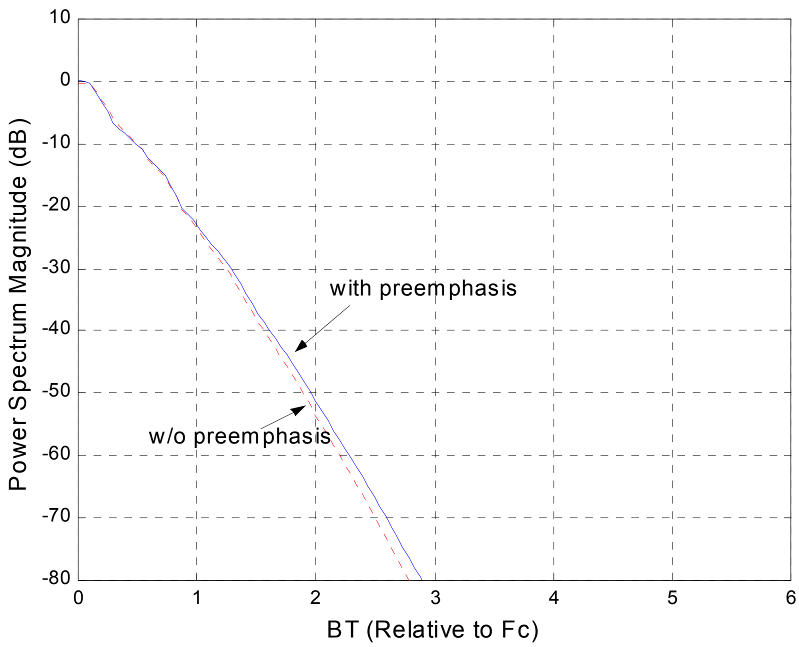

Figure 5.17 Comparison of bandwidth efficiencies of 16-HK signals with and without preemphasis. The preemphasis introduces trivial effects on the transmit bandwidth.

The presence of the simple pre/deemphasis shows the promise of BER improvement, especially on the high E_b/N_o. However, the modules are not yet optimized. Properly designed pre/deemphasis modules could further lower the BER of HK, especially on a larger dimensional system.

Another concern is focused to the penalty on RF bandwidth introduced by the preemphasis. The preemphasis amplifies the high frequency component of the FM modulating signal. Hence, the RF bandwidth is possibly expanded. Fortunately, the simulation results show that the expansion of the RF bandwidth is insignificant. Figure 5.16 compares the original baseband Hermite modulating waveform and the pre-emphasized waveform. The pre-emphaized waveform is attenuated to maintain the same power as the original waveform. As a result, the FM demodulated waveforms at the receiver for both cases are identical. Figure 5.17 illustrates the minimum change in the RF spectrum when the preemphasis is used.

The PSD is not the only concern on the RF spectrum allocation. The PSD implies the average deviation. The maximum instantaneous frequency deviation is also important. The filter with cutoff frequency set at the HK bandwidth will remove some portion of the power from the transmitted or received signal. The maximum frequency deviation of HK can roughly be estimated by the peak to average power ratio (PAR) discussed in Chapter 4. For example, an 8-dimensional HK has a PAR of 10.28. The maximum to average frequency deviation ratio is roughly 3.2. A distortion free filter must allow more than 3 times the average bandwidth for the HK waveform. Nevertheless, the occurrence statistics of the maximum deviation is not studied in this dissertation. These statistics would be useful to predict the degradation due to filtering. In the simulation, only noise is filtered to fit into the signal bandwidth while the wanted signal is not filtered. Taking the filtering into account, the overall BER performance will certainly degrade because of the frequency deviation beyond the filter cutoff frequency.

5.8 Chapter Summary

In this chapter, Hermite waveforms are used as a modulating signal in FM systems. The system is named Hermite Keying (HK). The bandwidth is compared to MSK and GMSK. SNR at the outputs of the FM limiter/discriminator and Hermite baseband detector are investigated. BER of the HK is compared with non-coherent FSK. The BERs for each dimension of the HK signal are not identical because of the uneven SNR at output of Hermite baseband detector. Significant BER improvement is achieved by using pre/deemphasis. It is shown that the pre/deemphasis has insignificant effect on HK transmit bandwidth.

Chapter 6
Performance in a Mobile Satellite Channel

In a mobile communication system, blocking of the signal, and signal arrival via multipath are persistent problems. Multiple copies of the transmit signal possibly arrive at the receiver at different times. The delay on the multipath severely degrades the communication link, especially when it becomes large relative to the symbol period. Hermite pulses span, depending on the system dimension, over some certain bit periods. Consequently, for the same delay spread, the ratio of delay and symbol period is reduced. Possibly, the degradation caused by the delay diminishes in Hermite transmit systems. The immunity to delay spread of Hermite system is investigated in this chapter.

6.1 Choice of Channel Model

A number of mobile channel models are proposed for different kinds of communication links. A model of a cellular communication channel treats the received signal as the sum of three components: the wanted signal in the main path, its delayed multipath signal and a co-channel interference signal. Each signal envelope is Rayleigh distributed and the phase is uniformly distributed over $(0, 2\pi)$ [RAP02]. Additionally, the signal powers vary rapidly (fast fading). It has been shown analytically that BER degradation due to multipath, when $\pi/4$ differential quadrature phase shift keying ($\pi/4$-QPSK) is used as the modulation technique, increases as the ratio of delay spread to symbol period increases [LIU90]. The results are confirmed by simulation in [FUN93]. As a result, high data rate transmission, with its short bit period, undergoes more severe BER degradation.

Instead of using the cellular channel, a mobile satellite channel is chosen. The mobile satellite channel consists of a direct lognormal path and a Rayleigh-distributed delayed multipath [LOO85]. The difference between the cellular model and the mobile satellite model is in the characteristics of the direct path component. The direct path of the mobile satellite model is assumed to be under shadowing. The net result is that its amplitude varies lognormally. However, the model does not include the effects of random phase on the direct path. In contrast, the power envelope of the main path in the cellular channel is Rayleigh distributed and the carrier phase is also random. Since the aim is to investigate the benefits of the spread symbol period using Hermite Keying (HK) against the distortion caused by the delayed multipath component, the less complicated mobile satellite model is the better choice.

6.2 Brief Survey of Non-Frequency Selective Mobile Satellite Fading Channels

Many mobile satellite models assume no multipath delay. Available models are surveyed in this section. Without the multipath delay, the received power fluctuates but the waveform is not distorted. The channel is considered a flat or non-frequency selective channel. On the other hand, if the received waveform is distorted by the delayed multipath component, the channel is said to be a frequency selective fading. BER performance of the HK technique in the frequency selective fading is investigated in the section after next.

Signal fading in mobile communications can be categorized into two types: large-scale fading and small-scale fading. The large-scale fading reflects the statistical path loss attenuation caused by prominent terrain contours. This kind of fading is usually referred to as shadowing [SKL97a]. Shadowed paths introduce variation of the mean of the local received power. Lognormal is widely accepted as best describing the distribution of the shadowing phenomenon in space [JAK74]. Meanwhile, rapid and dramatic changes in the received signal power experienced over short travel distances is called small scale fading. Either speed of the transceiver or radio multipath propagation can influence small scale fading. The envelope of the resulting power is commonly described by a Rayleigh distribution. The Rayleigh distribution is modeled on the assumption that no non-fading dominant path exists.

Mobile-to-satellite communication channels experience both kinds of fading. A model by Loo [LOO85], splits the received power into LOS and multipath components. The model assumes that only the LOS path is under shadowing and log-normally distributed. Meanwhile, the multipath obeys the Rayleigh distribution with constant power. The total received power is just the sum of the two components. Loo's model is suitable for rural environments. There is no multipath delay in Loo's model.

Based on statistics from data recorded, a model by Lutz et al. [LUT91] makes use of the states of the mobile. If the mobile is in an unobstructed area, for example, the channel is modeled as the sum of a direct path from satellite and Rayleigh distributed signals reflected from a number of surrounding objects. As a consequence, the resulting amplitude of the received signal is a Ricean process. On the other hand, if the mobile is under shadowing, the received signal power is described by a conditional Rayleigh distribution with a mean that varies lognormally. The distribution parameters depend strongly on satellite elevation angles. Most of the time, mobiles travel across unobstructed and shadowing areas. Details on superimposing the two distributions along with the distribution parameters are provided in the literature [LUT91].

Later, a Rice lognormal model was published [COR94]. The model extends Loo's assumption by adding lognormal fading on both direct and diffuse paths. By tuning the model parameters, the model is claimed to fit all types of environment (rural, suburban and urban). Furthermore, the model is valid for both terrestrial and satellite links. Suzuki model [SUZ77], a widely accepted model for urban areas, views the fading channel as a Rayleigh lognormal process. It is, in fact, a special case of a Rice Lognormal Model. In addition, Loo and Rice Lognormal models are shown to be a merged model [VAT95].

The above channels are not modeled with multipath delay. The models focus on the statistic of the received power. The transmitted bits are prone to be erroneous when the received power fades. However, if a long delay is experienced via multipath, the channel encounters frequency-selective fading. The combination of the wanted (direct) path and the delayed path introduces a distorted received signal. Additional degradation of BER performance of the system is expected.

Note that a BER performance degradation under frequency selective fading is analyzed by Liu and Feher [LIU91]. In the analysis, $\pi/4$ QPSK is transmitted to a two-ray modeled channel with delay on the multipath. The analytical results conclude that the degradation of BER is affected by the longer delay on the multipath channel and the power ratio of direct and multipath (C/M). An interesting result is that for the same C/M, irreducible BER, or BER floor, increases proportionally with the delay. Simulation results in [FUN93] agree with Liu and Feher's analysis. In Hermite Keying (HK), symbol periods span over several bit periods. Tolerance to frequency selective fading possibly improves. However, waveform distortion does affect the orthogonality of the Hermite pulses. The interaction of the two on BER performance is investigated in the following sections.

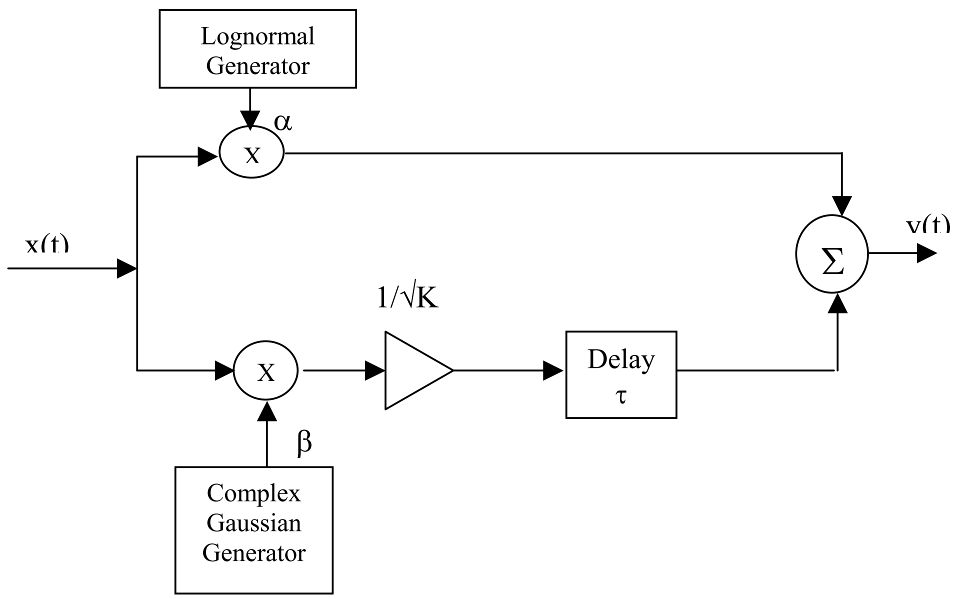

Figure 6.1 A frequency-selective fading model for a mobile satellite channel.

6.3 Frequency-Selective Mobile Satellite Channel Model

Extended from the Loo's model [LOO85], a model for mobile satellite communication channels under frequency-selective fading is developed [DEG95]. The model is shown in Figure 6.1. According to the model, the direct path component is under shadowing. Its received signal power obeys lognormal fading. Meanwhile, the scattered path is delayed and Rayleigh distributed.

Let $x(t)$ and $y(t)$ be the complex envelope representation of the input and output of the channel, respectively. The channel output $y(t)$ can be expressed by

$$y(t) = \alpha(t)x(t) + \tfrac{1}{\sqrt{K}}\beta(t)x(t-\tau) \tag{6.1}$$

where $x(t)$ is the input signal, $\alpha(t)$ is the lognormal shadowing process, $\beta(t)$ is a zero-mean, unity-power complex Gaussian process with independent real and imaginary components, τ is a fixed time delay and K is the ratio of the direct power to the multipath power..

The $\alpha(t)$ is, basically, a time-varying envelope of the transit signal $x(t)$. Lognormality implies that X_{dB}, the envelope power of $x(t)$ in decibels, defined by $20\log(\alpha(t))$, is normal or Gaussian distributed with mean μ_{dB} and variance $(\sigma_{dB})^2$.

$$X_{dB} = 20\log\alpha \sim N(\mu_{dB}, \sigma_{dB}) \tag{6.2}$$

The subscript dB reflects the way the lognormal distribution is defined by definition of decibels. The shadowing multiplicative factor $\alpha(t)$ can be generated indirectly through a Gaussian process.

$$\gamma(t) \sim N(\mu_\gamma, \sigma_\gamma) \tag{6.3}$$

where $\mu_\gamma = \mu_{dB}$ and $\sigma_\gamma = \sigma_{dB}$

The subscript dB is replaced by γ in order to be consistent with the one used in the literature. The standard deviation σ_γ is usually referred to as dB spread. The lognormal $\alpha(t)$ process is related to $\gamma(t)$ by

$$\alpha(t) = 10^{\gamma(t)/20} \tag{6.4}$$

In analysis, the natural logarithm is more convenient than the base 10 logarithm. Let X_{ln} be a logarithmic quantity defined by $\ln(\alpha)$. X_{ln} and X_{dB} are related by

$$X_{\ln} = \frac{\ln(10)}{20} X_{dB} \tag{6.5}$$

X_{ln} is now Gaussian distributed with mean and variance defined respectively by

$$\mu_{\ln} = \mu_{dB} \tag{6.6}$$

$$\sigma_{\ln}^2 = h^2 \sigma_{dB}^2 \tag{6.7}$$

where $h = \ln(10)/20 = 0.115$. Therefore, $\alpha(t)$ can be alternatively generated by

$$\alpha(t) = \exp[\lambda(t)] \tag{6.8}$$

where $\lambda \sim N(\mu_{\ln}, \sigma_{\ln})$.

Depending on which mean and variance system is chosen, the probability density function (pdf) of α can be written in various ways. A widely adopted pdf is described by [LOO91]

$$p(\alpha) = \frac{1}{\sqrt{2\pi}\sigma_{\ln}} \cdot \frac{1}{\alpha} \exp\left[-\tfrac{1}{2} \left(\frac{\ln \alpha - \mu_{\ln}}{\sigma_{\ln}} \right)^2 \right] \quad \textbf{(6.9)}$$

On the scattered path, the envelope of the complex Gaussian process $\beta(t)$ is Rayleigh distributed [PAP65]. The signal strength of the path of this model is controlled by the path gain $1/\sqrt{K}$. The envelope of the signal from the scattered path is then delayed by τ. The non-zero τ introduces the frequency-selective characteristics of the channel.

In summary, the carrier to multipath ratio (C/M) in dB is defined by

$$\left[\frac{C}{M} \right]_{dB} = 10 \log_{10} K + \mu_\gamma + \frac{\sigma_\gamma^2}{20 \log_{10} e} \quad \textbf{(6.10)}$$

If a clear line of sight (LOS) exists, both μ_γ and σ_γ are zero. C/M then depends only on K, the power ratio of the direct and scattered path components. Moreover, the channel is completely frequency-flat fading if the delay spread τ is zero. A channel with C/M lower than 5 dB is considered as being under heavy multipath condition [DEG95].

A set of measured data reported in [LUT91] are selected and shown in Table 6.1. These parameters depend on types of antennas used, satellite elevations and environments. In clear view, the Rice factor is used. Conversely, in deep shadow, the channel is modeled as lognormal (μ_{10} and σ_{10}). Note that unlike many authors, the lognormal parameters in [LUT91] are defined over dB power. The ratio of the clear view and deep shadow for a mobile traveling in an environment with a satellite angle is shown in the column of Time under Shadowing. Nevertheless, the measured parameters do not complete the model in Figure 6.1 since the delay on the multipath channel is not yet included.

Table 6.1 Ricean and lognormal parameters selected from [LUT91]. All parameters are selected for an identical type of antenna. The lognormal parameters μ_{10} and σ_{10} are defined over lognormal received power P, 10 $\log_{10}(P)$.

Satellite Elevation	Environment	Time under Shadowing	Direct to Multipath Ratio (Rice-factor)	Lognormal Mean, μ_{10}	Lognormal σ_{10}
13°	Highway	24%	10.2 dB	-8.9 dB	5.1 dB
13°	City	89%	3.9 dB	-11.5 dB	2.0 dB
24°	Highway	25%	11.9 dB	-7.7 dB	6.0 dB
24°	Old City	66%	6.0 dB	-10.8 dB	2.8 dB
34°	Highway	0.8%	11.7 dB	-8.8 dB	3.8 dB
34°	City	58%	6.0 dB	-10.6 dB	2.6 dB
43°	Highway	0.2%	14.8 dB	-12.0 dB	2.9 dB
43°	City	54%	5.5 dB	-13.6 dB	3.8 dB

6.4 Summary of System Parameters Used in Simulation

According to the mobile satellite model, many parameters can be varied. They are listed as the follows:

1. The AWGN floor, N_o.
2. The shadowing mean and dB spread of the lognormal direct path: μ_{dB} and σ_{dB}.
3. The power ratio of the direct and scattered path C/M. It is indicated by K in Figure 6.1.
4. The delay spread τ on the scattered path. Together with the symbol period T, the ratio τ/T, which indicates the degree of frequency-selectiveness, is formed.
5. Dimension of the Hermite signals. This directly affects the τ/T ratio.

The constant envelope Hermite Keying (HK) defined in Chapter 5 with pre/deemphasis is the input of the channel. Chapter 5 discusses the BER performance of the HK in AWGN. This chapter extends the BER performance evaluation to a frequency-selective fading channel. In addition to AWGN, the received HK signal is impaired by the amplitude variation and the delayed multipath. A worse BER is expected. A few parameters are examined at a time. Then, the interacting effects of the parameters for the more complete model are close up.

6.5 BER Degradation due to Slow Lognormal Fading

Assume the multipath does not exist, i.e., the channel is lognormal. Let $P_e(E_b/N_o)$ be a BER for the given E_b/N_o for an unvarying channel. Lognormal channels fluctuate the E_b/N_o and hence the associated BER. Theoretically, the overall probability becomes

$$P_{e,LN} = \int_0^\infty p(\alpha) P_e(\alpha^2 E_b / N_o) d\alpha \qquad \textbf{(6.11)}$$

where α is lognormally distributed. However, closed forms of the analytical BER are generally complicated and not provided for all modulation techniques. Simulation is an alternative to determine the BER, and was used in this investigation of mobile satellite channels.

The lognormal channel used in the simulation is illustrated in Figure 6.2. Pre/deemphasis units are used on the 8-HK transmitter/receiver. With them, the BER of the 8-dimensional HK is, as shown in Chapter 5, slightly worse than for non-coherent FSK. The link is assumed to be slow fading. Thus, the received power level $\alpha^2(t)$ does not change during the symbol period. In our simulation, the power level is randomized every two symbol periods.

The simulation assumes that an E_b/N_o of 15 dB is received if the channel experiences no fading. At 15 dB, BER of 10^{-6} is guaranteed on the 8-HK system. Taking lognormal fading into account, the mean powers in dB (μ_{dB}) are set to drop from the unfaded power (E_b/N_o of 15 dB) by 3 levels: 0, 3 and 6 dB. The simulated dB spreads (σ_{dB}) vary from 0-8 dB. The simulation BER results are illustrated in Figure 6.3.

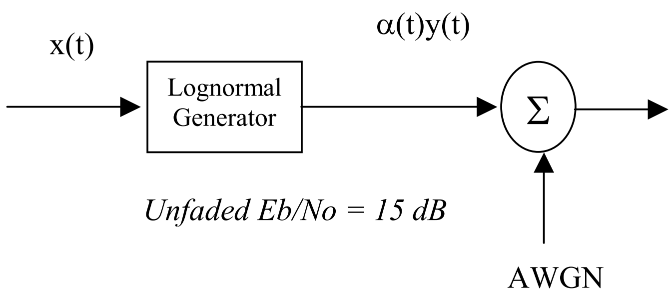

Figure 6.2 Model of the slow lognormal fading channel used in the simulation. The received signal envelope $\alpha(t)$ is lognormally distributed. The system invokes pre/deemphasis.

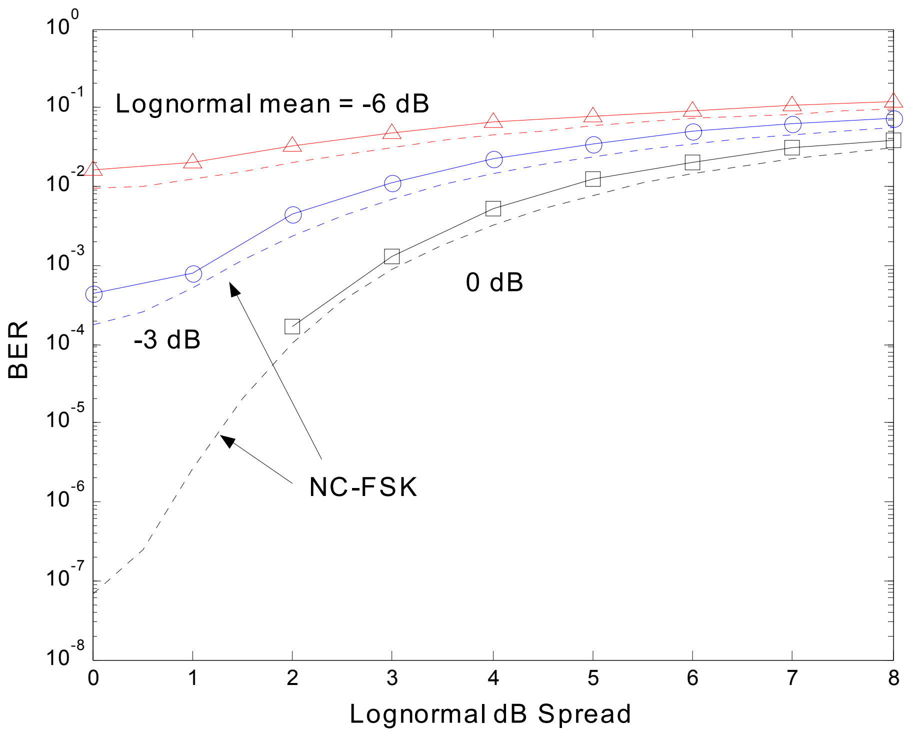

Figure 6.3 BER of a simulated 8-dimensional Hermite Keying (8-HK) in lognormal fading channels, assuming unfaded *Eb*/*No* of 15 dB. The dashed lines are the BER of non-coherent FSK in the same channel obtained from the numerical integration method. In Chapter 5, the BER of the NC-FSK in AWGN is slight better than the BER of 8-HK. The same statistic of the received signal power variation maintains the slight advantage of NC-FSK over the 8-HK.

The BER for equivalent links using non-coherent FSK is also included in Figure 6.3. The plots are numerically generated, for the given E_b/N_o of 15 dB and lognormal parameters, by using the probability of error in lognormal channel defined in (6.11), with probability of lognormal factor $p(\alpha)$ and the analytical BER of FSK defined in (6.9) and (5.30), respectively.

$$p_{FSK,LN}(\zeta,\sigma_{\ln},\mu_{\ln}) = \int_0^\infty \frac{1}{\sqrt{2\pi}h\sigma_{dB}} \cdot \frac{1}{\alpha} \exp\left[-\tfrac{1}{2}\left(\frac{\ln\alpha - \mu_{dB}}{h\sigma_{dB}}\right)^2\right] \times 0.5 \cdot \exp\left(-0.5\alpha^2\zeta\right) \cdot d\alpha \qquad \textbf{(6.12)}$$

where $\zeta = E_b/N_o$. This simulation has an E_b/N_o of $10^{(15/10)} = 31.6$.

Compared with the simulated overall BER of HK, the FSK slightly outperforms. As concluded in Chapter 5, the BER of the FSK is slightly better than of the 8-HK with the simple pre/deemphasis. Therefore, the simulation results are not surprising.

6.6 Degradation due to Delayed Multipath

Assume the Rayleigh scattered path is present without delay ($\tau = 0$). The channel is a frequency-flat channel. Depending on the characteristics of the direct path, the channel model illustrated in Figure 6.1 turns into either a simple Ricean channel or a lognormal satellite mobile channel. In the case of the Ricean channel, the power on the direct path is constant. In contrast, the direct path power of the latter is lognormal. The probability density functions of the received signal envelope, $p(\alpha)$ for both cases are provided in [LOO91]. As long as the BER can be written in terms of E_b/N_o, the BER of the link can be obtained by numerical integration similar to the calculation of FSK in a lognormal channel in the previous section.

Analysis becomes more complicated in the presence of delay spread on the scattered path. Analytical BER for specific modulations and model channels have been published. For instance, BER of π/4-QPSK in a Rayleigh frequency selective fading channel is analyzed in [LIU91]. However, in the HK case, the analytical relationship between BER and E_b/N_o in a closed from is not available. Simulation is a quick approach to determine the BER performance of the system, especially when many channel parameters are varied.

6.6.1 Effects of Direct Path to Multipath Power Ratio (C/M)

Let us maintain the constancy of the power on the direct path and remove the AWGN (infinite E_b/N_o). No co-channel interference is assumed. The signal dispersion is affected only by the multipath. Three parameters to be examined are then

(a) the delay spread τ

(b) the power ratio of the direct and multipath K and

(c) the dimension of the HK system.

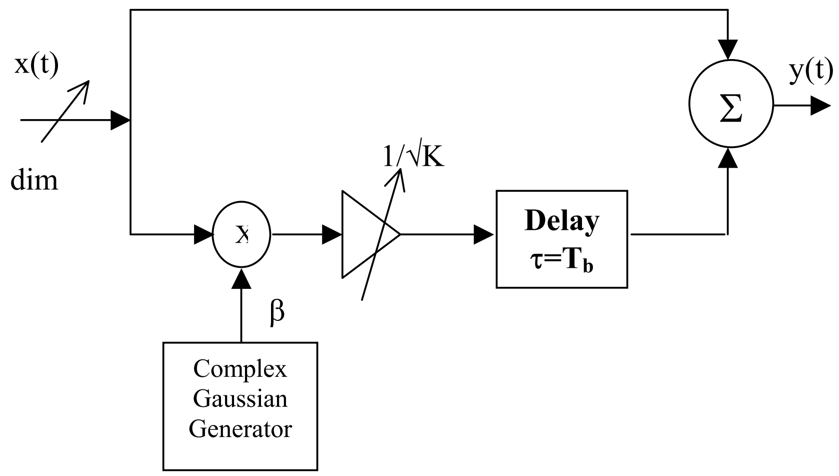

Figure 6.4 Block diagram for a frequency selective fading channel simulation. The direct path is free of fluctuation and the delay spread is fixed to T_b. No AWGN is assumed. The results are shown in Figure 6.5 and Figure 6.6.

The first investigation fixes the delay spread to one bit period ($\tau = T_b$) and varies the direct path carrier to multipath power ratio (C/M) from 0 to 10 dB. The BER performance is simulated on 1-, 4- and 8-dimensional systems. The simulation block diagram is summarized in Figure 6.4. Figure 6.5 lists the BER of a 4-HK link dimension-wise. The average BER of different dimensional systems are compared in Figure 6.6. In this simulation, the system is not affected by noise. The received signal is distorted by the delayed copy of itself via the multipath. The average BER of the four systems increases as the power of the multipath decreases. As shown in Figure 6.5, the BER on the 0^{th} dimension of the 4-dimensinal system is the least. The results are consistent with HK in AWGN.

According to Figure 6.6, under C/M of 7 dB, the numbers of dimensions used do not significantly affect the average BER. At higher C/M, using the 1-dimensional system shows a BER advantage over the 4- and 8-dimensioanl systems. Nevertheless, the disadvantage of the larger dimensional systems is subtle if the channel undergoes deep lognormal fading (C/M < 5 dB).

An interesting result is on the BER of the 0^{th} dimension. The BER improves significantly as the number of dimensions grows. Especially, in low C/M, the 0^{th} order waveform of the 8-dimensional system tolerates the frequency selective fading better than the 0^{th} order waveform of the 4-dimensional system. As a result, one advantage of the larger system is that the information carried on the 0^{th} dimension is secured in frequency selective fading. Thus, the 0^{th} dimension can be used to keep the most important bits in some applications; for example, the most significant bit of a datum acquired from sampling images, or the addresses in a data packet. Therefore dimensionality does help in this application.

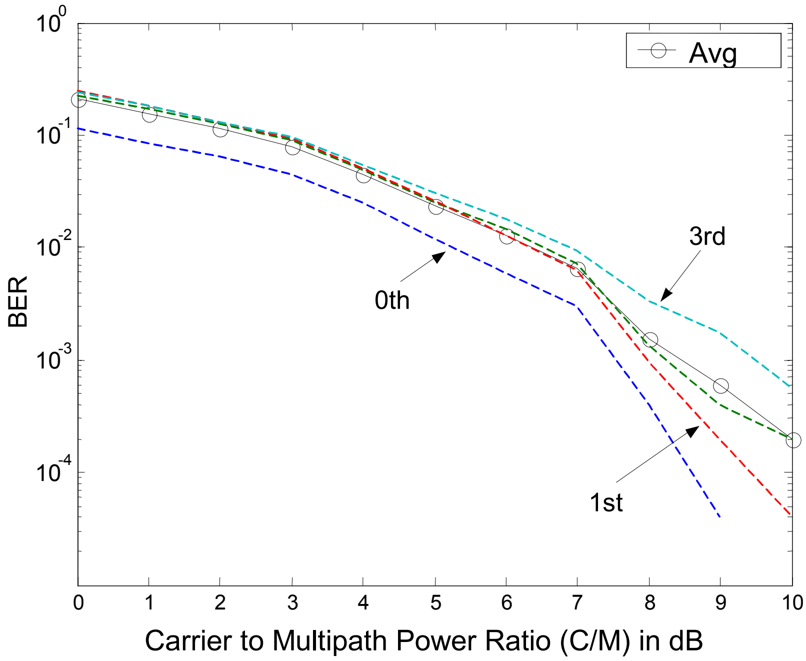

Figure 6.5 BER vs. Carrier to multipath power ratio (C/M) of a four-dimensional system listed by dimension. The delay on the Rayleigh multipath is fixed at the bit period, $\tau = T_b$. Infinite E_b/N_o and no lognormal effect on the direct path are assumed.

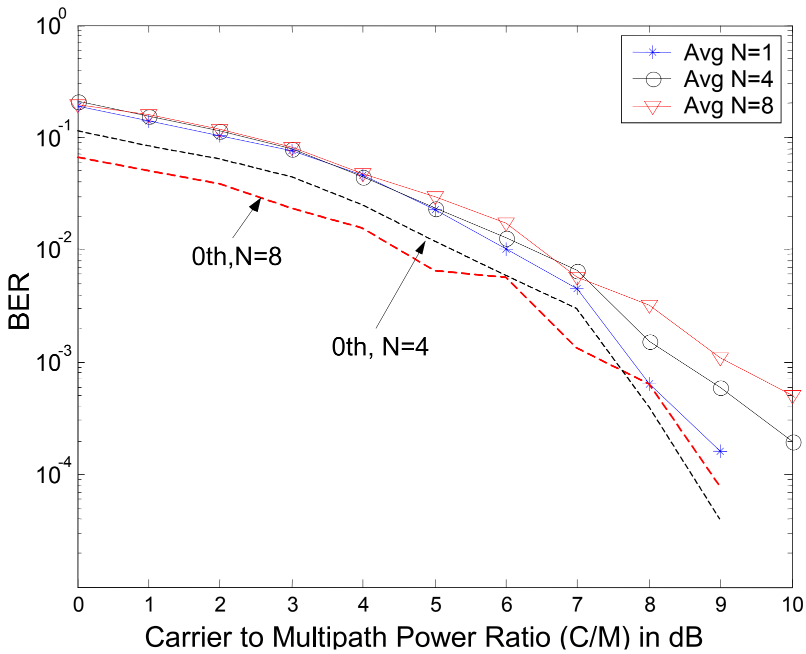

Figure 6.6 Comparison of the average BER of 1-, 4- and 8-dimensional systems. Under C/M of 7 dB, the average BER are roughly the same. However, the BER associated with the lowest (the 0^{th}) dimension, illustrated by the dashed lines, improves on the 8-dimensional system. The assumptions used are as of Figure 6.5.

6.6.2 Effects of Delay Spread

The previous section concludes that the higher the C/M, the lower the BER. In this section, C/M is fixed to 6 dB and the delay spread varies from $0.1T_b$ to T_b. The set up is as depicted in Figure 6.7 and the resulting BER are illustrated in Figure 6.8 and Figure 6.9.

According to Figure 6.8, the average BER increases as the delay spread increases. Again, the 0^{th} dimension of the 4-dimensional system yields significantly better BER margin compared with the BER of the other higher dimensions. As shown in Figure 6.9 the margin of the BER of the 0^{th} dimension and the average BER is emphasized in the 8-dimensional system. Dimensionality helps in securing the information carried on the 0^{th} dimension. Note that in the 8-dimensional system, no error is found on the channel with multipath delay of $0.1T_b$. The simulator monitors over 10 million trial bits.

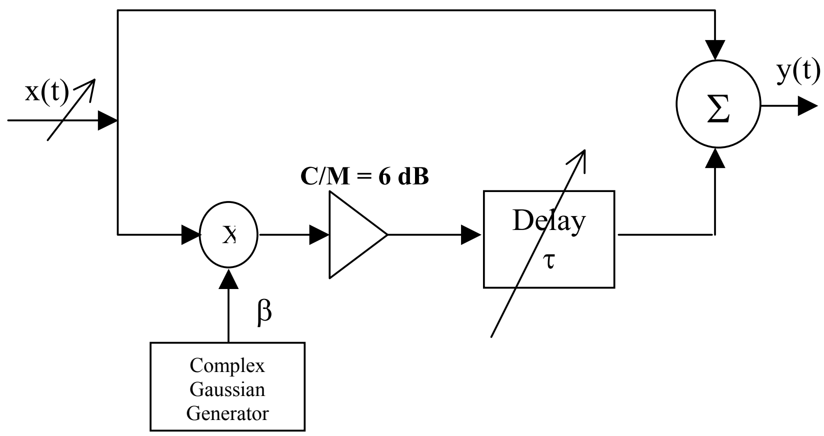

Figure 6.7 Block diagram for a frequency selective fading channel simulation. The direct path is free of fluctuation and the direct to multipath power ratio is fixed at 6 dB. The results are shown in Figures 6.8 and 6.9.

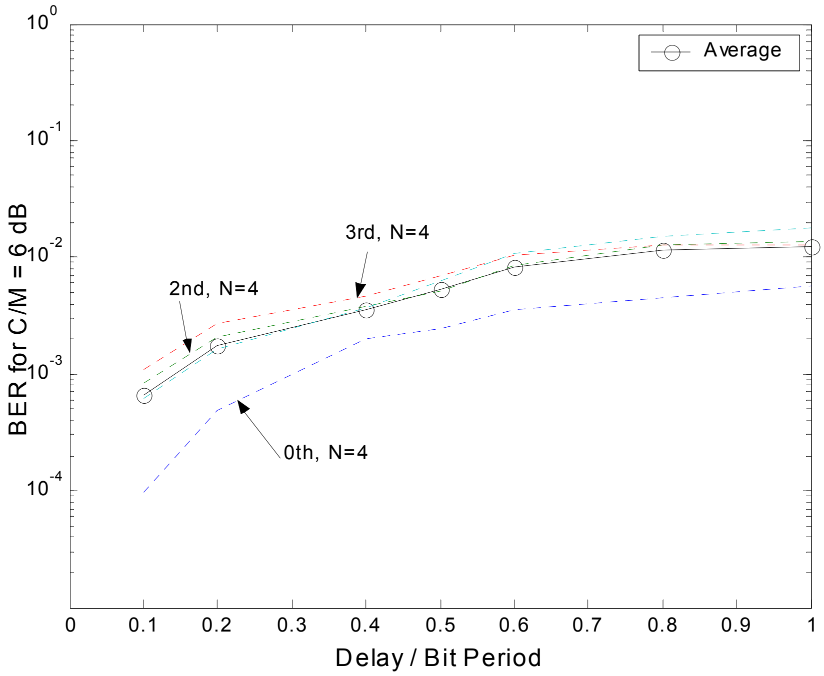

Figure 6.8 BER vs. delay spread of a four-dimensional system listed by dimension. The C/M is fixed at 6 dB. Infinite E_b/N_o and no lognormal effect on the direct path are assumed.

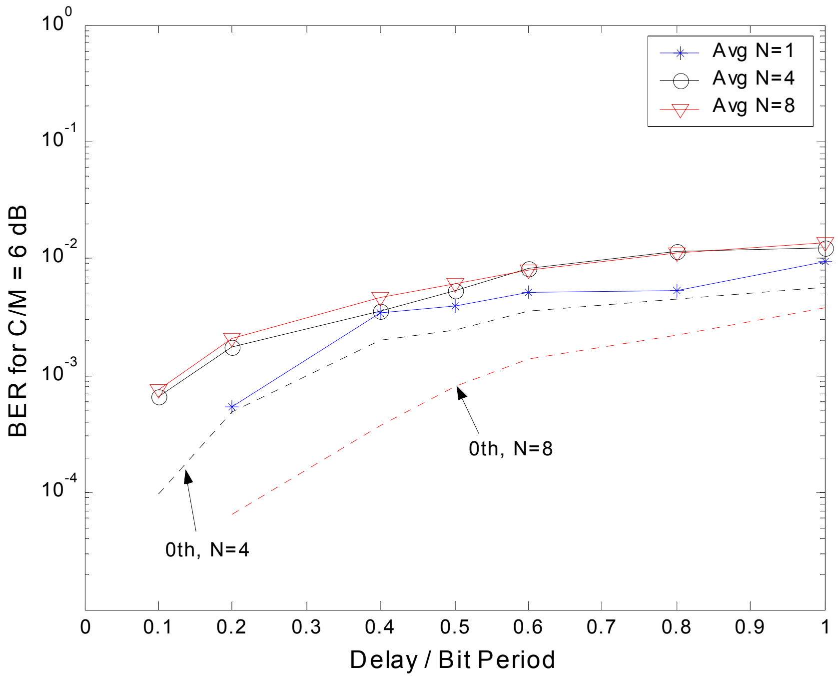

Figure 6.9 Comparison of the average BER of 1-, 4- and 8-dimensional systems. The BER of the lowest order (the 0^{th}) dimension are illustrated by the dashed lines. The assumptions used are as of Figure 6.8.

6.6.3 Effects of Combination of C/M and E_b/N_o

Earlier the bit energy to noise power density ratio was assumed to be infinite. This section deals with finite E_b/N_o. As C/M gets sufficiently large, i.e., the multipath fades out, and the BER approaches zero. However, if noise is present, the BER cannot go to zero. The irreducible BER is limited by the AWGN. The simulation block diagram is illustrated in Figure 6.10.

Figure 6.11 shows BER versus C/M at various E_b/N_o. The simulation assumes a multipath delay of $0.5T_b$ and has the E_b/N_o set at 8, 10, 12 and infinite dB. C/M is then increased from 0 to 30 dB. With infinite E_b/N_o, the BER approaches zero as the C/M increases. However, finite E_b/N_o defines an irreducible BER floor. There is no significant difference between 1- and 4-dimensional systems.

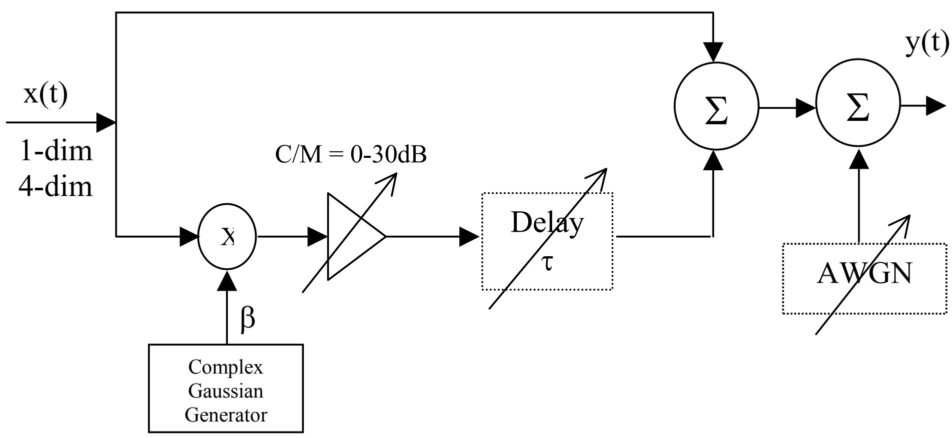

Figure 6.10 A model of frequency selective fading channel with AWGN included. The simulation assumes that the direct path is free of fluctuation. The BER results are summarized in Figure 6.11 and Figure 6.12.

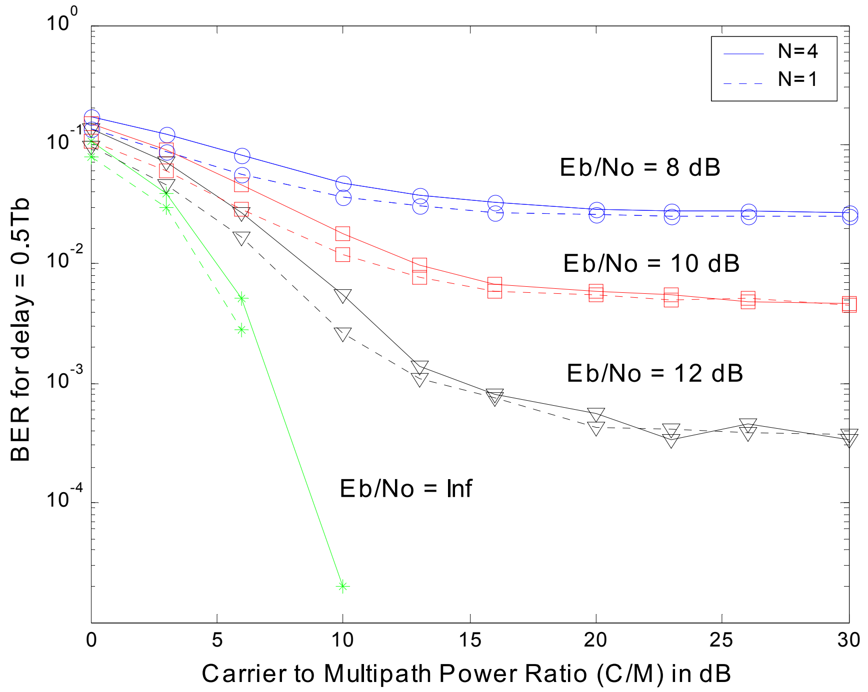

Figure 6.11 Average BER vs. C/M of 1- and 4-dimensional systems for the given E_b/N_o. The delay spread is fixed at $0.5T_b$. No lognormal effect on the direct path is assumed.

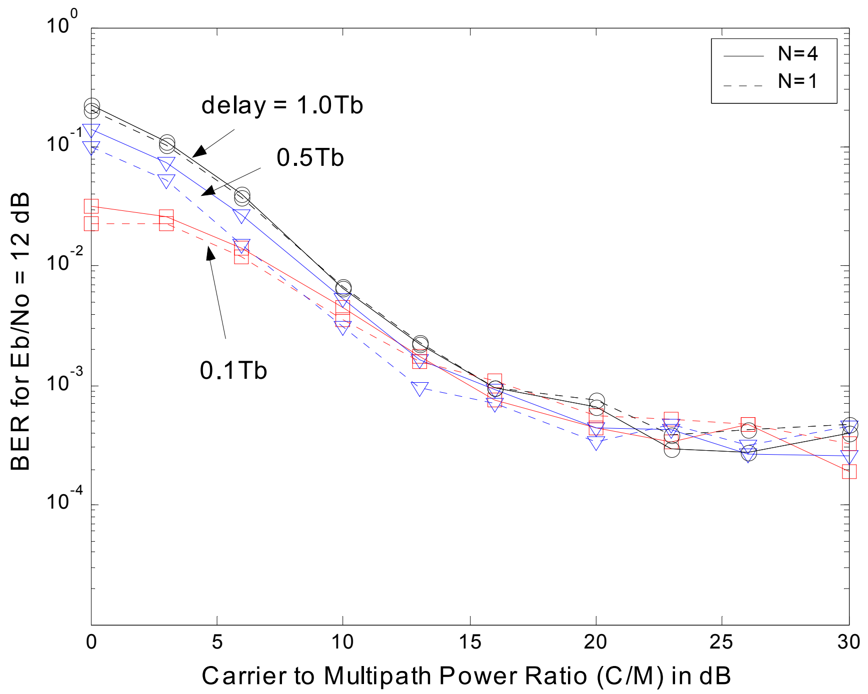

Figure 6.12 Average BER vs. C/M of 1- and 4-dimensional systems for the given delay spreads. E_b/N_o is fixed at 12 dB. No effect of the lognormal is assumed.

The simulation results illustrated in Figure 6.12 demonstrate how delay spread influences the BER with the presence of AWGN. Three delay spreads, $0.1T_b$, $0.5T_b$ and $1T_b$, are examined with an E_b/N_o of 12 dB. The BER is evaluated for for 1- and 4-dimensioanl Hermite Keying systems. For the same C/M, longer delays increase BER. In all cases, larger C/M ratios improve the BER. However, the BER improvement stops around 5×10^{-4} at a C/M ratio of about 15 dB. There, the BER is limited by the 12-dB E_b/N_o.

According to Figure 6.11, either a C/M of 5 dB or an E_b/N_o of 12 dB prevents the BER from going below 10^{-3}. Forward error correction (FEC), which adds redundant bits to the data stream, is capable of correcting some error bits. Therefore, such an error control technique is needed to lower the irreducible errors. FEC is beyond the scope of this dissertation.

In conclusion, given a fixed delay and E_b/N_o, the higher C/M, the lower BER. The BER improvement of the system is bounded by the E_b/N_o. Increasing C/M, meaning the multipath is non-existing, gives no further reduction in BER. Given a fixed E_b/N_o and C/M, the BER deteriorates, as multipath delay gets longer. For a large C/M, the BER is dominated only by E_b/N_o. No significant result is found on the 1- and 4-dimensional systems.

In the case of frequency selective fading channels, the BER associated with lower order pulses of HK is significantly less than the average BER. The lower order pulses should be used to carry the most important data of the transmission. For instance, in a transmitted packet, address data is more crucial than the user data. Address bits should be transmitted using the lower order Hermite pulses. As a result, the uneven BER is an advantage of using HK in frequency selective fading channels.

In the derivation of the optimal synchronization method, white noise is assumed. The BER on each dimension is supposed to be identical. In AWGN case, the FM noise in HK is not white but the pre/deemphasis partially eliminates the difference between the dimensional BER. As a consequence, optimal synchronization, which includes all dimensions in determining the synchronization, is valid. However, in frequency selective fading, uneven BER of HK with pre/deemphasis is observed. It is possibly more robust to use only outputs from the lower order correlators to implement the synchronizer since they are more reliable. The BER on the higher order dimension is worse so it possibly reduces the reliability of the synchronizer. Further research on robust synchronization is needed.

6.7 Chapter Summary

In this chapter, models for a satellite mobile channel are reviewed. Discussion focuses on the frequency-selective model. The model parameters are discussed in detail. The effects of lognormal distributed direct path on the BER of Hermite Keying system are investigated. The simulation examines the BER degradation caused by multipath delay and also the power ratio of direct and multipath signals. Finally, AWGN is included in the model. C/M and AGWN determine the floor of irreducible BER.

Chapter 7
Results Summary and Conclusions

In this dissertation, a new method for the transmission of digital data is introduced. The approach makes use of the orthogonality properties of Hermite waveforms that are used to represent digital data. Hermite waveforms are derived from Hermite functions and have the property that all orders of waveform are orthogonal. Multilevel signaling can be implemented by simultaneous transmission of several Hermite waveforms coded with different sections of a data stream. Although the waveforms extend to infinity, the transmission of truncated waveforms leads to minimal inter-symbol interference, and the bandwidth required is comparable to that needed in conventional digital transmission systems using square root raised cosine (RRC) filtering.

The investigation of the new communication system begins with an analysis of bandwidth efficiency of the chosen waveforms. The discussion covers structures of the baseband transmitter and receiver, synchronization, techniques to carry the waveforms over radio links, the bandwidth and power efficiencies of Hermite waveforms when transmitted by modulation of an RF carrier, and finally performance in fading channels. The results are briefly summarized and conclusions are drawn in this chapter.

7.1 Summary and Conclusion on Bandwidth Efficiency

This dissertation analyzes the spectral efficiency of Hermite-based techniques in terms of bandwidth per data bit rate by using simulation. It is found that in baseband communications, the bandwidth required to transmit binary data at a rate of R_b using antipodal Hermite pulses is $0.625R_b$. This bandwidth is identical to the bandwidth needed by a raised cosine pulse with a roll-off factor of 0.25. The theoretical limit for zero ISI using binary waveforms is $0.5R_b$. Nevertheless, it is unlikely that a baseband system can use a bandwidth less than $0.625R_b$ in practice. Therefore, the bandwidth efficiency of the antipodal Hermite technique is considered excellent for baseband communications.

Transmitting Hermite waveforms as RF signals can be implemented in either of two ways by using amplitude or frequency modulation. Using AM, a total occupied bandwidth of $1.25R_b$ Hz is needed to transmit at a bit rate of R_b bits/second. The bandwidth efficiency of the Hermite technique matches the bandwidth of BPSK filtered by a square root raised cosine filter with a roll-off factor of 0.25. Typically, a roll off factor 0.25 is close to the minimum that can be used in practice with RRC filtering. Note that first null bandwidth of unfiltered BPSK exceeds $2R_b$. QPSK makes use of quadrature carriers to double the bandwidth efficiency of BPSK. The same approach can be applied to AM Hermite transmission as well. Therefore, the bandwidth efficiency of AM Hermite transmissions is also excellent in a radio frequency link.

One difficulty is that Hermite waveforms are peaky. The peak to average power ratio is a linear function of the number of orthogonal pulses used (dimension). Hermite Keying (HK), in which the waveform is modulated onto an RF carrier using a linear FM modulator, is proposed as the best method for transmission of baseband Hermite waveforms. Despite peaky modulating waveform, the shape of HK power spectral density is monotonically decreasing; unlike the case of MSK, no side lobes are observed in the HK spectrum. It is found that when 99.9% of power of the HK signal is transmitted, the occupied bandwidth of HK is less than that of MSK even though FM preemphasis is used. Hermite keying offers superior spectral efficiency to many common digital modulation techniques. Therefore, HK has excellent bandwidth efficiency.

In conclusion, the bandwidth efficiency of Hermite-based modulations can compete with other practical techniques for digital data transmission in both baseband and RF communications. One may choose Hermite-based modulation techniques over others whenever multi-level signaling is needed without worry of bandwidth efficiency.

7.2 Summary and Conclusion on Bit Error Rate

It is shown that an optimal receiver for a signal consisting of *N* orthogonal pulses (N-dimensional signal) can be implemented by using an array of dimension-wise matched filters. In transmission of single-dimensional signals, the optimal relationship between the bit error rate (BER) and the ratio of bit energy and noise power spectral density (E_b/N_o) is commonly known. This dissertation concludes that the relationship between BER and E_b/N_o also applies to the case of N-dimensional Hermite signals detected by using dimension-wise matched filters.

Antipodal Hermite baseband waveform, an N-dimensional signal, more or less, allows some degree of intersymbol interference (ISI). However, the ISI insignificantly affects the BER. The BER performance of the antipodal N-dimensional Hermite waveforms is identical to that of other single-dimensional antipodal techniques. An E_b/N_o ratio of 10.6 dB is required to reach a bit error rate 10^{-6}, identical to the theoretical result for a polar binary waveform.

Amplitude modulation is a simple method to carry the Hermite waveforms over radio links. Analysis shows that AM-Hermite modulation yields the same BER as BPSK and QPSK. BER is identical to the baseband case. In both baseband and AM Hermite cases, errors are distributed evenly to all dimensions. The results from simulation using complex envelope representation confirm the analytical results. Without extra power efficiency gained from channel coding, modulation techniques alone cannot achieve performance superior to the BER performance of BPSK. Therefore, AM-Hermite performs very well in terms of power efficiency.

A constant envelope signal and simplicity of the detectors are always preferred in radio communications. The BER performance of constant-envelope Hermite Keying (HK) with a limiter/discriminator, a simple FM detector, is compared to the BER performance of non-coherent FSK. With the inclusion of a simple preemphasis/deemphasis process, the average BER of HK is very close to FSK in a channel corrupted by white noise. Thus, the performance of HK with a simple FM detector is satisfactory.

To conclude the usefulness of having an extended symbol period, HK is tested in a frequency selective fading channel. A summary of the BER performance of HK in the fading channel is as follows. Both the delay and the power of the multipath plays an important roll in BER degradation. Furthermore, the delay of the multipath spreads the errors unevenly to the Hermite dimensions. The number of errors found on the high order Hermite pulses is greater than the number on the lower order pulses; BER for the 0^{th} dimension is considerably less than BER for the higher dimensions. The difference is underlined either when the channel experiences long delay or the number of Hermite pulses used is large. However, the larger dimension tends not to improve average BER. Only the data carried by the 0^{th} pulse is more secure.

It can be concluded that the BER performance of HK in a fading channel is about the same as GMSK (single-dimension HK) since the dimensionality does not improve the average BER. Nevertheless, using N-dimensional HK can secure some important bits by carrying them on the 0^{th} order pulse. This is beneficial to some applications. For example, digital data that is converted from an analog waveform can take advantage of the uneven error distribution. The most significant bit of the sample is kept on the 0^{th} pulse. Because of fewer errors on the bits, fidelity will be gained when the received digital data is converted back to analog signal. Therefore, N-dimensional HK is useful in frequency-selective fading environment and in certain applications. It is a better choice than GMSK, at least for some specific applications.

7.3 PSD and Optimal Synchronization of Antipodal N- dimensional waveforms

This dissertation aims to answer how efficiently the newly introduced modulation technique performs in terms of bandwidth and power. The conclusion has been drawn in the previous two sections. There are also interesting byproducts that are developed during the efficiency investigation: derivations of the PSD of antipodal N-dimensional waveforms and an optimal synchronization technique for the waveforms.

A derivation for the power spectral density (PSD) for N-dimensional antipodal waveforms is extended from the commonly known single-dimensional waveform. The shape of the PSD of an antipodal single-dimensional waveform can be obtained by the squared absolute value of the waveform Fourier transform. For N-dimensional waveforms, the derivation in this dissertation concludes that the PSD is the sum of the squared absolute values of Fourier transforms of all participating orthogonal pulses. The derived PSD for N-dimensional system assumes an equiprobable transmission of zeroes and ones in the data stream.

Optimal synchronizers in AWGN for antipodal signals are already available. In this dissertation, the theory is developed for optimal synchronization for more complicated N-dimensional signals. Realization of the N-dimensional synchronizers is also developed. Based on the newly developed theory, a simplified synchronizer that makes use of matched filters, which are already available for detection of the Hermite waveforms, is then designed. The synchronizer performs well at an E_b/N_o of 3 dB and the speed of acquisition is comparable to that of other synchronizers used for digital data transmission. This dissertation adds a valuable theory to communication engineering.

7.4 Conclusion

A new method for the transmission of digital data using multi-level signaling is introduced in this dissertation; Hermite Keying. Its performance is extensively evaluated. The results suggest that the new technique shows potential of usability in specific applications. This dissertation contributes new theories on N-dimensional transmission, which certainly is beneficial to advanced study in Communications. Further research is required to extend the technique to other applications, and to determine the relative merits of Hermite keying. The analysis in this dissertation has been based on simulation and must be verified by the construction and testing of an N-dimensional Hermite transmission system.

7.5 Suggested Further Research

This dissertation focuses on the transmission of Hermite waveforms using amplitude and frequency modulations, with the assumption that the system can be implemented using simple non-coherent detectors. Phase modulation is another method to carry the baseband Hermite waveform over a radio frequency channel. It is expected that the BER should be improved over the FM technique proposed in the dissertation. The transmission techniques discussed in this dissertation are restricted to receivers that have non-coherent detectors. Coherent detectors for Hermite Keying have not been investigated. The BER performance of coherent detectors, in general, is better than that of non-coherent detectors. It is worth studying such detectors.

It would be interesting to investigate the usefulness of HK in a complete digital transmission system of which both address data and user data are transmitted. It is possible that the digital modulation techniques that have uniform BER might lose the destination address or package identification information. As a consequence, retransmission of the data is needed. Hence, the overall throughput of the system decreases. Hermite Keying offers a way to provide more secure addressing and package ID bits by using lower order Hermite waveforms for these bits in the packet, and higher order waveforms for the data bits. The BER for lower order waveforms has been demonstrated to be lower than for the higher order waveforms. Throughput improvement should be possible in noisy channels. In that case, Hermite Keying is an attractive modulation technique. A channel coding technique for uneven BER should also be investigated.

References

[ABR95] Abrado, A., G. Benelli, and G. R. Cau, "Multiple-symbol differential detection of GMSK for mobile communications," *IEEE Trans. Veh. Technol,* vol. VT-44, pp. 379-389, August 1995.

[BEA84] Beauchamp, K. G., *Applications of Walsh and Related Functions,* Academic Press, London, 1984.

[BER93] Berrou, C., A. Glavieux, and P. Thitimajshima, "Near Shannon Limit Error-Correcting Coding and Decoding: Turbo Codes," *ICC*, pp. 1064-1070, 1993.

[BOS60] Bose, R. C. and D. K. Ray Chaudhuri, "On a Class of Error Correcting Binary Group Codes," *Information Control*, no. 3, pp. 68-79, March 1960.

[CAM83] Campanella, J. and Schaefer, D., "Time-Division Muliple-Access Systems (TDMA)," in *Digital Communications—Satellite/Earth Station Engineering*, edited by Feher, K., Prentice Hall, Eaglewood Cliffs, N.J., Chapter 8, 1983.

[CAS91] Casas, E. F. and Leung, C., "OFDM for Data Communication over Mobile Radio FM Channel—Part I: Analysis and Experimental Results," *IEEE Trans. Communications*, vol. 39, no. 5, pp. 783-793, May 1991.

[CAS99] Casakis-Qiorps, F. J and Sanchez-Perez, R., "Robust FM Data Transmission in Multiple Propagation Environments," *Vehicular Technology Conference Proceedings, Fall IEEE-50th,* vol. 5, pp. 2959-2963, September 1999.

[CHA66] Chang, R. W., "High Speed Multichannel Data Transmission with Bandlimited Orthogonal Signals," *Bell Sys. Tech. J.,* vol. 45, pp. 1775-1796, December 1966.

[CHA68] Chang, R. W. and Gibby, R. A., "A Theoretical Study of Performance of an Orthogonal Multiplexing Data Transmission Scheme," *IEEE Trans. Communication Technology*, vol. COM-16, no. 4, pp. 529-540, August 1968.

[CHU87] Chuang, J., "The Effects of Time Delay Spread on Portable Communications Channel with Digital Modulation," *IEEE Journal on Selected Areas in Communications*, vol. JSAC-5, no. 5, pp. 879-889, June 1987.

[CRA99] Cramer, J. M., Shcoltz, R. A. and Win, M. Z., "On the Analysis of UWB Communication Channels," *Proc. MILCOM '99*, vol. 2, pp. 1191-1195.

[COR94] Corazza, G. E. and F. Valataro, "A statistic model for land mobile satellite channels and its application to nongeostationary orbit system," *IEEE Trans. Veh. Technol.,* vol. 34, pp 738-742, August 1994.

[COU97] Couch, L. W., *Digital and Analog Communications,* 5th ed., Prentice Hall, Upper Saddle River, New Jersey, 1997.

[CIM85] Cimini, L. J. Jr., "Analysis and Simulation of a Digital Mobile Channel Using Orthogonal Frequency Division Multiplexing," *IEEE Trans. Communications*, vol. COM-22, no. 7, pp. 665-675, July 1985.

[DEG95] De Gaudenzi, R. et al, "A performance comparison of orthogonal code division multiple-access techniques for mobile satellite communications," *IEEE J. Select. Areas Comm.,* vol. 13, No. 2, pp 325-332, February 1995.

[ELT89] El-Tannay, M.S., et. Al., "Data detection and timing recovery for a noncoherent discriminator-based GMSK receiver", *IEEE 39th J. Veh. Techol. Con.,* vol.l, pp 243-248, May 1989.

[EUR94] European Telecommunication Standard, "Radio Broadcasting Systems: Digital Audio Broadcasting," *ETSI Final Draft*, pr ETS 300 401, November 1994.

[FUN93] Fung, V., et al., "Bit error simulation for π/4-DQPSK mobile radio communications using two-ray and measurement-based impulse response models," *IEEE J. Select. Areas Comm.,* vol. 11, no. 3, pp 393-405, April 1993.

[FOL92] Folland, G. B., *Fourier Analysis and Its Application*, Brook/Cole, California, 1992.

[GUN94] Gunther, C. G. and J. Habermann, "DOQPSK-Differential Demodulation of Filtered Offset QPSK," *IEEE 44th J. Veh. Technol. Con.,* vol.3, pp 1542 -1546, June 1994.

[GRO76] Gronemeyer, S. A. and McBride, A. L., "MSK and Offset QPSK modulation," *IEEE Trans. Commun.,* vol. COM-24, pp. 809-820, August 1976.

[HA90] Ha, T. T, *Digital Satellite Communications*, 2nd ed, McGraw-Hill, New York, 1990.

[HAR72] Harmuth, H. F., *Transmission of Information by Orthogonal Functions,* Springer-Verlag 2nd ed, New York, 1972.

[HIR81] Hirosaki, B., "An Orthogonally Multiplexed QAM System Using the Discrete Fourier Transform," *IEEE Trans. Communications*, vol. COM-29, no. 7, pp. 982-989, July 1981.

[ISH80] Ishisuka, M. and Hirade, K., "Optimal Gaussian Filter and Deviated-Frequency-Locking Scheme for Coherent Detection of MSK," *IEEE Trans. Commun.,* vol. COM-28, no. 6, pp. 850-857, June 1980.

[ISH84] Ishizuka, M. and Y. Yasuda, "Improved coherent detection of GMSK," *IEEE Trans. Commun.*, vol. 32, pp. 308-311, March 1984.

[JAK74] Jake, W. C., Jr., *Microwave Mobile Communications*, Wiley-Interscience, New York, 1974.

[LIN73] Lindsey, W. C., and M. K. Simon, *Telecommunication Systems Engineer,* Prentice Hall, Inc., New Jersey, 1973.

[LIU90] Liu, C-L. and K. Feher, "Performance of non-coherent π/4-QPSK in a frequency-selective fast Rayleigh fading channel," *Proc. IEEE Int. Conf. Commun.,* Atlanta, GA, Apr. 1990, pp. 335.7.1-335.7.5.

[LIU91] Liu, C. and K. Feher, "Bit error rate performance of π/4-DQPSK in a frequency-selective fast Rayleigh fading channel," *IEEE Trans. Veh. Technol.* vol. 40, no.3, pp 558-568, August 1991.

[LOO85] Loo, C., "A statistical model for a land mobile satellite link," *IEEE Trans. Veh. Technol*., vol. VT-34, pp 122-127, August 1985.

[LOO91] Loo, C. and N. Secord, "Computer models for fading channels with applications to digital transmission," *IEEE Trans. Veh Techno.* vol. 40, no. 4, pp 700-707, November 1991

[LUT91] Lutz, E. et al. "The land mobile satellite communication channel – Reconding, statistics, and channel model," *IEEE Trans. Veh. Techno.* vol. 40, no. 2, pp 375-386, May 1991.

[MAT99] Math Works, Inc., *Matlab Version 5.3*, Natick, MA, 1999.

[MAR90] Martens, J. B., "The Hermite Transform—Theory," *IEEE Trans. Acoustics, Speech, and Signal Processing*, vol. 38, no. 9, pp. 1595-1606, September 1990.

[MIT03] Mitchell, C. and Kohno, R., "High Data Rate Transmissions Using Orthogonal Modified Hermite Pulses in UWB Communications," *International Conferences on Telecommunications, ICT 2003*, vol. 2, pp. 1278-1283.

[MIC02] Michael, L. B., Ghavami, M. and Kohno, R., "Multiple Pulse Generator for Ultra-Wideband Communication Using Hermite Polynomial Based Orthogonal Pulse," *IEEE Conference on Ultra Wideband Systems and Technologies, Digest of papers 2002*, pp. 47-51.

[MUR00] Murakami, Y. et al., "A New Design of Pilot Symbol in 16QAM Channels," *IEEE Vehicular Technology Conference Proceeding,* vol. 3, pp. 2064-2068, May 2000.

[MUR81] Murota, K. and K. Hirade, "GMSK modulation for digital mobile radio telephony," *IEEE Trans. Comm.,* vol. COMM-29, no. 7, pp 1044-1050, July 1981.

[NYQ28] Nyquist, H., "Certain topics in telegraph transmission theory," *Transactions of the AIEE,* vol. 47, pp. 617-644, February 1928.

[OPP89] Oppenheim, A. V. and R. W. Schafer, *Discrete-Time Signal Processing*, Prentice Hall, New Jersey, 1989.

[PAP65] Papoulis, A., *Probability Random Variables and Stochastic Process*,: McGraw-Hill, New York, 1965.

[PAW88] Pawula, R. F., "Refinements to the theory of error rates for narrow-band digital FM," *IEEE Trans. Commun.,* vol. COM-36, pp. 509-513, April 1988.

[PAW99] Pawula, R.F., "Improved Performance of Coded FM." *IEEE Trans. Commun.,* vol. 47, no. 11, pp. 1701-1708, November 1999.

[PIC82] Pickholtz, R. L., et al, "Theory of Spread-Spectrum Communication—A Tutorial," *IEEE Trans. Commun.*, vol. COM-30, no. 5, pp. 855-884, May 1982.

[POL88] Polacek, M, et al, "On FM Threshold Extension by Click Noise Elimination," *IEEE Trans. Commun*, vol. 36, no. 3, pp. 375-380, March, 1988.

[PRA86] Pratt, T. and C. W. Bostian, *Satellite Communication,* John Wiley and Son, New York, 1986.

[PRO95] Proakis, J. G., *Digital Communications,* 3rd ed., McGraw-Hill Book Company, New York, 1995.

[RAO99] Rao, M. M., et al., "Simultaneous Extrapolation in Time and Frequency Domains Using Hermite Expansions," *IEEE Trans. Antennas and Propagation*, vol. 47, no. 6, pp. 1108-1115, June 1999.

[RAP02] Rappaport, T. S., *Wireless Communications,* 2nd ed., Prentice Hall, NJ 2002.

[RIC63] Rice, S. O., *Noise in FM Receivers,* Time Series Analysis, M. Rosenblatt, Ed., Wiley, New York, 1963.

[SAL67] Saltzberg, B. R., "Performance of an Efficient Parallel Data Transmission System," *IEEE Trans. Communication Technology*, vol. COM-15, no. 6, pp. 805-811, December 1967.

[SAL87] Saleh, A. A. M., and Valenzeula, R. A., "A Statistical Model for Indoor Multipath Propagation," *IEEE Journal on Selected Areas in Communications*, vol. JSAC-5, no. 2, pp. 128-137, February 1987.

[SAL94] Salt, J. E. and S. Kumar, "Effects of filtering on the performance of QPSK and MSK modulation in D-S spread spectrum systems using RAKE receivers," *IEEE J. Select. Areas Comm.,* vol. 12, no. 4, pp 707-715, May 1994.

[SAR80] Sarwate, D. V. and M. B. Pursley, "Crosscorrelation Properties of Pseudorandom and Related Sequences," *Proc. IEEE,* Vol. 68, pp. 593-619, May 1980.

[SHA48] Shannon, C. E., "Mathematical Theory and Communication," *Bell System Technical Journal*, vol. 27, pp. 379-423, July 1948.

[SKL97a] Sklar, B., "Rayleigh fading channels in mobile digital communication systems part I: Characterization," *IEEE Commun. Magazine,* vol. 35, no. 7, pp. 90-100, July 1997.

[SKL97b] Sklar, B., "Rayleigh fading channels in mobile digital communication systems part II: Mitigation," *IEEE Commun. Magazine,* vol. 35, no. 7, pp. 102-109, July 1997.

[SUZ77] Suzuki, H., "A statistical model for urban radio propagation," *IEEE Trans. Commun.,* vol. COM-25, pp 673-680, July 1977.

[TIA93] TIA/EIA Interim Standard-95, “Mobile Station—Base Station Compatibility Standard for Dual-Mode Wideband Spread Spectrum Cellular System,” July 1993.

[VAN67] Van Trees, H. L., *Detection, Estimation and Modulation Theory,* John Wiley & Son, Inc. New York, N.Y., 1967.

[VAR91] Varshney, P. and S. Kumar, “Performance of GMSK in a land mobile radio channel,” *IEEE Trans. Veh. Technol,* vol. COM-44, pp. 607-614, August 1991.

[VAT95] Vatalaro, F., “Generalized Rice-lognormal channel model for wireless communications,” *Electron. Lett.* vol. 31, no. 22, pp 1899-1900, October 1995.

[WAL93] Walton, M. R. and Hanrahan, H. E., “Hermite Wavelets for Multicarrier Data Transmission,” *Proceedings of South African Symposium on Communications and Signal Processing*, pp. 40-45, August 1993.

[WEI71] Weinstein, S. B. and Ebert, P. M., “Data Transmission by Frequency-Division Multiplexing Using the Discrete Fourier Transform,” *IEEE Trans. Communication Technology*, vol. COM-19, no. 5, pp. 628-634, October, 1971.

[WIE33] Wiener, N., *The Fourier Integral and Certain of Its Applications,* Cambridge University Press, London, 1933.

[WIN98] Win, M. Z. and Scholtz, R. A., “Impulse Radio: How It Works,” *IEEE Communications Letter*, vol. 2, no. 2, pp. 36-38, February, 1998.

[WU95] Wu, Y. and Zou, W. Y., “Orthogonal Frequency Division Multiplexing: A Multi-Carrier Modulation Scheme,” *IEEE Trans. on Consumer Electronics*, vol. 41, no. 3, pp. 392-399, August, 1995.

[ZIE90] Ziemer, R. E. and W. H. Tranter, *Principles of Communications: System, Modulation and Noise*, Houghton Mifflin, Boston, 1990.

[ZIE92] Ziemer, R.E. and Peterson, R. L., *Introduction to Digital Communications*, Macmillan Publishing Company, 1992.

Vita

Wachira Chongburee received his Bachelor Degree in Electrical Engineering from Kasetsart University, Thailand in 1991. He focused on Digital Signal Processing when he pursued his Master's Degree at Virginia Tech, and later on Communications for his Doctoral Degree at the same institution. He currently is a Kasetsart University faculty member back home in Thailand. In addition to teaching and conducting research, he is interested in establishing a telecommunication business.